Stony Brook University

Oxidized Graphene Nanoparticles as a Delivery System for the Bioactive Sphingolipid Ceramide

A Dissertation Presented

by

Cassandra Suhrland

to

The Graduate School

in Partial Fulfillment of the

Requirements

for the Degree of

Doctor of Philosophy

in

Biomedical Engineering

Stony Brook University

August 2016

Stony Brook University

The Graduate School

Cassandra Suhrland

We, the dissertation committee for the above candidate for the

Doctor of Philosophy degree, hereby recommend

acceptance of this dissertation.

Dr. Balaji Sitharaman – Dissertation Advisor
Associate Professor, Department of Biomedical Engineering

Dr. Eric Brouzes - Chairperson of Defense
Assistant Professor, Department of Biomedical Engineering

Dr. Mei Lin Chan - Committee Member of Dissertation Defense
Assistant Professor, Department of Biomedical Engineering

Dr. Jean-Philip Truman - Committee Member of Dissertation Defense
Research Assistant Professor, Department of Medicine

This dissertation is accepted by the Graduate School

Nancy Goroff
Interim Dean of the Graduate School

Abstract of the Dissertation

Oxidized Graphene Nanoparticles as a Delivery System for the Bioactive Sphingolipid Ceramide

by

Cassandra Suhrland

Doctor of Philosophy

in

Biomedical Engineering

Stony Brook University

2016

In recent years there has been a growing appreciation for the active functions certain lipids have in cellular metabolism. These "bioactive lipids" have been found to be an important part of many cell signaling processes. In particular, the bioactive sphingolipid ceramide has emerged as an important player in cancer biology. Dysregulation of ceramide metabolism has been shown to impart resistance to drug and radiation treatment in certain types of cancer, with low levels of specific ceramide species conferring resistance to apoptosis. It has also been shown that restoring levels of these ceramides in cancer cells through exogenous delivery also restores sensitivity to radiation and drug treatment. As such, the exogenous delivery of ceramide to represents an untapped therapeutic target for the treatment of resistant cancers. However, as a lipid, ceramide is extremely hydrophobic and has virtually no solubility in aqueous solution; it requires a delivery system for successful entry into cells. Current methods of ceramide delivery have serious drawbacks, and as a result, there is currently no clinically approved method for the therapeutic delivery of ceramide.

In this work, we present the use of oxidized graphene nanoribbons (O-GNRs) derived from multi-walled carbon nanotubes as a delivery system for ceramide. We developed a novel method for the noncovalent reversible loading of ceramide onto O-GNRs. Using this method, we were able to load significant amounts of both short chain and long chain ceramides onto O-GNRs. We found that the short-chain C_6 ceramide was able to directly induce high levels of apoptosis in cancer cells when loaded onto O-GNRs. We also found that long chain C_{16} and C_{24} ceramides were able to modulate the resistance of cancer cells to drug and radiation treatment when loaded onto O-GNRs. However, we found that O-GNRs have significant biological effects that interfere with the effects of ceramide on drug and radiation treatment, suggesting a critical need to

optimize the properties of these nanoparticles for use with ceramide. Despite these limitations, these results represent a promising first step on the path to therapeutic delivery of ceramide.

Dedication

For my family

Who have stood by my side and have always been there for me, no matter what.

Table of Contents

List of Figures/Tables/Illustrations

Figure 5.4 Effects of uptake inhibitors (I) on the viability of HeLa cells treated with C6 ceramide and C16 ceramide loaded O-GNRs (A, B) or UV irradiation and C24 ceramide loaded O-GNRs (C, D) as measured by Prestoblue. Dynasore, gefitinib, and EIPA showed significant decreases in viability on cells treated with C16 loaded O-GNRs and C6 (A, B). Filipin showed a significant increase in cells treated with C16 loaded O-GNRs and C6 (B). For C24 treatment, dynasore lowered the viability of UV-irradiated cells with C24 loaded O-GNRs (C) while treatment with gefitinib, filipin, and EIPA showed no significant effect (C, D). * indicates significant difference from "Untreated" and † indicates significant difference from "C6" (A, B) or "UV" (C, D). For High and Low concentrations: for dynasore Hi = 80 μM, Lo = 40 μM; for Gefitinib Hi = 1 μM, Lo = 0.5 μM; for EIPA Hi = 0.5 mM, Lo = 0.25 mM; for Filipin, Hi = 3 μg/mL, Lo = 2 μg/mL.

Figure 5.5 Effects of uptake inhibitors on apoptosis induced by C16 ceramide loaded O-GNRs and C6 ceramide (A) or C24 ceramide loaded O-GNRs and UV irradiation (B). For cells treated with C16 loaded O-GNRs and C6 ceramide, dynasore and EIPA treatment led to an increase in apoptosis, filipin led to a decrease in apoptosis, and gefitinib had no significant effect (A). For cells treated with C24 loaded O-GNRs and UV, no inhibitor had an effect on the level of apoptosis observed (B). * indicates significant difference from "Untreated." Concentration of inhibitors: dynasore = 80 μM, Gefitinib = 1 μM, EIPA = 0.5 mM, Filipin, = 3 μg/mL.

Figure 5.6 Confocal Microscopy images of HeLa cells treated with fluorescent C12 NBD ceramide loaded onto O-GNRs (A-D) or fluorescent C12 NBD ceramide only (E-H). Ceramide loaded onto O-GNRs (A) shows ceramide more localized to endosomes after 2 hours than free ceramide (E). Cells treated with Dynasore and ceramide-loaded O-GNRs (B) and Gefitinib and ceramide-loaded O-GNRs (C) show significantly less fluorescence than cells not treated with inhibitors of O-GNR uptake (A). However, cells treated with Dynasore and free ceramide (F) and Gefitinib and free ceramide (G) show no difference than cells treated with free ceramide alone (E). Cells treated with free ceramide and endosome disruptor desipramine (H) show significantly less endosome localization than cells treated with free ceramide only (E). However, cells treated with desipramine and ceramide-loaded O-GNRs (D) show no difference in endosome localization compared to cells treated with ceramide-loaded O-GNRs only (A).

Figure 5.7 Transmission electron microscopy images of HeLa cells incubated with ceramide loaded O-GNRs after 24 hr. Both C16 loaded O-GNRs (A, C) and C24 loaded O-GNRs (B, D) show high degrees of nanoparticle uptake. There is also evidence of membrane "blebbing" (arrows) associated with the uptake mechanism (A, C). Zoomed-in views of these regions of interest (C, D) also show O-GNRs localized to endosomes.

Acknowledgments

I would first like to thank my advisor Dr. Balaji Sitharaman, for his support, guidance, and patience in my time at Stony Brook. Thank you for giving me the opportunities you have, and for believing in me and shaping my growth as a scientist.

I would also like to thank the members of committee Dr. Eric Brouzes, Dr. Mei Lin Chan, and Dr. Jean-Philip Truman. I am grateful that all of you agreed to be a part of my committee, and I am grateful for your feedback on my work. I would especially like to thank Jean-Philip, for originally approaching us with this goal of delivering ceramide, and for his help in understanding the many intricacies of ceramide.

I would like to thank the fellow members of my lab, Dr. Gaurav Lalwani, Dr. Sayan Mullick Chowdhury, Dr. Shruti Kanakia, Dr. Behzad Farshid, Dr. Sunny Patel, Shawn Xie, Jason Rashkow, Yahfi Talukdar, and Stephen Lee. We were a small army of grad students working on many projects, with nanoparticles as the central unifying force. Working with you guys has been a blast, and though it was difficult to watch all of you slowly trickle out of the lab, I'm proud to have watched you grow and move onto new things.

I would like to thank the Department of Biomedical Engineering at Stony Brook. It has been a place that has not only introduced me to new and exciting research, but also great people as well.

I would also like to thank Susan Van Horn and the Central Microscopy Facility at Stony Brook University for her assistance with obtaining TEM images.

I would like to thank Izolda Mileva and the Lipidomics Facility for her help with mass spectrometry.

Finally, I would like to thank my family. My parents, Mark and Jeri, my sister Breanne, and my brother-in-law Chris. Words cannot adequately express how grateful I am to all of you, how much you've given me, and how much I love you. Who I am today, and what I have been able to accomplish, would never have been possible without all of you.

List of Publications

Cassandra Suhrland, Sayan Mullick Chowdhury, Zina Sanchez, Pankaj Chaudhary, MA Suresh Kumar, Stephen Lee, Louis A. Peña, Michael Waring, Balaji Sitharaman, and Mamta Naidu" Graphene nanoribbons as a drug delivery agent for lucanthone mediated therapy of glioblastoma multiforme." Nanomedicine: Nanotechnology, Biology and Medicine 11.1 (2015): 109-118.

Cassandra Suhrland, Daniel J. Dedora, Shilpi Goenka, Sayan Mullick Chowdhury, Gaurav Lalwani, Lilianne R. Mujica-Parodi, and Balaji Sitharaman. "Sulfobutyl ether β-cyclodextrin (Captisol®) and methyl β-cyclodextrin enhance and stabilize fluorescence of aqueous indocyanine green." Journal of Biomedical Materials Research Part B: Applied Biomaterials (2015).

Sunny C. Patel, Stephen Lee, Gaurav Lalwani, Cassandra Suhrland, Sayan Mullick Chowdhury, and Balaji Sitharaman. "Graphene-based platforms for cancer therapeutics." Therapeutic delivery 7.2 (2016): 101-116.

Cassandra Suhrland, Jean-Philip Truman, Lina M. Obeid, and Balaji Sitharaman. "Oxidized Graphene Nanoparticles as a Delivery System for the Pro-Apoptotic Sphingolipid C6 Ceramide." *In Preparation*

Cassandra Suhrland and Balaji Sitharaman. "Oxidized Graphene Nanoribbons Protect HeLa Cells from UV-Induced Apoptosis Through Buffering of Reactive Oxygen Species." *In Preparation*

Cassandra Suhrland, Jean-Philip Truman, Lina M. Obeid, and Balaji Sitharaman. "Delivery of Long Chain C16 and C24 in HeLa Cells Using Oxidized Graphene Nanoribbons." *In Preparation*

Chapter 1

Ceramide: A Review of Metabolism, Roles in Apoptosis and Cancer, and Delivery Methods

For many years, lipids have been viewed largely as passive actors in cellular metabolism, mainly assigned to structural roles in cell membranes or for the storage of energy in adipose tissue. However, in recent years there has been a growing appreciation for the critical, active roles lipids play in healthy and disease states alike. In particular, the enigmatic group of lipids known as sphingolipids has emerged as having many messengers for a wide variety of cellular functions[1-4]. Of these sphingolipids, ceramide has emerged as a key regulator of cellular processes of clinical relevance[5-7]. It has been shown that ceramide metabolism plays a large role in the progression of cancer[8], a group of diseases which are responsible hundreds of thousands of deaths and tens of billions of dollars in healthcare costs annually[9]. However, as a lipid ceramide is extremely hydrophobic, even compared to other biologically relevant lipids such as the more familiar phospholipids. This has limited its therapeutic applications, and as a result, there are currently no clinically available methods for the therapeutic delivery of ceramide.

In this chapter, we will review the metabolic pathways of ceramide synthesis, the role of ceramide in apoptotic signaling, the dysregulation of ceramide metabolism in cancer, the currently available methods for ceramide delivery, and possible avenues for new methods of ceramide delivery.

Sphingolipid Metabolism and Ceramide

There are three major pathways of ceramide synthesis in cells. The synthesis of all sphingolipids begins with the first major pathway, the '*de novo*' pathway, which synthesizes sphingolipids using basic fatty acids and other cofactors (Fig 1.1). This process begins with the condensation of palmitoyl-coenzyme A (CoA) and the amino acid serine into 3-ketosphinganine[10-12]. This product undergoes a reduction reaction by the enzyme 3-ketosphinganine reductase to yield dihydrosphingosine[10,13]. At this point, a second aliphatic tail

is acylated to dihydrosphingosine catalyzed by one of six ceramide synthases (CerS) and a variable chain length fatty acyl-CoA as the substrate, yielding dihydroceramide[14-21]. The specific CerS used depends on the length of the fatty acyl-CoA aliphatic chain, and the resulting ceramide is identified by the nomenclature C_n, where n is the carbon length of the fatty acyl tail. To convert from dihydroceramide to ceramide, the dihydroceramide desaturases (DES) create a 4,5 trans double bond into the sphingosine portion of ceramide[22,23]. The vast majority of enzymes and the processes involved in *de novo* ceramide synthesis is contained on and localized to the endoplasmic reticulum (Fig. 1.2)[24].

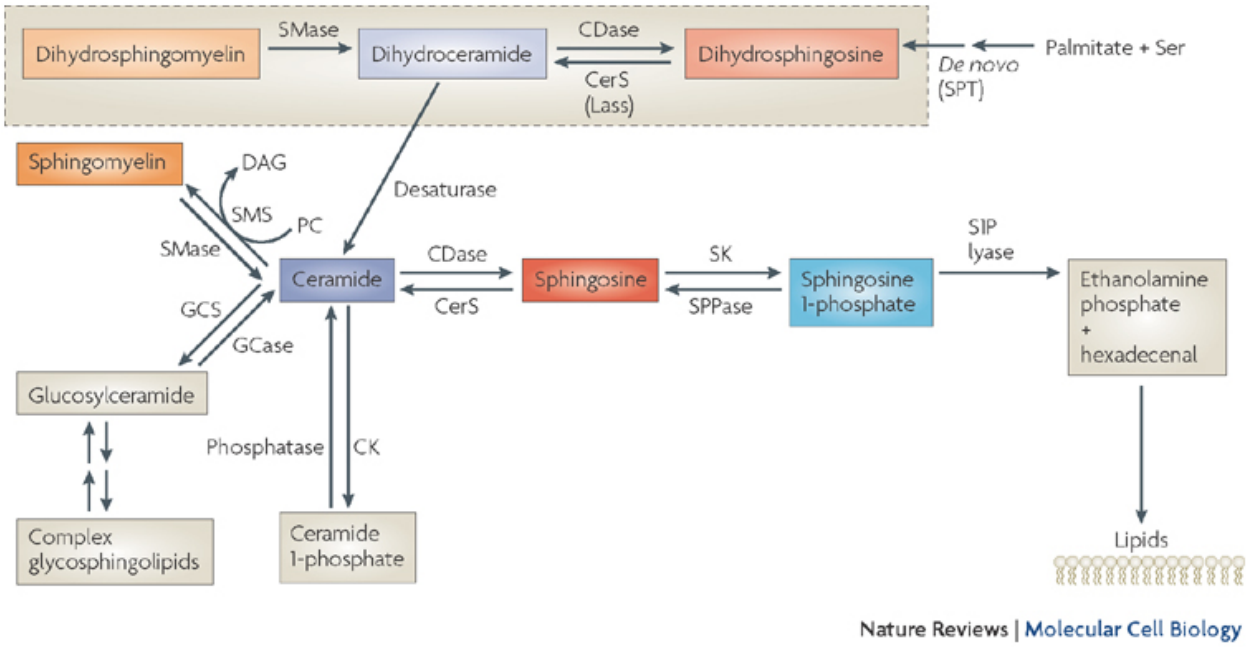

Figure 1.1. Ceramide is considered to be the central hub of sphingolipid metabolism, and is synthesized de novo from the condensation of palmitate and serine to form 3-keto-dihydrosphingosine (not shown). In turn, 3-keto-dihydrosphingosine is reduced to dihydrosphingosine followed by acylation by (dihydro)-ceramide synthase (also known as Lass or CerS). Ceramide is generated by the action of desaturases. From here, ceramide can be converted to other interconnected bioactive lipid species. The only exit pathway from the sphingolipid pathways is mediated by sphingosine-1-phosphate (S1P) lyase, which metabolizes S1P. Both ceramide and dihydroceramide have been shown to be bioactive and, in fact, >50 distinct molecular species may be classified as ceramide. Each may have its own separate metabolic network, resulting in unprecedented levels of complexity in sphingolipid signalling. In this figure, only a pathway for a generic ceramide and a generic dihydroceramide (shown in the dotted outline box) are depicted. It does not show the multiplicity or subcellular localization of

these pathways. CDase, ceramidase; CK, ceramide kinase; DAG, diacylglycerol; GCase, glucosyl ceramidase; GCS, glucosylceramide synthase; PC, phosphatidylcholine; SK, sphingosine kinase; SMase, sphingomyelinase; SMS, sphingomyelin synthase; SPPase, sphingosine phosphate phosphatase; SPT, serine palmitoyl transferase. Adapted with permission from "Principles of bioactive lipid signalling: lessons from sphingolipids." Nature Reviews Molecular Cell Biology (2008). Copy 2008 Nature Publishing Group.

From here ceramide serves as a sort of crossroads for the synthesis of complex sphingolipids, which are synthesized from ceramide using specific substrates and enzymes. One of the most abundant complex sphingolipids, sphingomyelin, is synthesized using phosphatidylcholine and sphingomyelin synthase[25,26]. The reverse of this reaction comprises the second major pathway of ceramide synthesis, dubbed the 'sphingomyelinase' pathway for the name of the enzyme that catalyzes the hydrolysis of sphingomyelin into ceramide and phosphocholine (Fig. 1.1)[26]. Unlike the enzymes of the *de novo* pathway, sphingomyelinases (SMases) are located on the membranes of several subcellular structures and organelles (Fig. 1.2). Acid sphingomyelinase (aSMase) is localized mainly to lysosomes and the extracellular leaflet, with the aSMases at each location having slightly different structures and functionality[27]. Neutral sphingomyelinases (nSMases) exist on both the inner leaflet of the plasma membrane and outer leaflet of the mitochondria, as well as the nucleus and Golgi[28-33]. There also exists alkaline sphingomyelinase (alkSMase), but its structure is fundamentally different from other SMases and its role in intracellular sphingolipid metabolism and signaling is not entirely clear[34].

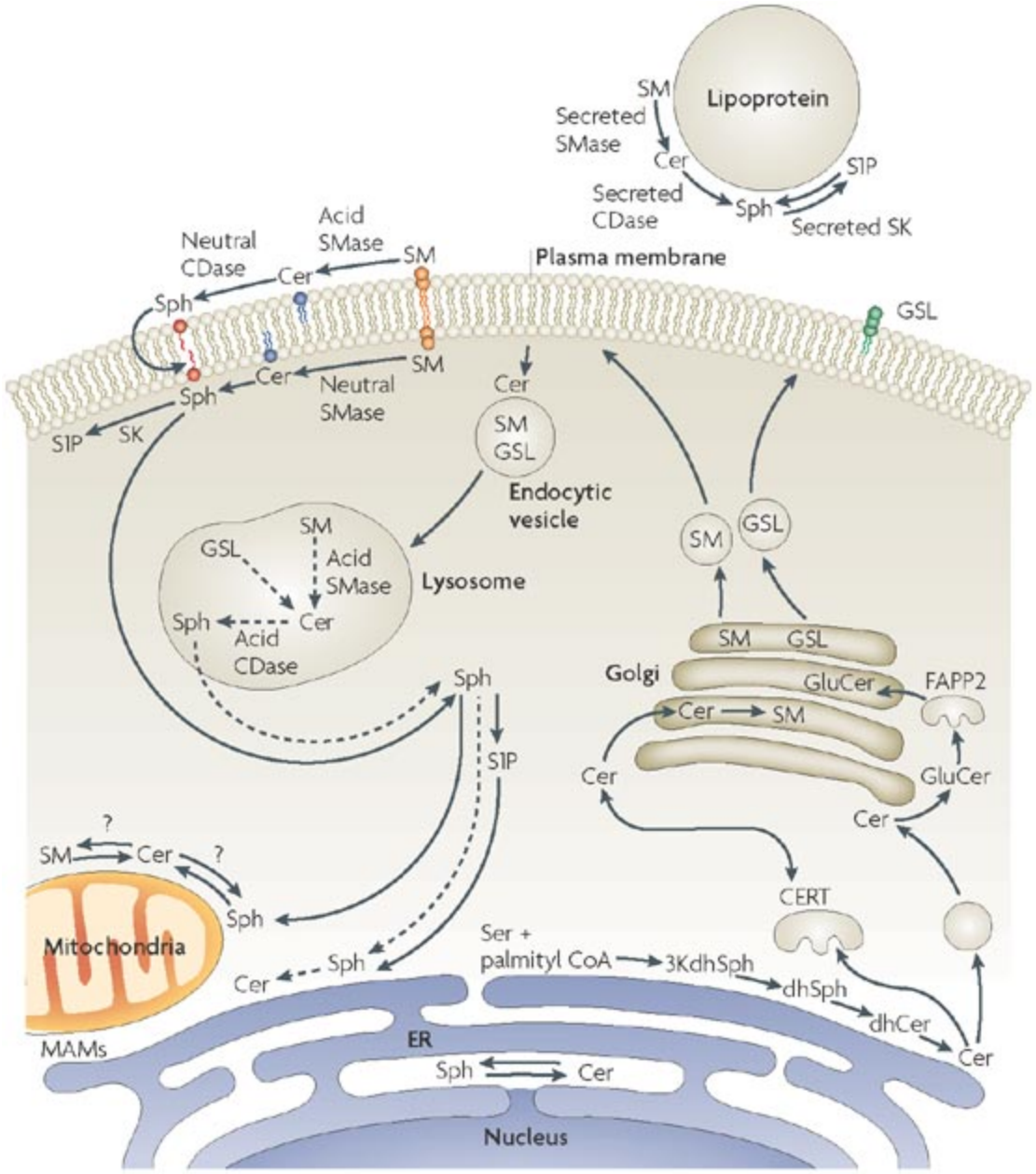

Nature Reviews | Molecular Cell Biology **Figure 1.2.** De novo synthesis of sphingolipids occurs in the endoplasmic reticulum (ER) and possibly in ER-associated membranes, such as the perinuclear membrane and mitochondria-associated membranes (MAMs; see figure). Ceramide (Cer) formed in this compartment is transported to the Golgi, which is the site of synthesis of sphingomyelin (SM) and glucosylceramide (GluCer), with the latter serving as the precursor for complex glycosphingolipids (GSLs). The transport of Cer to the Golgi occurs either through the action of the transfer protein CERT, which specifically delivers Cer for SM synthesis, or through vesicular transport, which delivers Cer for the synthesis of GluCer. In turn, transfer of GluCer for GSL synthesis requires the action of the recently identified transport protein FAPP2[35]. GluCer appears to be synthesized on the cytosolic side of the Golgi, and requires flipping to the inside of the Golgi for the synthesis of complex

GSLs, possibly with the aid of the ABC transporter, P-glycoprotein (also known as MDR1) (not shown). Delivery of SM and complex GSLs to the plasma membrane appears to occur by vesicular transport. Acid sphingomyelinase (aSMase) that is present in the outer membrane leaflet or neutral SMases in the inner leaflet of the bilayer can metabolize SM to Cer and subsequently other bioactive lipids. The mechanisms by which sphingolipids may cross lipid bilayers are discussed in. This metabolic network also extends to the circulatory system, where many of the enzymes (acid SMase, neutral ceramidase (CDase) and sphingosine kinase (SK)) have been detected, often in association with lipoproteins that are rich in SM and Cer. Internalization of membrane sphingolipids proceeds through the endosomal pathway whereby SM and GluCer may reach the lysosomal compartment, where they are degraded by the actions of SMases and glucosidases to form Cer. Cer is hydrolysed by acid CDase to form sphingosine (Sph). Sph may exit the lysosome, although its ionizable positive charge favours partitioning in lysosomes. Therefore, it is postulated that the action of SK1 at or near the lysosome may be required to 'trap' Sph through phosphorylation. Subsequent dephosphorylation by S1P phosphatases in the ER would recycle the salvaged Sph to Cer (a similar role for SK in delivering exogenous sphingoid bases to internal metabolic pathways has been demonstrated in yeast). Sph formed from this salvage pathway is also sufficiently soluble in cytosol to move among membranes. The salvage pathway is shown by the dashed arrows. 3KdhSph, 3-keto-dihydrosphingosine; dhCer, dihydroceramide; dhSph, dihydrosphingosine; S1P, sphingosine-1-phosphate. Adapted with permission from "Principles of bioactive lipid signalling: lessons from sphingolipids." Nature Reviews Molecular Cell Biology (2008). Copy 2008 Nature Publishing Group.

The third major pathway of ceramide synthesis is dubbed the 'salvage' pathway (Fig 1.1). Similarly to the sphingomyelinase pathway, the salvage pathway regenerates ceramides from the catabolism of complex sphingolipids, including sphingomyelin[36]. However, unlike in the sphingomyelinase pathway, the salvage pathway involves breaking down all the way to sphingosine, which is then fed into one of the ceramide synthases to yield ceramide[37]. As the salvage pathway uses the same ceramide synthases as the de novo pathway, the locations of synthesis are similar, with free sphingosine being trafficked mainly from lysosomal degradation of complex sphingolipids (Fig. 1.2.).

Ceramide Signaling in Apoptosis

Although sphingolipid metabolism has been shown to be an important component of many cell signaling processes, ceramide metabolism, in particular, has been heavily implicated in apoptotic signaling. Apoptosis, or "programmed cell death," is an important biological process for removing dysfunctional cells from an organism, characterized by chromatin condensation, cell shrinkage, and a shift to a round morphology. There are many factors involved in apoptotic signaling, but overall, apoptosis is classified into two main pathways: the extrinsic and intrinsic pathways[38].

The extrinsic pathway is characterized by signal transduction from death receptors on the cell surface, typically induced by specific ligands. Some of these receptor-ligand pairs include Fas and Fas Ligand[39], Tumor Necrosis Factor (TNF) Receptor 1 (TNFR1) and TNF[40], and TRAIL-R1 and TRAIL[41]. Upon binding of the ligand to the receptor, the intracellular portion of the death receptor known as the death domain binds to the Fas-associated death domain (FADD) protein[42]. The FADD complex associates with procaspase-8 to create the death-induced signaling complex (DISC) and activate the initiator caspase-8[42]. This leads either directly or indirectly to the activation of downstream caspases involved in executing the final steps of apoptosis[43].

The intrinsic pathway of apoptosis is characterized by mitochondrial outer membrane permeabilization (MOMP) and the loss of mitochondrial membrane potential (MMP), which is considered a 'point of no return' in apoptosis where no antiapoptotic factors can 'rescue' the cell from the induction of apoptosis[44]. The intrinsic pathway is triggered by intracellular stressors such as oxidative stress or DNA damage and involves members of the Bcl-2 family. Upon activation of the intrinsic pathway, the proapoptotic members of the Bcl-2 family, Bax and Bid, translocate to the mitochondria and reduce MMP by disrupting the integrity of the membrane[45-

[47]. There are also antiapoptotic members of the Bcl-2 family, Bcl-2 and Bcl-xL, which can inhibit the actions of the proapoptotic factors on MMP[45].

Although they are distinct pathways, there exist points of crosstalk between the intrinsic and extrinsic pathways, and both pathways can be activated simultaneously by the same stimuli[48]. Eventually, both pathways converge on the activation of 'executioner' caspases -3, -6 and -7, leading to apoptosis[49].

Ceramide and Effectors of Apoptosis

Ceramides have been shown to have important roles in both of these pathways of apoptosis[5,50,51]. The evidence for ceramide's critical role in apoptosis comes from three central observations across many studies. The first is that ceramide accumulates during induction of apoptotic signaling. The second is that the inhibition of this accumulation of ceramide blunts apoptosis. The third is that external delivery of ceramide or stimulation of endogenous ceramide production can induce or enhance apoptosis[6]. Of the three ceramide metabolic pathways, the *de novo* and sphingomyelinase pathways have been implicated more than the salvage pathway[6], although select studies have shown a role for the salvage pathway in inducing apoptosis[52,53]. The generation of ceramides from each of these pathways also follow different temporal patterns, with ceramides generated from SMases being rapid and transient on the order of minutes, and *de novo* generated ceramide over the course of several hours[54-56].

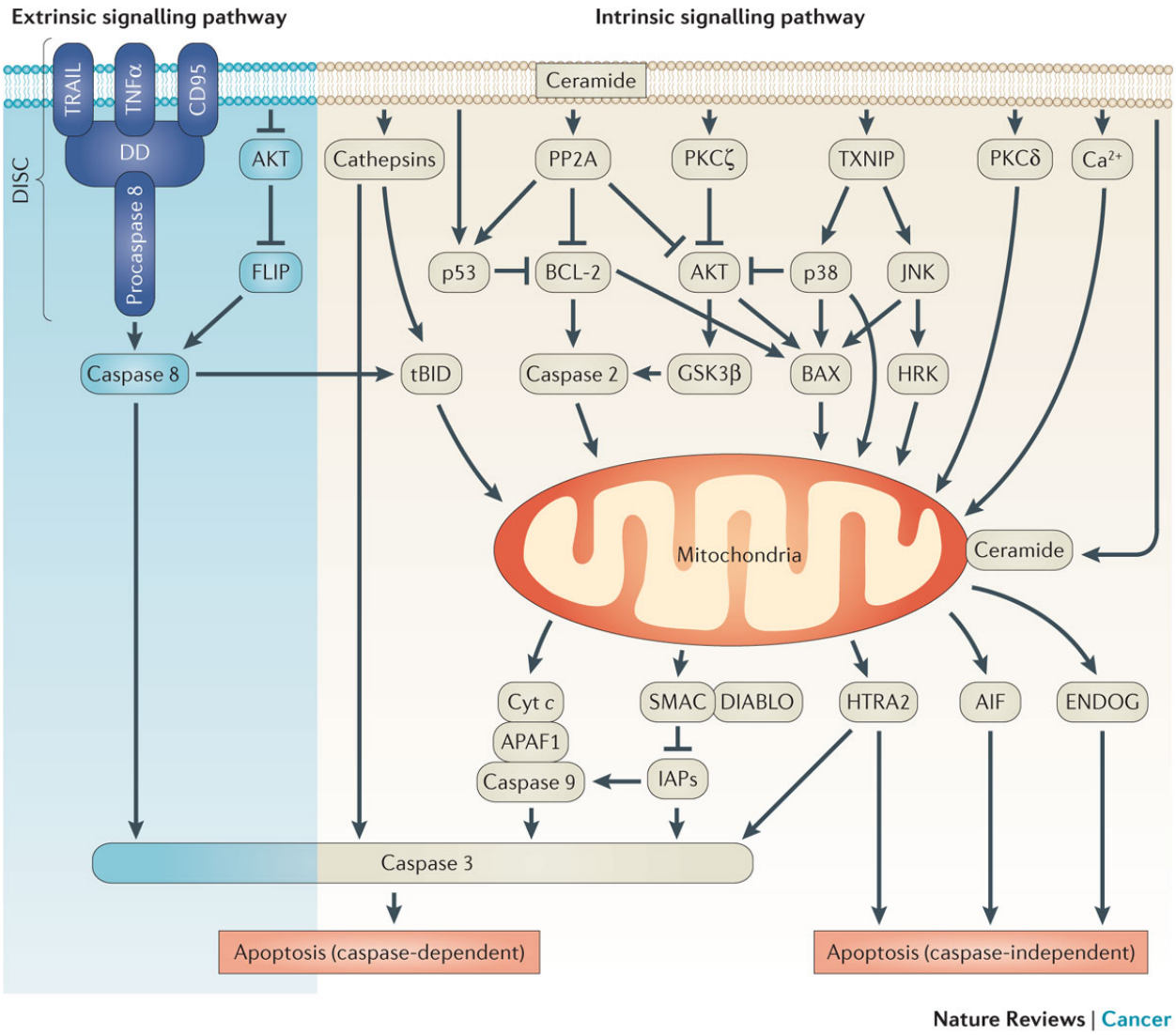

Figure 1.3. By the binding of ligand to cell surface receptors that target the activation of the extrinsic apoptosis pathway, the intracellular death domain (DD), interacts with FAS-associated death domain (FADD). The FADD complex interacts with procaspase 8 to form a death-inducing signalling complex (DISC) that is required for the activation of caspase 8. Subsequently, caspase 8 cleaves BH3-interacting domain death agonist (BID) to form a truncated form, tBID, which is capable of reducing mitochondrial transmembrane potential and activating caspase 3. An endogenous inhibitor of apoptosis, FLICE-inhibitory protein (FLIP), which is caspase-related but which has no protease activity, is thought to function by competing with caspase 8 for binding to the DISC. FLIP is predominantly expressed as long (FLIPL) and short (FLIPS) splice forms. Both FLIP splice forms are recruited to DISCs, preventing the full activation of caspase 8 and thereby inhibiting apoptosis. FLIP has been found to be overexpressed in a number of cancers. The intrinsic mitochondrial pathway of ceramide-induced apoptosis is mainly regulated by caspases and BCL-2 family members. Loss of mitochondrial outer membrane potential subsequently leads to the release of pro-apoptotic proteins: cytochrome c (Cyt c), apoptosis-inducing factor (AIF), second mitochondria-derived activator of caspase (SMAC)–direct

inhibitor of apoptosis protein (IAP)-binding protein with low PI (DIABLO), endonuclease G (ENDOG) and HTRA serine peptidase 2 (HTRA2; also known as OMI), which is the 'engine' that drives the intrinsic ceramide-induced apoptosis pathway. Consequently, mitochondrial apoptosis can be either caspase-dependent or caspase-independent. On release to the cytosol, cytochrome c triggers caspase 3 activation through the formation of what is termed the cytochrome c-apoptotic protease-activating factor 1 (APAF1)–caspase 9-containing apoptosome complex, whereas SMAC–DIABLO triggers caspase 3 activation by blocking IAPs through its amino-terminal IAP-binding motif. Similarly, AIF and ENDOG can be released from the mitochondria on outer mitochondrial membrane permeabilization, and move to the nucleus to promote nuclear chromatin condensation and DNA fragmentation. HTRA2 can promote apoptosis by caspase activation through the neutralization of IAPs or by a caspase-independent path, simply via HTRA2 protease activity. GSK3β, glycogen synthase kinase 3β; HRK, harakiri; JNK, JUN N-terminal kinase; PKC, protein kinase C; PP2A, protein phosphatase 2A; TRAIL, TNF-related apoptosis-inducing ligand; TXNIP, thioredoxin interacting protein. Adapted with permission from "Ceramide-orchestrated signalling in cancer cells." Nature Reviews Cancer (2013) Copyright 2013 Nature Publishing Group.

In the extrinsic pathway, ceramide plays a critical role involving the receptors themselves. Induction of Fas and TRAILR results in ceramide accumulation on the plasma membrane and nucleus (Fig 1.3)[57-59]. Ceramide generated on the plasma membrane from aSMase aggregates into ceramide-rich domains, which are involved in clustering Fas and TRAILR, a required step in receptor-induced apoptosis[60]. They also assist in the formation of the DISC, and in amplifying downstream signaling by the DISC[61-68]. Some studies suggest that Fas-induced apoptosis specifically may be ceramide dependent[69,70]. These effects can be attenuated by the CerS inhibitor fumonisin B1, which was able to protect leukemia cells from Fas-induced apoptosis[59]. Conversely, apoptosis could not be induced in neuroblastoma cells by Fas Ligand alone, depending on the addition of C_2 and C_6 ceramide in order to induce apoptosis[71]. Slightly downstream of Fas, FLICE inhibitory protein (FLIP), which is an inhibitor of caspase-8 and part of the Fas DISC, can be downregulated by ceramide[72-74]. Similarly to Fas signaling, resistance to TRAIL-induced apoptosis also been shown to be linked to low levels of ceramide[74-77]. This has been partially linked to CerS6, where direct knockdown of CerS6 expression also inhibited

TRAIL-induced apoptosis[76]. Similarly, low levels of ceramide has been linked to defects in TNFR induced apoptosis[78,79]. However, there are also data to suggest that ceramide alone is not sufficient for TNF-induced apoptosis[80,81]. There are also data that suggest TNF and ceramide may have distinct pathways[82-84]. The complexity of ceramide and TNF interaction and signaling pathways may also suggest complicated interactions between different steps of signal transduction, as well as signaling that involves both extrinsic and intrinsic pathways of apoptosis[85-88].

In the intrinsic pathway, ceramide plays an important role as a messenger through localization to the mitochondria, the 'center' of the intrinsic pathway (Fig. 1.3). Ceramide-rich platforms in the plasma membrane have the ability to fuse with mitochondria, leading to ceramide accumulation in the mitochondria and eventually to apoptosis in a process sometimes called 'the kiss of death'[89,90]. There also exist ER membranes that are physically joined to mitochondria, so that it is possible for mitochondrial accumulated ceramide to be generated from the *de novo* or salvage pathways and transferred directly without the need for membrane fusion[91]. There have also been some studies pointing to the possibility of ceramide-generating enzymes localizing to mitochondrial membranes and directly synthesizing mitochondrial ceramide directly *in situ*[30,31,92,93].

MOMP, a key event in the intrinsic pathway, can be induced by ceramide through the formation of channels that allow the leakage of small proapoptotic factors such as cytochrome c[94-96]. There is also evidence for a role for Bax in the formation of these channels, where ceramide and Bax work in a synergistic manner rather than through the actions of ceramide alone[97,98]. Ceramide itself can aid in the translocation of Bax from the cytoplasm to the

mitochondria through activation of p38 MAPK or AKT downregulation (Fig. 1.3)[99]. Ceramide can also cause a transient, pH-driven conformational change in Bax[100,101].

AKT, which is associated with pro-survival effects[102], can be downregulated through the upregulation of ceramide accumulation[103]. This downregulation by ceramide may be dependent upon activation by PKCζ[104]. There is also evidence for induction of MOMP through activation of glycogen synthase kinase 3β (GSK3β), cathepsin D, or activation of protein phosphatase 2A (PP2A)[105-108]. These, in turn, activate caspase 2 and 8 to cleave Bid to form tBid which then relocates to the mitochondria[109-111]. PP2A, in particular, is an important mediator of ceramide's induction of apoptosis[112,113]. Protein kinase Cδ (PKCδ) is also involved in ceramide-driven apoptosis through the release of cytochrome c and activation of caspase-9[114]. This ceramide driven release can also be inhibited by the antiapoptotic Bcl-2 through blocking the action of caspase 2[111,115,116].

The MAP kinases p38 and c-Jun N-terminal kinase (JNK), which are involved in several cell functions including apoptosis, have also been shown to be upregulated by ceramide[117-121]. This activation is mediated by thioredoxin interaction protein (TXNIP) through apoptosis signal-regulating kinase, which acts upstream of p38 and JNK[122]. Ceramide is also involved in activating p53, a 'tumor suppressor' which is inactivated or downregulated in many cancers[123-125]. Ceramide can also inhibit the actions of a family of proteins known as inhibitors of apoptosis (IAPs). Ceramide can downregulate or inhibit the actions of the IAP survivin through the expression of Bax and P53[126-129]. Ceramide also promotes the degradation of xIAP and cIAP1 to enhance sensitivity to apoptosis[130].

Dysregulation of Ceramide Metabolism in Apoptosis-Resistant Cancers

Apoptosis is an important part of cancer progression, as resistance to apoptosis is one of the central features of cancer[131-134]. Given the important roles ceramide serves in signaling apoptosis, it comes as no surprise that ceramide metabolism is often altered and impaired in cancer cells. This dysregulation of ceramide metabolism has been shown to impart resistance to chemotherapeutic drugs that normally induce apoptosis, as well as other pro-apoptotic stimuli such as radiation therapy[135-139].

There are key enzymes in metabolic pathways of ceramide that have been shown to play a role in resistant cancers, especially ones that deplete ceramide. One of the most important is glucosylceramide synthase (GCS). GCS and increased glucosylceramide levels have been implicated in several types of resistant cancers, especially breast cancer[140-143]. Accordingly, inhibition of GCS activity has been shown to sensitize resistance cancers to treatment with a number of chemotherapeutic drugs, including doxorubicin and paclitaxel[134,144-146]. Glucosylceramide itself is not necessarily a passive actor in cancer metabolism and may play a role in the metastasis and immune evasion in cancer, as well [147,148]. Ceramidase, another enzyme in the ceramide metabolic pathway which catalyzes the hydrolysis of ceramide into sphingosine and free fatty acid, has also been shown to have increased activity in certain types of resistant cancers, particularly prostate cancer[149-157]. Ceramidase activity produces sphingosine, which can be phosphorylated by sphingosine kinase into sphingosine-1-phosphate, a sphingolipid with many pro-survival effects[7,158]. As with GCS, targeting ceramidase activity is capable of restoring sensitivity to apoptosis[156,159].

Ceramide Delivery

Although the metabolic products of GCS and ceramidase have important biological actions of their own, the central unifying result between them - as well a central unifying feature of many cancers - is the depletion of ceramide levels. Given the importance of ceramide in apoptotic signaling, it is possible that restoring levels of ceramide through exogenous delivery may offer a way to overcome the resistance of certain cancers to treatment. There is much evidence demonstrating that C_2 and C_6 ceramides can reduce resistance to or enhance the sensitivity of chemotherapeutic drugs and other pro-apoptotic stimuli[8,160]. There is also evidence that delivering longer chain ceramides such as C_{16} ceramide can have a similar effect. Delivery of C_{16} ceramide was shown to reverse resistance to radiation in endothelial cells[161]. Furthermore, Fas-resistant hepatocytes from aSMase knockout mice had their sensitivity to Fas-induced apoptosis restored with delivery of C_{16} ceramide[162]. A similar effect was found in CerS-deficient *C. elegans*, with sensitivity to radiation restored upon delivery of C_{16} ceramide[163]. Thus, delivery of exogenous ceramides to cells represents a potential approach to treating resistant cancers. However, there are several challenges associated with ceramide delivery that have thus far limited its clinical application in drug delivery, mostly relating to its lack of solubility in aqueous solution.

Short Chain versus Long Chain Ceramide

Ceramides are often classified into two main categories: short chain and long chain ceramides. As the names imply, this classification is based largely on the length of the fatty acyl chain. Short chain ceramides are synthetic ceramides with a fatty acyl chain length under 12, but most commonly C_6 and C_2[60]. Long chain ceramides refer to ceramides with a fatty acyl chain length anywhere from 12 to 28 carbons, but most commonly of lengths C_{16} to C_{24} ceramide[60].

From a delivery perspective, there are several other differences between short chain and long chain ceramides that further separate the two categories. First, short chain ceramides are generally more directly cytotoxic than long chain ceramides. Second, these cytotoxic effects of short-chain ceramides are relatively uniform across many different types of cells, whereas the effects of long chain ceramides are can be cell specific[6]. Third, short chain ceramides do not require a special delivery system: they can be dissolved in organic solvents such as ethanol or DMSO, added directly to cell media, and enter cells with moderate efficiency. Conversely, long chain ceramides cannot form micelles in aqueous solution, and thus have extremely poor uptake into cells[60]. Fourth, the difficulties in delivering long chain ceramide has led to a majority of studies favoring short-chain ceramides; accordingly, more methods for delivery of short chain ceramides exist.

Despite these difficulties in delivering long chain ceramides, there does exist a 'gold standard' for the study of long chain ceramides: the dodecane-ethanol system. First pioneered by Ji et al. in 1995, this system relies on dissolving long chain ceramides in a 98:2 ethanol:dodecane v:v solution prior to delivery to cells[164]. This system putatively overcomes ceramide's high packing parameter and allows the formation of micelles by introducing dodecane molecules into the structure. Since then it has been used many times to deliver long chain ceramides to cells and further elucidate their functions and cellular effects[161-163]. However, despite being a valuable research tool, it would not be suitable for clinical application except in extremely limited circumstances, necessitating the exploration of other methods.

Liposomes

Liposomes are the most widely studied and applied method for ceramide delivery, as they most closely mimic ceramide's 'home' of cellular membranes. One of the earliest studies of the

therapeutic ceramide liposomes was by Shabbits et al. in 2003, who examined C_6 and C_{16} ceramide liposomes[165]. They found that C_6 ceramide liposomes containing DSPC and cholesterol had good uptake and cytotoxicity, and that the uptake of C_6 ceramide likely occurred due to passive exchange between the cell membrane and the liposome rather than endocytosis of the full liposome. However, they found that liposomes offered no significant advantage in terms of cytotoxicity compared to free C_6 ceramide in solution[165]. They also formulated C_{16} ceramide liposomes with cholesteryl hemisuccinate and found that it initially offered a modest increase in cytotoxicity. When they switched to a cell line that actively endocytoses liposomes, they found a much larger increase in toxicity[165]. Another study by Stover and Kester in the same year used ceramide liposomes containing C_6 ceramide, the lipids DOPC and DOPE, cholesterol, and PEGylated C_8 ceramide were able to induce apoptosis more effectively than free ceramide, demonstrating that the formulation of liposomes can have a strong effect on their efficacy (Fig 1.4)[166].

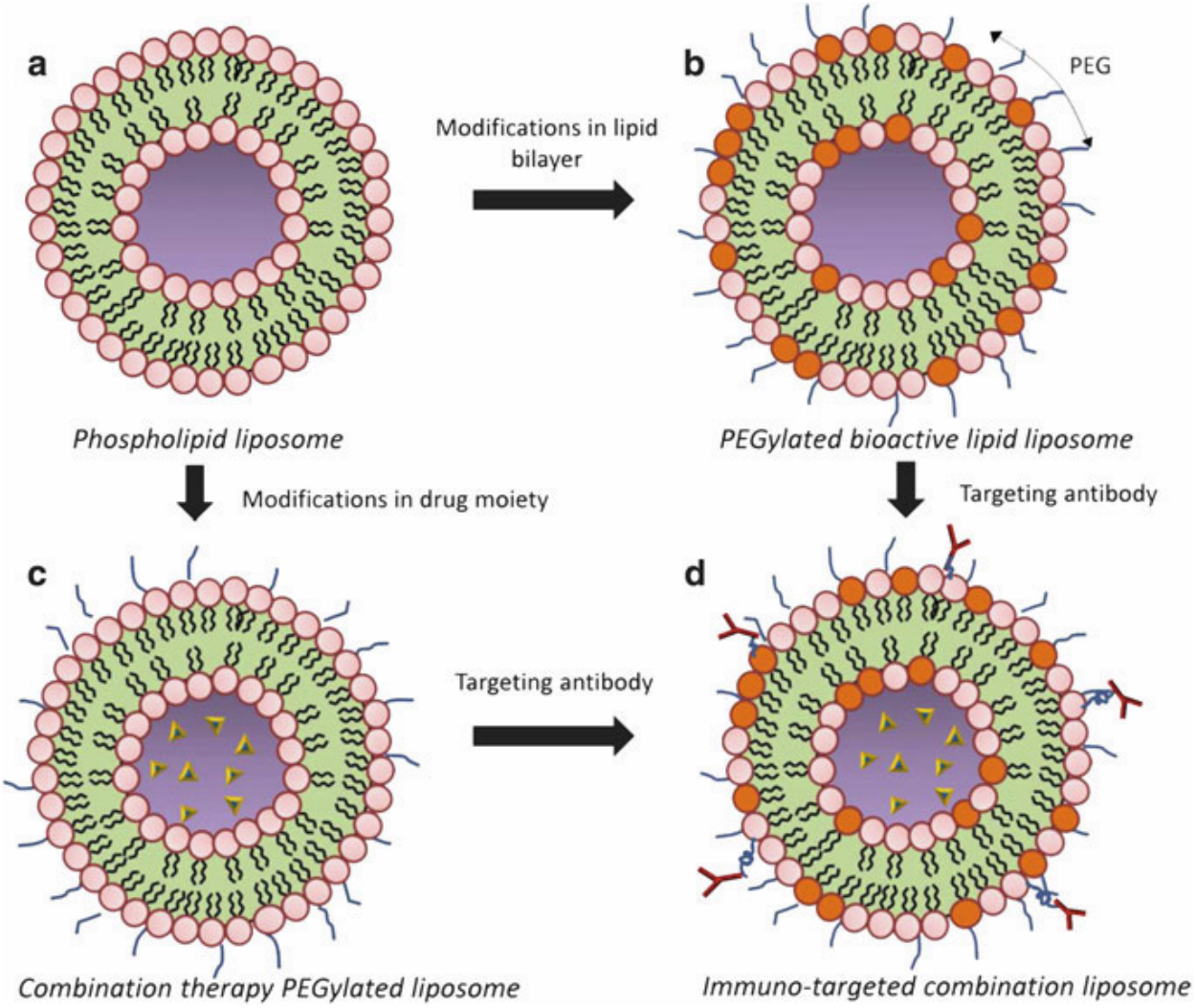

Fig. 1.4. The evolution of the nanoliposome. (a) Liposomes of various lipid mixtures (phospholipids and cholesterol) can be created at the nanoscale, less than 100 nm. (b) Second-generation nanoliposomes can be composed of various concentrations of bioactive lipids, including sphingolipids. (c) In addition, nanoliposomes can be created to contain therapeutic concentrations of active pharmaceutical ingredients (API). Nanoliposomal vehicles for bioactive lipids or APIs can then undergo surface passivation with PEG to increase biological circulation time. (d) In addition, discrete phospholipids can be bio-conjugated with targeting molecules, including antibodies, to create immuno-liposomes for enhanced tissue targeting. Adapted with permission from "The therapeutic potential of nanoscale sphingolipid technologies." Sphingolipids: Basic Science and Drug Development. Springer Vienna, 2013. Copyright Springer Publishing 2013.

Since then there have been many attempts at different formulations, such as liposomes incorporating the GCS inhibitor PDMP[167], the PKC inhibitor safingol[168], transferrin[169], PEGylated C_{16} ceramide[170], and PLGA nanoparticles[171]. There have also been ceramide liposomes encapsulating other drugs such as doxorubicin and curcumin for combinational effects[170,172]. Ceramide liposomes have also been tested *in vivo* in mouse models with substantial success[173-175]. However, the rapid release of ceramide from these liposomes, while beneficial for release into tissues, could also potentially limit the systemic distribution of ceramide[176]. The effect of formulation on liposome distribution is complex, and it remains to be seen if current or future ceramide liposome formulations can find the 'killer' combination of different elements that will pass clinical trials and translate into an effective cancer treatment.

Other Ceramide Delivery Systems

Liposomes have dominated the effort for the therapeutic applications of ceramides, but there have been other efforts that hold promise as delivery systems for ceramides. One such method is the loading of calcium phosphosilicate nanoparticles (CPSNPs) with C_6 or C_{10} ceramide, which showed potent inhibitory effects on cell growth *in vitro*[177,178]. There has also been success using polyethyleneoxide-modified-polyepsilon-caprolactone (PEO-PCL) nanoparticles with C_6 ceramide in combination with paclitaxel and tamoxifen to overcome multi-drug resistant cancers[179-181]. For sustained release, thermally activated linear-dendritic nanoparticles were able to deliver C_6 ceramide to MDA-MB-231 cells over the course of one month[182]. Perhaps most interesting is the use of carbon nanotubes as a delivery system for C_6 ceramide, which could be aligned and ceramide then drawn into the center, and then released *in situ* using inductive heating for a 'trojan horse' style of drug delivery[183]. All these of these methods have potential for the therapeutic delivery of ceramide, but are still in the early stages of

development. Furthermore, they all deal with the delivery of short chain ceramides in favor of longer chain ceramides, leaving an empty niche for the development of a delivery system for long chain ceramides that also has applications for short chain ceramides.

Graphene Oxide, Drug Delivery, and Lipid Interactions

Graphene oxide (GO) is a two-dimensional nanoparticle composed largely of carbon in a sp^2 arrangement but with introduced 'defects' of moieties containing hydrogen and oxygen[184]. GO is usually synthesized from pure carbon precursors such as graphite or carbon nanotubes (CNTs), using concentrated acids to introduce these defects, yielding oxidized graphene nanoplatelets (GNPs) and oxidized graphene nanoribbons (O-GNRs), respectively[185,186]. Whereas 'pristine' graphene is extremely hydrophobic, GO has appreciable dispersibility in aqueous solution while also retaining regions of hydrophobicity[184]. This status as a 'hybrid' of hydrophilic and hydrophobic regions - i.e. a surfactant - has previously been exploited to impart water solubility to hydrophobic anticancer drugs such as doxorubicin, paclitaxel, camptothecin and tamoxifen, and enhance their toxicity to cancer cells[187-191]. Furthermore, O-GNRs derived from multiwalled CNTs (MWCNTs) have been shown to have a cell-specific uptake by activating epidermal growth factor receptor (EGFR), which is overexpressed in many types of cancers[192-194]. Given these properties of GO nanoparticles and O-GNRs specifically, they could potentially serve as an excellent delivery system for ceramides (Fig. 1.5.). However, previous loading of hydrophobic anticancer drugs has exploited a phenomenon known as 'pi-stacking' which allows for a non-covalent reversible interaction between the aromatic structure of these anticancer drugs and GO[188]. The long aliphatic tails of ceramide's fatty acid moieties would not necessarily be able to interact in the same way.

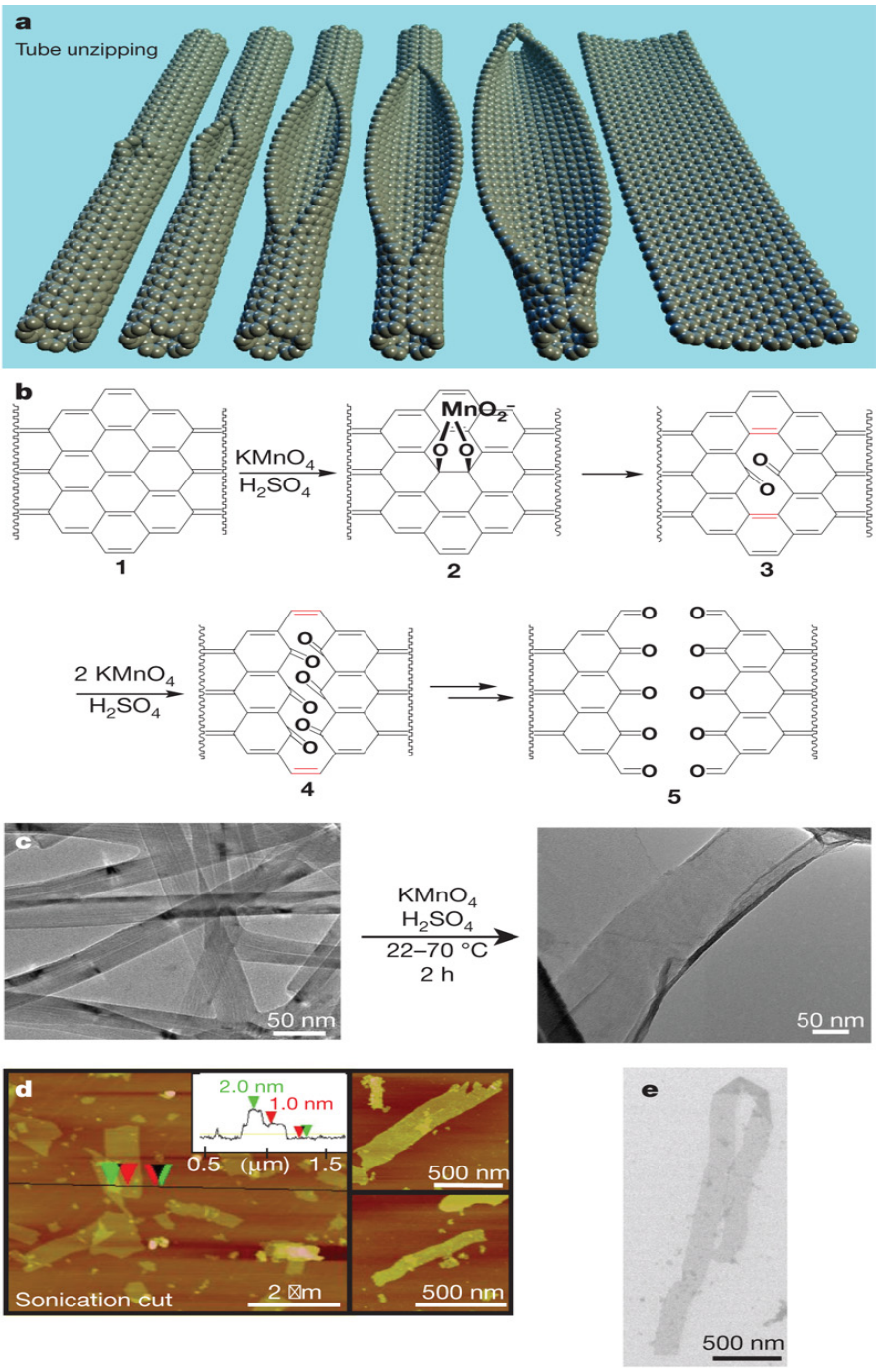

Figure 1.5 a, Representation of the gradual unzipping of one wall of a carbon nanotube to form a nanoribbon. Oxygenated sites are not shown. **b**, The proposed chemical mechanism of nanotube unzipping. The manganate ester in 2 could also be protonated. **c**, TEM images depicting the transformation of MWCNTs (left) into oxidized nanoribbons (right). The right-hand side of the ribbon is partly folded onto itself. The dark structures are part of the carbon imaging grid. **d**,

AFM images of partly stacked multiple short fragments of nanoribbons that were horizontally cut by tip-ultrasonic treatment of the original oxidation product to facilitate spin-casting onto the mica surface. The height data (inset) indicates that the ribbons are generally single layered. The two small images on the right show some other characteristic nanoribbons. **e**, SEM image of a folded, 4-mum-long single-layer nanoribbon on a silicon surface. Adapted with permission from "Longitudinal unzipping of carbon nanotubes to form graphene nanoribbons." Nature (2009) Copyright 2009 Nature Publishing Group.

There have been some studies that have examined the interactions between GO and lipids. However, the majority of these studies have been focused on lipids as intact membranes in the form of supported lipid bilayers (SLBs). The goals of these studies have focused largely around recreating cell membranes for examining the properties of proteins or other membrane-bound molecules, or for studying the interactions between graphene oxide and cell membranes or liposomes, often requiring composite materials and/or immobilized surfaces[195-200]. Even then, a review of the literature reveals no studies at all between GO and sphingolipids or ceramides. However, the use of 1,2-distearoyl-sn-glycero-3-phosphoethanolamine (DSPE) conjugated to PEG may provide an answer for the development of GO as a delivery system for ceramide. DSPE-PEG is a surfactant that has previously been used to impart additional water dispersibility to GO nanoparticles[192,193,201]. The DSPE moiety is a lipid which lays across the hydrophobic parts of graphene and is held in place by hydrophobic interactions, while the PEG moiety is hydrophilic and imparts additional water solubility to GO. A loading method which takes advantage of these hydrophobic interactions could load ceramide onto GO nanoparticles without the need for immobilization of the particles or the need to pre-form liposomes or liposomal layers.

Conclusions

Ceramide is a unique sphingolipid with many interesting and complicated biological properties and effects on cellular metabolism. Its importance in apoptotic signaling and cancer

biology makes it a desirable target for therapeutic delivery. While there is much that remains to be understood of ceramide's many signaling functions, the main limitation in developing therapeutic applications has been in delivery systems for ceramide. The methods for delivery of ceramide have made considerable advances in recent years, but these advances have thus far failed to translate into clinical applications. Furthermore, the short chain ceramides have been the focus of these innovations in delivery, while long chain ceramides have been neglected despite many promising applications. The current state of the field for ceramide delivery leaves much room for improvement. Graphene oxide nanoparticles have many properties that are favorable for the loading of delivery of ceramide, and can be used in this regard given a loading method that can overcome the challenges in working with ceramide.

The work presented in this thesis details such a method and its application in delivering ceramide to cells. Chapter 2 describes the development of the loading method and the challenges presented there. Chapter 3 describes the application of this method in the delivery of the short-chain C_6 ceramide to HeLa and other cell lines using oxidized graphene nanoribbons (O-GNRs). Chapter 4 describes an interesting property of graphene oxide to buffer ROS and prevent ultraviolet radiation-induced apoptosis in cells, and what challenges that may present for combinational treatment of radiation and ceramide treatment. Chapter 5 describes the delivery of long chain ceramides C_{16} and C_{24} to HeLa cells in combination with ultraviolet radiation or C_6 ceramide treatment, and the potential obstacles that O-GNRs may present in therapeutic delivery of these long-chain ceramides. Chapter 6 concludes the research and explores future directions for the research at hand and the field of ceramide delivery at large.

References

1 Gault, C. R., Obeid, L. M. & Hannun, Y. A. An overview of sphingolipid metabolism: from synthesis to breakdown. *Advances in experimental medicine and biology* **688**, 1-23 (2010).

2 Hla, T. & Dannenberg, Andrew J. Sphingolipid Signaling in Metabolic Disorders. *Cell Metabolism* **16**, 420-434, doi:10.1016/j.cmet.2012.06.017.

3 Harnett, M. M. in *Cell Signaling in Vascular Inflammation* (ed Jahar Bhattacharya) 91-101 (Humana Press, 2005).

4 Li, Y. *et al.* The pleiotropic roles of sphingolipid signaling in autophagy. *Cell death & disease* **5**, e1245, doi:10.1038/cddis.2014.215 (2014).

5 Smyth, M. J., Obeid, L. M. & Hannun, Y. A. Ceramide: a novel lipid mediator of apoptosis. *Advances in pharmacology (San Diego, Calif.)* **41**, 133-154 (1997).

6 Mullen, T. D. & Obeid, L. M. Ceramide and apoptosis: exploring the enigmatic connections between sphingolipid metabolism and programmed cell death. *Anti-cancer agents in medicinal chemistry* **12**, 340-363 (2012).

7 Espaillat, M. P., Shamseddine, A. A., Adada, M. M., Hannun, Y. A. & Obeid, L. M. Ceramide and sphingosine-1-phosphate in cancer, two faces of the sphinx. *Translational Cancer Research* **4**, 484-499 (2015).

8 Morad, S. A. & Cabot, M. C. Ceramide-orchestrated signalling in cancer cells. *Nature reviews. Cancer* **13**, 51-65, doi:10.1038/nrc3398 (2013).

9 Siegel, R. L., Miller, K. D. & Jemal, A. Cancer statistics, 2016. *CA: A Cancer Journal for Clinicians* **66**, 7-30, doi:10.3322/caac.21332 (2016).

10 Braun, P. E. & Snell, E. E. Biosynthesis of Sphingolipid Bases: II. KETO INTERMEDIATES IN SYNTHESIS OF SPHINGOSINE AND DIHYDROSPHINGOSINE BY CELL-FREE EXTRACTS OF HANSENULA CIFERRI. *Journal of Biological Chemistry* **243**, 3775-3783 (1968).

11 Merrill, A. H., Jr. Characterization of serine palmitoyltransferase activity in Chinese hamster ovary cells. *Biochimica et biophysica acta* **754**, 284-291 (1983).

12 Hanada, K. Serine palmitoyltransferase, a key enzyme of sphingolipid metabolism. *Biochimica et biophysica acta* **1632**, 16-30 (2003).

13 Braun, P. E., Morell, P. & Radin, N. S. Synthesis of C18- and C20-Dihydrosphingosines, Ketodihydrosphingosines, and Ceramides by Microsomal Preparations from Mouse Brain. *Journal of Biological Chemistry* **245**, 335-341 (1970).

14 Venkataraman, K. *et al.* Upstream of growth and differentiation factor 1 (uog1), a mammalian homolog of the yeast longevity assurance gene 1 (LAG1), regulates N-stearoyl-sphinganine (C18-(dihydro)ceramide) synthesis in a fumonisin B1-independent manner in mammalian cells. *The Journal of biological chemistry* **277**, 35642-35649, doi:10.1074/jbc.M205211200 (2002).

15 Mizutani, Y., Kihara, A. & Igarashi, Y. Mammalian Lass6 and its related family members regulate synthesis of specific ceramides. *Biochem J* **390**, 263-271, doi:10.1042/bj20050291 (2005).

16 Spassieva, S. *et al.* Necessary role for the Lag1p motif in (dihydro)ceramide synthase activity. *The Journal of biological chemistry* **281**, 33931-33938, doi:10.1074/jbc.M608092200 (2006).

17 Guillas, I. *et al.* Human homologues of LAG1 reconstitute Acyl-CoA-dependent ceramide synthesis in yeast. *The Journal of biological chemistry* **278**, 37083-37091, doi:10.1074/jbc.M307554200 (2003).

18 Laviad, E. L. *et al.* Characterization of ceramide synthase 2: tissue distribution, substrate specificity, and inhibition by sphingosine 1-phosphate. *The Journal of biological chemistry* **283**, 5677-5684, doi:10.1074/jbc.M707386200 (2008).

19 Mizutani, Y., Kihara, A. & Igarashi, Y. LASS3 (longevity assurance homologue 3) is a mainly testis-specific (dihydro)ceramide synthase with relatively broad substrate specificity. *Biochem J* **398**, 531-538, doi:10.1042/bj20060379 (2006).

20 Riebeling, C., Allegood, J. C., Wang, E., Merrill, A. H., Jr. & Futerman, A. H. Two mammalian longevity assurance gene (LAG1) family members, trh1 and trh4, regulate dihydroceramide synthesis using different fatty acyl-CoA donors. *The Journal of biological chemistry* **278**, 43452-43459, doi:10.1074/jbc.M307104200 (2003).

21 Lahiri, S. & Futerman, A. H. LASS5 is a bona fide dihydroceramide synthase that selectively utilizes palmitoyl-CoA as acyl donor. *The Journal of biological chemistry* **280**, 33735-33738, doi:10.1074/jbc.M506485200 (2005).

22 Ternes, P., Franke, S., Zahringer, U., Sperling, P. & Heinz, E. Identification and characterization of a sphingolipid delta 4-desaturase family. *The Journal of biological chemistry* **277**, 25512-25518, doi:10.1074/jbc.M202947200 (2002).

23 Geeraert, L., Mannaerts, G. P. & van Veldhoven, P. P. Conversion of dihydroceramide into ceramide: involvement of a desaturase. *Biochem J* **327**, 125-132 (1997).

24 Mandon, E. C., Ehses, I., Rother, J., van Echten, G. & Sandhoff, K. Subcellular localization and membrane topology of serine palmitoyltransferase, 3-

dehydrosphinganine reductase, and sphinganine N-acyltransferase in mouse liver. *The Journal of biological chemistry* **267**, 11144-11148 (1992).

25 Ullman, M. D. & Radin, N. S. The enzymatic formation of sphingomyelin from ceramide and lecithin in mouse liver. *The Journal of biological chemistry* **249**, 1506-1512 (1974).

26 Huitema, K., van den Dikkenberg, J., Brouwers, J. F. & Holthuis, J. C. Identification of a family of animal sphingomyelin synthases. *Embo j* **23**, 33-44, doi:10.1038/sj.emboj.7600034 (2004).

27 Smith, E. L. & Schuchman, E. H. The unexpected role of acid sphingomyelinase in cell death and the pathophysiology of common diseases. *FASEB journal : official publication of the Federation of American Societies for Experimental Biology* **22**, 3419-3431, doi:10.1096/fj.08-108043 (2008).

28 Strub, G. M., Maceyka, M., Hait, N. C., Milstien, S. & Spiegel, S. Extracellular and Intracellular Actions of Sphingosine-1-Phosphate. *Advances in experimental medicine and biology* **688**, 141-155 (2010).

29 Mizutani, Y. *et al.* Nuclear localization of neutral sphingomyelinase 1: biochemical and immunocytochemical analyses. *Journal of cell science* **114**, 3727-3736 (2001).

30 Novgorodov, S. A. *et al.* Novel pathway of ceramide production in mitochondria: thioesterase and neutral ceramidase produce ceramide from sphingosine and acyl-CoA. *The Journal of biological chemistry* **286**, 25352-25362, doi:10.1074/jbc.M110.214866 (2011).

31 Wu, B. X., Rajagopalan, V., Roddy, P. L., Clarke, C. J. & Hannun, Y. A. Identification and characterization of murine mitochondria-associated neutral sphingomyelinase (MA-

nSMase), the mammalian sphingomyelin phosphodiesterase 5. *The Journal of biological chemistry* **285**, 17993-18002, doi:10.1074/jbc.M110.102988 (2010).

32 Rajagopalan, V. *et al.* Critical determinants of mitochondria-associated neutral sphingomyelinase (MA-nSMase) for mitochondrial localization. *Biochimica et biophysica acta* **1850**, 628-639, doi:10.1016/j.bbagen.2014.11.019 (2015).

33 Krut, O., Wiegmann, K., Kashkar, H., Yazdanpanah, B. & Kronke, M. Novel tumor necrosis factor-responsive mammalian neutral sphingomyelinase-3 is a C-tail-anchored protein. *The Journal of biological chemistry* **281**, 13784-13793, doi:10.1074/jbc.M511306200 (2006).

34 Duan, R. D. Alkaline sphingomyelinase: an old enzyme with novel implications. *Biochimica et biophysica acta* **1761**, 281-291, doi:10.1016/j.bbalip.2006.03.007 (2006).

35 D/'Angelo, G. *et al.* Glycosphingolipid synthesis requires FAPP2 transfer of glucosylceramide. *Nature* **449**, 62-67, doi:http://www.nature.com/nature/journal/v449/n7158/suppinfo/nature06097_S1.html (2007).

36 Schulze, H., Kolter, T. & Sandhoff, K. Principles of lysosomal membrane degradation: Cellular topology and biochemistry of lysosomal lipid degradation. *Biochimica et biophysica acta* **1793**, 674-683, doi:10.1016/j.bbamcr.2008.09.020 (2009).

37 Smith, E. R. & Merrill, A. H., Jr. Differential roles of de novo sphingolipid biosynthesis and turnover in the "burst" of free sphingosine and sphinganine, and their 1-phosphates and N-acyl-derivatives, that occurs upon changing the medium of cells in culture. *The Journal of biological chemistry* **270**, 18749-18758 (1995).

38 Jin, Z. & El-Deiry, W. S. Overview of cell death signaling pathways. *Cancer biology & therapy* **4**, 139-163 (2005).

39 Dhein, J., Walczak, H., Baumler, C., Debatin, K. M. & Krammer, P. H. Autocrine T-cell suicide mediated by APO-1/(Fas/CD95). *Nature* **373**, 438-441, doi:10.1038/373438a0 (1995).

40 Tartaglia, L. A., Rothe, M., Hu, Y. F. & Goeddel, D. V. Tumor necrosis factor's cytotoxic activity is signaled by the p55 TNF receptor. *Cell* **73**, 213-216 (1993).

41 Pan, G. *et al.* The receptor for the cytotoxic ligand TRAIL. *Science* **276**, 111-113 (1997).

42 Ashkenazi, A. & Dixit, V. M. Death receptors: signaling and modulation. *Science* **281**, 1305-1308 (1998).

43 Barnhart, B. C., Alappat, E. C. & Peter, M. E. The CD95 type I/type II model. *Seminars in immunology* **15**, 185-193 (2003).

44 Chipuk, J. E., Bouchier-Hayes, L. & Green, D. R. Mitochondrial outer membrane permeabilization during apoptosis: the innocent bystander scenario. *Cell Death Differ* **13**, 1396-1402 (2006).

45 Reed, J. C. in *Apoptosis and Cancer Chemotherapy* (eds John A. Hickman & Caroline Dive) 99-116 (Humana Press, 1999).

46 Luo, X., Budihardjo, I., Zou, H., Slaughter, C. & Wang, X. Bid, a Bcl2 interacting protein, mediates cytochrome c release from mitochondria in response to activation of cell surface death receptors. *Cell* **94**, 481-490 (1998).

47 Zamzami, N. *et al.* Bid acts on the permeability transition pore complex to induce apoptosis. *Oncogene* **19**, 6342-6350 (2000).

48 Goc, A. *et al.* Simultaneous modulation of the intrinsic and extrinsic pathways by simvastatin in mediating prostate cancer cell apoptosis. *BMC cancer* **12**, 409, doi:10.1186/1471-2407-12-409 (2012).

49 McIlwain, D. R., Berger, T. & Mak, T. W. Caspase functions in cell death and disease. *Cold Spring Harbor perspectives in biology* **5**, a008656, doi:10.1101/cshperspect.a008656 (2013).

50 Morales, A., Lee, H., Goni, F. M., Kolesnick, R. & Fernandez-Checa, J. C. Sphingolipids and cell death. *Apoptosis : an international journal on programmed cell death* **12**, 923-939, doi:10.1007/s10495-007-0721-0 (2007).

51 Pettus, B. J., Chalfant, C. E. & Hannun, Y. A. Ceramide in apoptosis: an overview and current perspectives. *Biochimica et biophysica acta* **1585**, 114-125 (2002).

52 Takeda, S., Mitsutake, S., Tsuji, K. & Igarashi, Y. Apoptosis occurs via the ceramide recycling pathway in human HaCaT keratinocytes. *Journal of biochemistry* **139**, 255-262, doi:10.1093/jb/mvj026 (2006).

53 Cuvillier, O. *et al.* Sphingosine generation, cytochrome c release, and activation of caspase-7 in doxorubicin-induced apoptosis of MCF7 breast adenocarcinoma cells. *Cell Death Differ* **8**, 162-171, doi:10.1038/sj.cdd.4400793 (2001).

54 Adam, D., Wiegmann, K., Adam-Klages, S., Ruff, A. & Kronke, M. A novel cytoplasmic domain of the p55 tumor necrosis factor receptor initiates the neutral sphingomyelinase pathway. *The Journal of biological chemistry* **271**, 14617-14622 (1996).

55 Brenner, B. *et al.* Fas/CD95/Apo-I activates the acidic sphingomyelinase via caspases. *Cell Death Differ* **5**, 29-37, doi:10.1038/sj.cdd.4400307 (1998).

56 Vit, J. P. & Rosselli, F. Role of the ceramide-signaling pathways in ionizing radiation-induced apoptosis. *Oncogene* **22**, 8645-8652, doi:10.1038/sj.onc.1207087 (2003).

57 Park, M. A. *et al.* Vorinostat and sorafenib increase CD95 activation in gastrointestinal tumor cells through a Ca(2+)-de novo ceramide-PP2A-reactive oxygen species-dependent signaling pathway. *Cancer research* **70**, 6313-6324, doi:10.1158/0008-5472.can-10-0999 (2010).

58 Park, M. A. *et al.* Vorinostat and sorafenib increase ER stress, autophagy and apoptosis via ceramide-dependent CD95 and PERK activation. *Cancer biology & therapy* **7**, 1648-1662 (2008).

59 Huang, S. T., Yang, R. C., Chen, M. Y. & Pang, J. H. Phyllanthus urinaria induces the Fas receptor/ligand expression and ceramide-mediated apoptosis in HL-60 cells. *Life sciences* **75**, 339-351, doi:10.1016/j.lfs.2003.12.013 (2004).

60 Stancevic, B. & Kolesnick, R. Ceramide-rich platforms in transmembrane signaling. *FEBS letters* **584**, 1728-1740, doi:10.1016/j.febslet.2010.02.026 (2010).

61 Dumitru, C. A. & Gulbins, E. TRAIL activates acid sphingomyelinase via a redox mechanism and releases ceramide to trigger apoptosis. *Oncogene* **25**, 5612-5625, doi:10.1038/sj.onc.1209568 (2006).

62 Miyaji, M. *et al.* Role of membrane sphingomyelin and ceramide in platform formation for Fas-mediated apoptosis. *The Journal of experimental medicine* **202**, 249-259, doi:10.1084/jem.20041685 (2005).

63 Grassme, H. *et al.* CD95 signaling via ceramide-rich membrane rafts. *The Journal of biological chemistry* **276**, 20589-20596, doi:10.1074/jbc.M101207200 (2001).

64 Cremesti, A. *et al.* Ceramide enables fas to cap and kill. *The Journal of biological chemistry* **276**, 23954-23961, doi:10.1074/jbc.M101866200 (2001).

65 Dumitru, C. A., Carpinteiro, A., Trarbach, T., Hengge, U. R. & Gulbins, E. Doxorubicin enhances TRAIL-induced cell death via ceramide-enriched membrane platforms. *Apoptosis : an international journal on programmed cell death* **12**, 1533-1541, doi:10.1007/s10495-007-0081-9 (2007).

66 Min, Y. *et al.* Death receptor 5-recruited raft components contributes to the sensitivity of Jurkat leukemia cell lines to TRAIL-induced cell death. *IUBMB life* **61**, 261-267, doi:10.1002/iub.166 (2009).

67 Grassme, H., Schwarz, H. & Gulbins, E. Molecular mechanisms of ceramide-mediated CD95 clustering. *Biochemical and biophysical research communications* **284**, 1016-1030, doi:10.1006/bbrc.2001.5045 (2001).

68 Grassme, H., Cremesti, A., Kolesnick, R. & Gulbins, E. Ceramide-mediated clustering is required for CD95-DISC formation. *Oncogene* **22**, 5457-5470, doi:10.1038/sj.onc.1206540 (2003).

69 Herr, I., Wilhelm, D., Böhler, T., Angel, P. & Debatin, K. M. Activation of CD95 (APO-1/Fas) signaling by ceramide mediates cancer therapy-induced apoptosis. *The EMBO Journal* **16**, 6200-6208, doi:10.1093/emboj/16.20.6200 (1997).

70 Wagenknecht, B., Roth, W., Gulbins, E., Wolburg, H. & Weller, M. C2-ceramide signaling in glioma cells: synergistic enhancement of CD95-mediated, caspase-dependent apoptosis. *Cell Death Differ* **8**, 595-602, doi:10.1038/sj.cdd.4400848 (2001).

71 Schaefer, J. T., Barthlen, W. & Schweizer, P. Ceramide induces apoptosis in neuroblastoma cell cultures resistant to CD95 (Fas/APO-1)-mediated apoptosis. *Journal of pediatric surgery* **35**, 473-479 (2000).

72 Yoon, G. *et al.* Ceramide increases Fas-mediated apoptosis in glioblastoma cells through FLIP down-regulation. *Journal of neuro-oncology* **60**, 135-141 (2002).

73 Nam, S. Y., Amoscato, A. A. & Lee, Y. J. Low glucose-enhanced TRAIL cytotoxicity is mediated through the ceramide-Akt-FLIP pathway. *Oncogene* **21**, 337-346, doi:10.1038/sj.onc.1205068 (2002).

74 Asakuma, J., Sumitomo, M., Asano, T., Asano, T. & Hayakawa, M. Selective Akt inactivation and tumor necrosis actor-related apoptosis-inducing ligand sensitization of renal cancer cells by low concentrations of paclitaxel. *Cancer research* **63**, 1365-1370 (2003).

75 Zhang, Y., Yoshida, T. & Zhang, B. TRAIL induces endocytosis of its death receptors in MDA-MB-231 breast cancer cells. *Cancer biology & therapy* **8**, 917-922 (2009).

76 White-Gilbertson, S. *et al.* Ceramide synthase 6 modulates TRAIL sensitivity and nuclear translocation of active caspase 3 in colon cancer cells. *Oncogene* **28**, 1132-1141, doi:10.1038/onc.2008.468 (2009).

77 Voelkel-Johnson, C., Hannun, Y. A. & El-Zawahry, A. Resistance to TRAIL is associated with defects in ceramide signaling that can be overcome by exogenous C6-ceramide without requiring down-regulation of cellular FLICE inhibitory protein. *Molecular cancer therapeutics* **4**, 1320-1327, doi:10.1158/1535-7163.mct-05-0086 (2005).

78 Colell, A., Morales, A., Fernandez-Checa, J. C. & Garcia-Ruiz, C. Ceramide generated by acidic sphingomyelinase contributes to tumor necrosis factor-alpha-mediated apoptosis in human colon HT-29 cells through glycosphingolipids formation. Possible role of ganglioside GD3. *FEBS letters* **526**, 135-141 (2002).

79 Cai, Z. *et al.* Alteration of the sphingomyelin/ceramide pathway is associated with resistance of human breast carcinoma MCF7 cells to tumor necrosis factor-alpha-mediated cytotoxicity. *The Journal of biological chemistry* **272**, 6918-6926 (1997).

80 Higuchi, M., Singh, S., Jaffrezou, J. P. & Aggarwal, B. B. Acidic sphingomyelinase-generated ceramide is needed but not sufficient for TNF-induced apoptosis and nuclear factor-kappa B activation. *Journal of immunology (Baltimore, Md. : 1950)* **157**, 297-304 (1996).

81 Kuroki, J. *et al.* Cell-permeable ceramide inhibits the growth of B lymphoma Raji cells lacking TNF-alpha-receptors by inducing G0/G1 arrest but not apoptosis: a new model for dissecting cell-cycle arrest and apoptosis. *Leukemia* **10**, 1950-1958 (1996).

82 Donato, N. J. & Klostergaard, J. Distinct stress and cell destruction pathways are engaged by TNF and ceramide during apoptosis of MCF-7 cells. *Experimental cell research* **294**, 523-533, doi:10.1016/j.yexcr.2003.11.021 (2004).

83 Guo, Y. L., Kang, B., Yang, L. J. & Williamson, J. R. Tumor necrosis factor-alpha and ceramide induce cell death through different mechanisms in rat mesangial cells. *The American journal of physiology* **276**, F390-397 (1999).

84 Karasavvas, N. & Zakeri, Z. Relationships of apoptotic signaling mediated by ceramide and TNF-alpha in U937 cells. *Cell Death Differ* **6**, 115-123, doi:10.1038/sj.cdd.4400482 (1999).

85 Kimura, K., Markowski, M., Edsall, L. C., Spiegel, S. & Gelmann, E. P. Role of ceramide in mediating apoptosis of irradiated LNCaP prostate cancer cells. *Cell Death Differ* **10**, 240-248, doi:10.1038/sj.cdd.4401145 (2003).

86 Goswami, R., Kilkus, J., Scurlock, B. & Dawson, G. CrmA protects against apoptosis and ceramide formation in PC12 cells. *Neurochemical research* **27**, 735-741 (2002).

87 De Nadai, C. *et al.* Nitric oxide inhibits tumor necrosis factor-alpha-induced apoptosis by reducing the generation of ceramide. *Proceedings of the National Academy of Sciences of the United States of America* **97**, 5480-5485, doi:10.1073/pnas.070062397 (2000).

88 Sawada, M. *et al.* Molecular mechanisms of TNF-alpha-induced ceramide formation in human glioma cells: P53-mediated oxidant stress-dependent and -independent pathways. *Cell Death Differ* **11**, 997-1008, doi:10.1038/sj.cdd.4401438 (2004).

89 Babiychuk, E. B. *et al.* The targeting of plasmalemmal ceramide to mitochondria during apoptosis. *PloS one* **6**, e23706, doi:10.1371/journal.pone.0023706 (2011).

90 Babiychuk, E. B., Monastyrskaya, K. & Draeger, A. Fluorescent annexin A1 reveals dynamics of ceramide platforms in living cells. *Traffic (Copenhagen, Denmark)* **9**, 1757-1775, doi:10.1111/j.1600-0854.2008.00800.x (2008).

91 Stiban, J., Caputo, L. & Colombini, M. Ceramide synthesis in the endoplasmic reticulum can permeabilize mitochondria to proapoptotic proteins. *Journal of lipid research* **49**, 625-634, doi:10.1194/jlr.M700480-JLR200 (2008).

92 Bionda, C., Portoukalian, J., Schmitt, D., Rodriguez-Lafrasse, C. & Ardail, D. Subcellular compartmentalization of ceramide metabolism: MAM (mitochondria-associated membrane) and/or mitochondria? *Biochem J* **382**, 527-533, doi:10.1042/bj20031819 (2004).

93 Birbes, H., El Bawab, S., Hannun, Y. A. & Obeid, L. M. Selective hydrolysis of a mitochondrial pool of sphingomyelin induces apoptosis. *FASEB journal : official publication of the Federation of American Societies for Experimental Biology* **15**, 2669-2679, doi:10.1096/fj.01-0539com (2001).

94 Siskind, L. J., Kolesnick, R. N. & Colombini, M. Ceramide channels increase the permeability of the mitochondrial outer membrane to small proteins. *The Journal of biological chemistry* **277**, 26796-26803, doi:10.1074/jbc.M200754200 (2002).

95 Siskind, L. J., Kolesnick, R. N. & Colombini, M. Ceramide forms channels in mitochondrial outer membranes at physiologically relevant concentrations. *Mitochondrion* **6**, 118-125, doi:10.1016/j.mito.2006.03.002 (2006).

96 Siskind, L. J. & Colombini, M. The lipids C2- and C16-ceramide form large stable channels. Implications for apoptosis. *The Journal of biological chemistry* **275**, 38640-38644, doi:10.1074/jbc.C000587200 (2000).

97 Lee, H. *et al.* Mitochondrial ceramide-rich macrodomains functionalize Bax upon irradiation. *PloS one* **6**, e19783, doi:10.1371/journal.pone.0019783 (2011).

98 Martinez-Abundis, E., Correa, F., Pavon, N. & Zazueta, C. Bax distribution into mitochondrial detergent-resistant microdomains is related to ceramide and cholesterol content in postischemic hearts. *The FEBS journal* **276**, 5579-5588, doi:10.1111/j.1742-4658.2009.07239.x (2009).

99 Kong, J. Y., Klassen, S. S. & Rabkin, S. W. Ceramide activates a mitochondrial p38 mitogen-activated protein kinase: A potential mechanism for loss of mitochondrial transmembrane potential and apoptosis. *Molecular and Cellular Biochemistry* **278**, 39-51, doi:10.1007/s11010-005-1979-6 (2005).

100 Belaud-Rotureau, M. A. *et al.* Early transitory rise in intracellular pH leads to Bax conformation change during ceramide-induced apoptosis. *Apoptosis : an international journal on programmed cell death* **5**, 551-560, doi:10.1023/a:1009693630664 (2000).

101 Kim, H. J., Oh, J. E., Kim, S. W., Chun, Y. J. & Kim, M. Y. Ceramide induces p38 MAPK-dependent apoptosis and Bax translocation via inhibition of Akt in HL-60 cells. *Cancer letters* **260**, 88-95, doi:10.1016/j.canlet.2007.10.030 (2008).

102 Benbrook, D. M. & Masamha, C. P. The pro-survival function of Akt kinase can be overridden or altered to contribute to induction of apoptosis. *Current cancer drug targets* **11**, 586-599 (2011).

103 Yu, T., Li, J., Qiu, Y. & Sun, H. 1-phenyl-2-decanoylamino-3-morpholino-1-propanol (PDMP) facilitates curcumin-induced melanoma cell apoptosis by enhancing ceramide accumulation, JNK activation, and inhibiting PI3K/AKT activation. *Mol Cell Biochem* **361**, 47-54, doi:10.1007/s11010-011-1086-9 (2012).

104 Powell, D. J., Hajduch, E., Kular, G. & Hundal, H. S. Ceramide disables 3-phosphoinositide binding to the pleckstrin homology domain of protein kinase B (PKB)/Akt by a PKCzeta-dependent mechanism. *Molecular and cellular biology* **23**, 7794-7808 (2003).

105 Sanvicens, N. & Cotter, T. G. Ceramide is the key mediator of oxidative stress-induced apoptosis in retinal photoreceptor cells. *Journal of neurochemistry* **98**, 1432-1444, doi:10.1111/j.1471-4159.2006.03977.x (2006).

106 Lin, C. F. *et al.* GSK-3beta acts downstream of PP2A and the PI 3-kinase-Akt pathway, and upstream of caspase-2 in ceramide-induced mitochondrial apoptosis. *Journal of cell science* **120**, 2935-2943, doi:10.1242/jcs.03473 (2007).

107 De Stefanis, D. *et al.* Increase in ceramide level alters the lysosomal targeting of cathepsin D prior to onset of apoptosis in HT-29 colon cancer cells. *Biological chemistry* **383**, 989-999, doi:10.1515/bc.2002.106 (2002).

108 Heinrich, M. *et al.* Cathepsin D targeted by acid sphingomyelinase-derived ceramide. *Embo j* **18**, 5252-5263, doi:10.1093/emboj/18.19.5252 (1999).

109 Darios, F., Lambeng, N., Troadec, J. D., Michel, P. P. & Ruberg, M. Ceramide increases mitochondrial free calcium levels via caspase 8 and Bid: role in initiation of cell death. *Journal of neurochemistry* **84**, 643-654 (2003).

110 Yuan, H., Williams, S. D., Adachi, S., Oltersdorf, T. & Gottlieb, R. A. Cytochrome c dissociation and release from mitochondria by truncated Bid and ceramide. *Mitochondrion* **2**, 237-244, doi:10.1016/s1567-7249(02)00106-x (2003).

111 Lin, C. F. *et al.* Bcl-2 rescues ceramide- and etoposide-induced mitochondrial apoptosis through blockage of caspase-2 activation. *The Journal of biological chemistry* **280**, 23758-23765, doi:10.1074/jbc.M412292200 (2005).

112 Dobrowsky, R. T., Kamibayashi, C., Mumby, M. C. & Hannun, Y. A. Ceramide activates heterotrimeric protein phosphatase 2A. *The Journal of biological chemistry* **268**, 15523-15530 (1993).

113 Mukhopadhyay, A. *et al.* Direct interaction between the inhibitor 2 and ceramide via sphingolipid-protein binding is involved in the regulation of protein phosphatase 2A activity and signaling. *FASEB journal : official publication of the Federation of American Societies for Experimental Biology* **23**, 751-763, doi:10.1096/fj.08-120550 (2009).

114 Sumitomo, M. *et al.* Protein kinase Cδ amplifies ceramide formation via mitochondrial signaling in prostate cancer cells. *The Journal of Clinical Investigation* **109**, 827-836, doi:10.1172/JCI14146 (2002).

115 Pinton, P. *et al.* The Ca2+ concentration of the endoplasmic reticulum is a key determinant of ceramide-induced apoptosis: significance for the molecular mechanism of Bcl-2 action. *Embo j* **20**, 2690-2701, doi:10.1093/emboj/20.11.2690 (2001).

116 Morales, M. C. *et al.* 4-HPR-mediated leukemia cell cytotoxicity is triggered by ceramide-induced mitochondrial oxidative stress and is regulated downstream by Bcl-2. *Free radical research* **41**, 591-601, doi:10.1080/10715760701218558 (2007).

117 Messner, M. C. & Cabot, M. C. Cytotoxic responses to N-(4-hydroxyphenyl)retinamide in human pancreatic cancer cells. *Cancer chemotherapy and pharmacology* **68**, 477-487, doi:10.1007/s00280-010-1504-9 (2011).

118 Mondal, S., Mandal, C., Sangwan, R., Chandra, S. & Mandal, C. Withanolide D induces apoptosis in leukemia by targeting the activation of neutral sphingomyelinase-ceramide cascade mediated by synergistic activation of c-Jun N-terminal kinase and p38 mitogen-activated protein kinase. *Molecular cancer* **9**, 239, doi:10.1186/1476-4598-9-239 (2010).

119 Hilchie, A. L. *et al.* Curcumin-induced apoptosis in PC3 prostate carcinoma cells is caspase-independent and involves cellular ceramide accumulation and damage to mitochondria. *Nutrition and cancer* **62**, 379-389, doi:10.1080/01635580903441238 (2010).

120 Maziere, C. *et al.* UVA radiation stimulates ceramide production: relationship to oxidative stress and potential role in ERK, JNK, and p38 activation. *Biochemical and biophysical research communications* **281**, 289-294, doi:10.1006/bbrc.2001.4348 (2001).

121 Sanchez, A. M. *et al.* Apoptosis induced by capsaicin in prostate PC-3 cells involves ceramide accumulation, neutral sphingomyelinase, and JNK activation. *Apoptosis : an international journal on programmed cell death* **12**, 2013-2024, doi:10.1007/s10495-007-0119-z (2007).

122 Chen, C. L. *et al.* Ceramide induces p38 MAPK and JNK activation through a mechanism involving a thioredoxin-interacting protein-mediated pathway. *Blood* **111**, 4365-4374, doi:10.1182/blood-2007-08-106336 (2008).

123 Pruschy, M. *et al.* Ceramide triggers p53-dependent apoptosis in genetically defined fibrosarcoma tumour cells. *British journal of cancer* **80**, 693-698, doi:10.1038/sj.bjc.6690411 (1999).

124 Kim, S. S. *et al.* P53 mediates ceramide-induced apoptosis in SKN-SH cells. *Oncogene* **21**, 2020-2028, doi:10.1038/sj.onc.1205037 (2002).

125 Deng, X., Gao, F. & May, W. S. Protein phosphatase 2A inactivates Bcl2's antiapoptotic function by dephosphorylation and up-regulation of Bcl2-p53 binding. *Blood* **113**, 422-428, doi:10.1182/blood-2008-06-165134 (2009).

126 Temme, A. *et al.* Nuclear localization of Survivin renders HeLa tumor cells more sensitive to apoptosis by induction of p53 and Bax. *Cancer letters* **250**, 177-193, doi:10.1016/j.canlet.2006.09.020 (2007).

127 Blanc-Brude, O. P. *et al.* Therapeutic targeting of the survivin pathway in cancer: initiation of mitochondrial apoptosis and suppression of tumor-associated angiogenesis. *Clinical cancer research : an official journal of the American Association for Cancer Research* **9**, 2683-2692 (2003).

128 Mesri, M. *et al.* Suppression of Vascular Endothelial Growth Factor-Mediated Endothelial Cell Protection by Survivin Targeting. *The American Journal of Pathology* **158**, 1757-1765 (2001).

129 Liu, X. *et al.* Targeting of survivin by nanoliposomal ceramide induces complete remission in a rat model of NK-LGL leukemia. *Blood* **116**, 4192-4201, doi:10.1182/blood-2010-02-271080 (2010).

130 Paschall, A. V. *et al.* Ceramide targets xIAP and cIAP1 to sensitize metastatic colon and breast cancer cells to apoptosis induction to suppress tumor progression. *BMC cancer* **14**, 24, doi:10.1186/1471-2407-14-24 (2014).

131 Gottesman, M. M. Mechanisms of cancer drug resistance. *Annual review of medicine* **53**, 615-627, doi:10.1146/annurev.med.53.082901.103929 (2002).

132 Gimenez-Bonafe, P., Tortosa, A. & Perez-Tomas, R. Overcoming drug resistance by enhancing apoptosis of tumor cells. *Current cancer drug targets* **9**, 320-340 (2009).

133 Makin, G. & Hickman, J. A. Apoptosis and cancer chemotherapy. *Cell and tissue research* **301**, 143-152 (2000).

134 Gouaze, V. *et al.* Overexpression of glucosylceramide synthase and P-glycoprotein in cancer cells selected for resistance to natural product chemotherapy. *Molecular cancer therapeutics* **3**, 633-639 (2004).

135 Ogretmen, B. & Hannun, Y. A. Biologically active sphingolipids in cancer pathogenesis and treatment. *Nature reviews. Cancer* **4**, 604-616, doi:10.1038/nrc1411 (2004).

136 Saddoughi, S. A., Song, P. & Ogretmen, B. Roles of Bioactive Sphingolipids in Cancer Biology and Therapeutics. *Sub-cellular biochemistry* **49**, 413-440, doi:10.1007/978-1-4020-8831-5_16 (2008).

137 Reynolds, C. P., Maurer, B. J. & Kolesnick, R. N. Ceramide synthesis and metabolism as a target for cancer therapy. *Cancer letters* **206**, 169-180, doi:10.1016/j.canlet.2003.08.034 (2004).

138 Senchenkov, A., Litvak, D. A. & Cabot, M. C. Targeting ceramide metabolism--a strategy for overcoming drug resistance. *Journal of the National Cancer Institute* **93**, 347-357 (2001).

139 Garzotto, M. *et al.* Reversal of radiation resistance in LNCaP cells by targeting apoptosis through ceramide synthase. *Cancer research* **59**, 5194-5201 (1999).

140 Morjani, H. *et al.* Elevation of glucosylceramide in multidrug-resistant cancer cells and accumulation in cytoplasmic droplets. *International journal of cancer* **94**, 157-165 (2001).

141 Lucci, A. *et al.* Glucosylceramide: a marker for multiple-drug resistant cancers. *Anticancer research* **18**, 475-480 (1998).

142 Lavie, Y., Cao, H.-t., Bursten, S. L., Giuliano, A. E. & Cabot, M. C. Accumulation of Glucosylceramides in Multidrug-resistant Cancer Cells. *Journal of Biological Chemistry* **271**, 19530-19536, doi:10.1074/jbc.271.32.19530 (1996).

143 Veldman, R. J. *et al.* Altered sphingolipid metabolism in multidrug-resistant ovarian cancer cells is due to uncoupling of glycolipid biosynthesis in the Golgi apparatus. *FASEB journal : official publication of the Federation of American Societies for Experimental Biology* **16**, 1111-1113, doi:10.1096/fj.01-0863fje (2002).

144 Liu, Y. Y., Han, T. Y., Giuliano, A. E. & Cabot, M. C. Expression of glucosylceramide synthase, converting ceramide to glucosylceramide, confers adriamycin resistance in human breast cancer cells. *The Journal of biological chemistry* **274**, 1140-1146 (1999).

145 Gouaze, V. *et al.* Glucosylceramide synthase blockade down-regulates P-glycoprotein and resensitizes multidrug-resistant breast cancer cells to anticancer drugs. *Cancer research* **65**, 3861-3867, doi:10.1158/0008-5472.can-04-2329 (2005).

146 Gouaze-Andersson, V. *et al.* Ceramide and glucosylceramide upregulate expression of the multidrug resistance gene MDR1 in cancer cells. *Biochimica et biophysica acta* **1771**, 1407-1417, doi:10.1016/j.bbalip.2007.09.005 (2007).

147 Inokuchi, J. *et al.* Inhibition of experimental metastasis of murine Lewis lung carcinoma by an inhibitor of glucosylceramide synthase and its possible mechanism of action. *Cancer research* **50**, 6731-6737 (1990).

148 Radin, N. S. Chemotherapy by slowing glucosphingolipid synthesis. *Biochemical pharmacology* **57**, 589-595 (1999).

149 Seelan, R. S. *et al.* Human acid ceramidase is overexpressed but not mutated in prostate cancer. *Genes, chromosomes & cancer* **29**, 137-146 (2000).

150 Norris, J. S. *et al.* Combined therapeutic use of AdGFPFasL and small molecule inhibitors of ceramide metabolism in prostate and head and neck cancers: a status report. *Cancer gene therapy* **13**, 1045-1051, doi:10.1038/sj.cgt.7700965 (2006).

151 Liu, X. *et al.* Modulation of ceramide metabolism enhances viral protein apoptin's cytotoxicity in prostate cancer. *Molecular therapy : the journal of the American Society of Gene Therapy* **14**, 637-646, doi:10.1016/j.ymthe.2006.06.005 (2006).

152 Holman, D. H. *et al.* Lysosomotropic acid ceramidase inhibitor induces apoptosis in prostate cancer cells. *Cancer chemotherapy and pharmacology* **61**, 231-242, doi:10.1007/s00280-007-0465-0 (2008).

153 Liu, X. *et al.* Involvement of sphingolipids in apoptin-induced cell killing. *Molecular therapy : the journal of the American Society of Gene Therapy* **14**, 627-636, doi:10.1016/j.ymthe.2006.07.001 (2006).

154 Cheng, J. C. *et al.* Radiation-induced acid ceramidase confers prostate cancer resistance and tumor relapse. *J Clin Invest* **123**, 4344-4358, doi:10.1172/jci64791 (2013).

155 Elojeimy, S. *et al.* Role of Acid Ceramidase in Resistance to FasL: Therapeutic Approaches Based on Acid Ceramidase Inhibitors and FasL Gene Therapy. *Molecular therapy : the journal of the American Society of Gene Therapy* **15**, 1259-1263 (2007).

156 Roh, J.-L., Park, J. Y., Kim, E. H. & Jang, H. J. Targeting acid ceramidase sensitises head and neck cancer to cisplatin. *European Journal of Cancer* **52**, 163-172, doi:http://dx.doi.org/10.1016/j.ejca.2015.10.056 (2016).

157 Ramirez de Molina, A. *et al.* Acid ceramidase as a chemotherapeutic target to overcome resistance to the antitumoral effect of choline kinase alpha inhibition. *Current cancer drug targets* **12**, 617-624 (2012).

158 Truman, J.-P., García-Barros, M. & Obeid, L. M. "Evolving concepts in cancer therapy through targeting sphingolipid metabolism". *Biochimica et biophysica acta* **1841**, 1174-1188, doi:10.1016/j.bbalip.2013.12.013 (2014).

159 Strelow, A. *et al.* Overexpression of acid ceramidase protects from tumor necrosis factor-induced cell death. *The Journal of experimental medicine* **192**, 601-612 (2000).

160 Kester, M. *et al.* Preclinical development of a C6-ceramide NanoLiposome, a novel sphingolipid therapeutic. *Biological chemistry* **396**, 737-747, doi:10.1515/hsz-2015-0129 (2015).

161 Truman, J. P. *et al.* Endothelial membrane remodeling is obligate for anti-angiogenic radiosensitization during tumor radiosurgery. *PloS one* **5**, e12310, doi:10.1371/journal.pone.0012310 (2010).

162 Paris, F. *et al.* Natural ceramide reverses Fas resistance of acid sphingomyelinase(-/-) hepatocytes. *The Journal of biological chemistry* **276**, 8297-8305, doi:10.1074/jbc.M008732200 (2001).

163 Deng, X. *et al.* Ceramide biogenesis is required for radiation-induced apoptosis in the germ line of C. elegans. *Science* **322**, 110-115, doi:10.1126/science.1158111 (2008).

164 Ji, L., Zhang, G., Uematsu, S., Akahori, Y. & Hirabayashi, Y. Induction of apoptotic DNA fragmentation and cell death by natural ceramide. *FEBS letters* **358**, 211-214, doi:http://dx.doi.org/10.1016/0014-5793(94)01428-4 (1995).

165 Shabbits, J. A. & Mayer, L. D. Intracellular delivery of ceramide lipids via liposomes enhances apoptosis in vitro. *Biochimica et biophysica acta* **1612**, 98-106 (2003).

166 Stover, T. & Kester, M. Liposomal delivery enhances short-chain ceramide-induced apoptosis of breast cancer cells. *The Journal of pharmacology and experimental therapeutics* **307**, 468-475, doi:10.1124/jpet.103.054056 (2003).

167 Jiang, Y. *et al.* Combinatorial therapies improve the therapeutic efficacy of nanoliposomal ceramide for pancreatic cancer. *Cancer biology & therapy* **12**, 574-585, doi:10.4161/cbt.12.7.15971 (2011).

168 Tan, K. B., Ling, L. U., Bunte, R. M., Chng, W. J. & Chiu, G. N. Liposomal codelivery of a synergistic combination of bioactive lipids in the treatment of acute myeloid leukemia. *Nanomedicine (London, England)* **9**, 1665-1679, doi:10.2217/nnm.13.123 (2014).

169 Koshkaryev, A., Piroyan, A. & Torchilin, V. P. Increased apoptosis in cancer cells in vitro and in vivo by ceramides in transferrin-modified liposomes. *Cancer biology & therapy* **13**, 50-60, doi:10.4161/cbt.13.1.18871 (2012).

170 Su, X. *et al.* Co-delivery of doxorubicin and PEGylated C16-ceramide by nanoliposomes for enhanced therapy against multidrug resistance. *Nanomedicine (London, England)* **10**, 2033-2050, doi:10.2217/nnm.15.50 (2015).

171 Zou, P., Stern, S. T. & Sun, D. PLGA/liposome hybrid nanoparticles for short-chain ceramide delivery. *Pharmaceutical research* **31**, 684-693, doi:10.1007/s11095-013-1190-5 (2014).

172 Dhule, S. S. *et al.* The combined effect of encapsulating curcumin and C6 ceramide in liposomal nanoparticles against osteosarcoma. *Molecular pharmaceutics* **11**, 417-427, doi:10.1021/mp400366r (2014).

173 Zhai, L., Sun, N., Han, Z., Jin, H. C. & Zhang, B. Liposomal short-chain C6 ceramide induces potent anti-osteosarcoma activity in vitro and in vivo. *Biochemical and biophysical research communications* **468**, 274-280, doi:10.1016/j.bbrc.2015.10.113 (2015).

174 Stover, T. C., Sharma, A., Robertson, G. P. & Kester, M. Systemic delivery of liposomal short-chain ceramide limits solid tumor growth in murine models of breast adenocarcinoma. *Clinical cancer research : an official journal of the American Association for Cancer Research* **11**, 3465-3474, doi:10.1158/1078-0432.ccr-04-1770 (2005).

175 Shabbits, J. A. & Mayer, L. D. High ceramide content liposomes with in vivo antitumor activity. *Anticancer research* **23**, 3663-3669 (2003).

176 Zolnik, B. S. *et al.* Rapid distribution of liposomal short-chain ceramide in vitro and in vivo. *Drug metabolism and disposition: the biological fate of chemicals* **36**, 1709-1715, doi:10.1124/dmd.107.019679 (2008).

177 Morgan, T. T. *et al.* Encapsulation of Organic Molecules in Calcium Phosphate Nanocomposite Particles for Intracellular Imaging and Drug Delivery. *Nano Letters* **8**, 4108-4115, doi:10.1021/nl8019888 (2008).

178 Kester, M. *et al.* Calcium phosphate nanocomposite particles for in vitro imaging and encapsulated chemotherapeutic drug delivery to cancer cells. *Nano Lett* **8**, 4116-4121, doi:10.1021/nl802098g (2008).

179 Devalapally, H., Duan, Z., Seiden, M. V. & Amiji, M. M. Modulation of drug resistance in ovarian adenocarcinoma by enhancing intracellular ceramide using tamoxifen-loaded biodegradable polymeric nanoparticles. *Clinical cancer research : an official journal of the American Association for Cancer Research* **14**, 3193-3203, doi:10.1158/1078-0432.ccr-07-4973 (2008).

180 Devalapally, H., Duan, Z., Seiden, M. V. & Amiji, M. M. Paclitaxel and ceramide co-administration in biodegradable polymeric nanoparticulate delivery system to overcome drug resistance in ovarian cancer. *International journal of cancer* **121**, 1830-1838, doi:10.1002/ijc.22886 (2007).

181 van Vlerken, L. E., Duan, Z., Seiden, M. V. & Amiji, M. M. Modulation of intracellular ceramide using polymeric nanoparticles to overcome multidrug resistance in cancer. *Cancer research* **67**, 4843-4850, doi:10.1158/0008-5472.can-06-1648 (2007).

182 Stover, T. C., Kim, Y. S., Lowe, T. L. & Kester, M. Thermoresponsive and biodegradable linear-dendritic nanoparticles for targeted and sustained release of a pro-

apoptotic drug. *Biomaterials* **29**, 359-369, doi:10.1016/j.biomaterials.2007.09.037 (2008).

183 Wu, C. H. *et al.* Trojan-horse nanotube on-command intracellular drug delivery. *Nano Lett* **12**, 5475-5480, doi:10.1021/nl301865c (2012).

184 Dreyer, D. R., Park, S., Bielawski, C. W. & Ruoff, R. S. The chemistry of graphene oxide. *Chemical Society reviews* **39**, 228-240, doi:10.1039/b917103g (2010).

185 Hummers, W. S. & Offeman, R. E. Preparation of Graphitic Oxide. *Journal of the American Chemical Society* **80**, 1339-1339, doi:10.1021/ja01539a017 (1958).

186 Kosynkin, D. V. *et al.* Longitudinal unzipping of carbon nanotubes to form graphene nanoribbons. *Nature* **458**, 872-876, doi:http://www.nature.com/nature/journal/v458/n7240/suppinfo/nature07872_S1.html (2009).

187 Yang, X. *et al.* High-Efficiency Loading and Controlled Release of Doxorubicin Hydrochloride on Graphene Oxide. *The Journal of Physical Chemistry C* **112**, 17554-17558, doi:10.1021/jp806751k (2008).

188 Sun, X. *et al.* Nano-Graphene Oxide for Cellular Imaging and Drug Delivery. *Nano Res* **1**, 203-212, doi:10.1007/s12274-008-8021-8 (2008).

189 Zhang, L., Xia, J., Zhao, Q., Liu, L. & Zhang, Z. Functional graphene oxide as a nanocarrier for controlled loading and targeted delivery of mixed anticancer drugs. *Small* **6**, 537-544, doi:10.1002/smll.200901680 (2010).

190 Xu, Z. *et al.* Delivery of paclitaxel using PEGylated graphene oxide as a nanocarrier. *ACS applied materials & interfaces* **7**, 1355-1363, doi:10.1021/am507798d (2015).

191 Misra, S. K., Kondaiah, P., Bhattacharya, S. & Rao, C. Graphene as a nanocarrier for tamoxifen induces apoptosis in transformed cancer cell lines of different origins. *Small* **8**, 131-143 (2012).

192 Mullick Chowdhury, S. *et al.* Cell specific cytotoxicity and uptake of graphene nanoribbons. *Biomaterials* **34**, 283-293, doi:10.1016/j.biomaterials.2012.09.057 (2013).

193 Mullick Chowdhury, S., Manepalli, P. & Sitharaman, B. Graphene nanoribbons elicit cell specific uptake and delivery via activation of epidermal growth factor receptor enhanced by human papillomavirus E5 protein. *Acta biomaterialia* **10**, 4494-4504, doi:10.1016/j.actbio.2014.06.030 (2014).

194 Normanno, N. *et al.* Epidermal growth factor receptor (EGFR) signaling in cancer. *Gene* **366**, 2-16, doi:http://dx.doi.org/10.1016/j.gene.2005.10.018 (2006).

195 Frost, R., Svedhem, S., Langhammer, C. & Kasemo, B. Graphene Oxide and Lipid Membranes: Size-Dependent Interactions. *Langmuir : the ACS journal of surfaces and colloids* **32**, 2708-2717, doi:10.1021/acs.langmuir.5b03239 (2016).

196 Chen, J. *et al.* Interaction of Graphene and its Oxide with Lipid Membrane: A Molecular Dynamics Simulation Study. *The Journal of Physical Chemistry C* **120**, 6225-6231, doi:10.1021/acs.jpcc.5b10635 (2016).

197 Okamoto, Y. *et al.* Fabrication of Supported Lipid Bilayer on Graphene Oxide. *Journal of Physics: Conference Series* **352**, 012017 (2012).

198 Wu, L., Zeng, L. & Jiang, X. Revealing the Nature of Interaction between Graphene Oxide and Lipid Membrane by Surface-Enhanced Infrared Absorption Spectroscopy. *Journal of the American Chemical Society* **137**, 10052-10055, doi:10.1021/jacs.5b03803 (2015).

199 Tsuzuki, K. *et al.* in *Journal of Physics: Conference Series.* 012016 (IOP Publishing).

200 Rui, L. *et al.* Reduced graphene oxide directed self-assembly of phospholipid monolayers in liquid and gel phases. *Biochimica et biophysica acta* **1848**, 1203-1211, doi:10.1016/j.bbamem.2015.02.018 (2015).

201 Robinson, J. T. *et al.* Ultrasmall Reduced Graphene Oxide with High Near-Infrared Absorbance for Photothermal Therapy. *Journal of the American Chemical Society* **133**, 6825-6831, doi:10.1021/ja2010175 (2011).

Chapter 2

Development of a Method for Loading Ceramides onto Oxidized Graphene Nanoribbon

Abstract

The bioactive sphingolipid ceramide has many interesting potential applications in therapeutic treatment. However, as a lipid, it not soluble in aqueous solution and requires a delivery system to be delivered *in vitro* or *in vivo*. Current delivery systems have serious drawbacks, limiting the potential of ceramide for therapeutic treatment. To this end, we have developed a method to load ceramide onto oxidized graphene nanoribbons (O-GNRs). We found that by slowly adding water to a solution of ethanol containing ceramide and O-GNRs, we were able to load a high amount of ceramide onto O-GNRs. We also found that the rate of addition and the presence of sonication were crucial to preventing undesirable effects such as the aggregation of the O-GNRs. These data represent an important step towards the therapeutic application of ceramide.

Introduction

There is a lack of a good delivery method for ceramide, and the delivery methods available often only work well for the short chain exogenous ceramides and/or cannot be adapted at all to the longer chain ceramides[1]. O-GNRs represent a good potential candidate as a delivery vehicle for ceramide due to their unique surface chemistry and amphiphilic nature[2]. However, the design of such a loading method must take into account the limitations of both ceramide and O-GNRs. Mixing different solvents together can cause O-GNRs to aggregate, and as previously mentioned, ceramide is not soluble in aqueous solution at all. However, by accounting for these parameters and controlling for them, we can develop a loading method that allows ceramide to be reversibly bound to O-GNRs. We describe the development of such a method, which took place in four main experimental steps: mixing in organic solvents, forced hydrophobic interaction by fractional distillation, forced hydrophobic interaction with a burette, and forced hydrophobic interaction with a syringe pump/prevention of aggregation with sonication. These steps proceeded in a trial-and-error manner, with results from the previous step being applied to the next step.

Chapter 2 Global Methods

Materials

C_{16}-Ceramide and NBD Ceramide (C_6 N-[6-[(7-nitro-2-1,3-benzoxadiazol-4-yl)amino]hexanoyl]-D-erythro-sphingosine) were purchased from Avanti Polar Lipids (Alabaster, AL, USA). All other materials and reagents were purchased from Sigma-Aldrich (St. Louis, MO, USA) unless otherwise noted.

Cell Culture

HeLa cells were obtained from ATCC (Manassas, VA, USA). Cells were grown in Dulbecco's Modified Eagle Medium (DMEM) supplemented with 10% fetal bovine serum and 1% penicillin-streptomycin. Cells were grown at 37 °C in a humidified atmosphere of 5% carbon dioxide.

O-GNR Synthesis

O-GNRs were synthesized from multi-walled carbon nanotubes (MWCNTs) using the longitudinal unzipping method with centrifugation instead of filtration for purification[3]. Briefly, MWCNTs (150mg) were dispersed in 30 mL of concentrated sulfuric acid. After 3 hr, 750mg of potassium permanganate was added and then the mixture was stirred for 1 hr. The mixture was then heated to approximately 60 °C for 1 hr in an oil bath to complete the reaction. It was then allowed to cool to room temperature and was washed with dilute hydrochloric acid. The product was isolated by flocculation using ethanol and ether, followed by centrifugation at 3000 rpm and drying overnight in a vacuum oven.

Prestoblue Viability

Cells were seeded at a density of 5000 cells/well in 96 well plates. Aggregated or non-aggregated nanoparticles were placed in each well. After 24 hours, the media was aspirated, and each well was rinsed twice with PBS. A mixture of 10 µL of Presto Blue Viability Reagent (Life Technologies, Grand Island, NY, USA) and 90 µL of DMEM with 10% FBS and 1% P/S were added to each well and placed back in the incubator. After 2 hours, the plates were removed, and the fluorescence intensity of each well was measured using a Molecular Devices SpectraMax M2e (Sunnyvale, CA, USA) with an excitation wavelength of 560 nm and an emission wavelength of 590 nm. The cell viability is expressed as a percent of the cells treated with aggregated O-GNRs with the formula $\left((I_{test} - I_{blank})/(I_{control} - I_{blank}) \times 100\%\right) - 100\%$,

where I_{test} is the fluorescence intensity of cells exposed to non-aggregated nanoparticles, $I_{control}$ is the fluorescence intensity of cells treated with aggregated nanoparticles, and I_{blank} is the fluorescence intensity from empty wells.

Imaging of O-GNR aggregation

Low magnitude images of O-GNRs were taken in 48 well plates using a Zeiss Axiovert 200M Fluorescent Microscope (Thornwood, NY, USA) using an objective lens of 2.5x.

Mixing in Organic Solvents

Rationale

One of the first studies involving graphene as a drug delivery agent involved PEG-coated graphene oxide and a camptothecin analogue, which led to a significant amount loaded onto the graphene oxide nanoparticles and a significant biological effect[4]. This loading was based on the pi-stacking phenomenon, where the aromatic ring structures present in graphene and camptothecin can interact in such a way that is more energetically favorable than dissociation. Since the fluorescently tagged NBD-ceramide contains an aromatic ring, it may be able to load onto graphene nanoparticles using the same pi-stacking phenomenon.

Methods

50 µL of a 200 µg/mL solution of C_6 NBD ceramide in ethanol or DMSO and 250 µL of a 1 mg/mL stock solution of O-GNRs in ethanol or DMSO were added to a 5mL glass scintillation and mixed for 24 hours on ice. After 24 hours, the solution was spun down at 13000 RPM, and the supernatant was collected. The fluorescence of the supernatant was read at an excitation wavelength of 465 nm and an emission wavelength of 535 nm in a Molecular Devices

SpectraMax M2e (Sunnyvale, CA, USA) in triplicate and averaged. To determine the loading efficiency, the stock solution of NBD ceramide was diluted down by the same factor as during the loading process, and the fluorescence was read and compared to the fluorescence of the supernatant.

Results/Discussion

Figure 2.1 shows that there is no significant difference between the fluorescence of the supernatant and the fluorescence of the stock solution for mixing in either ethanol or DMSO. This is surprising considering that NBD ceramide contains a fluorescent tag with an aromatic ring that should be able to bind to graphene via pi-stacking. These results suggest that loading ceramide onto graphene nanoparticles cannot be accomplished using the traditional methods for loading drugs onto graphene.

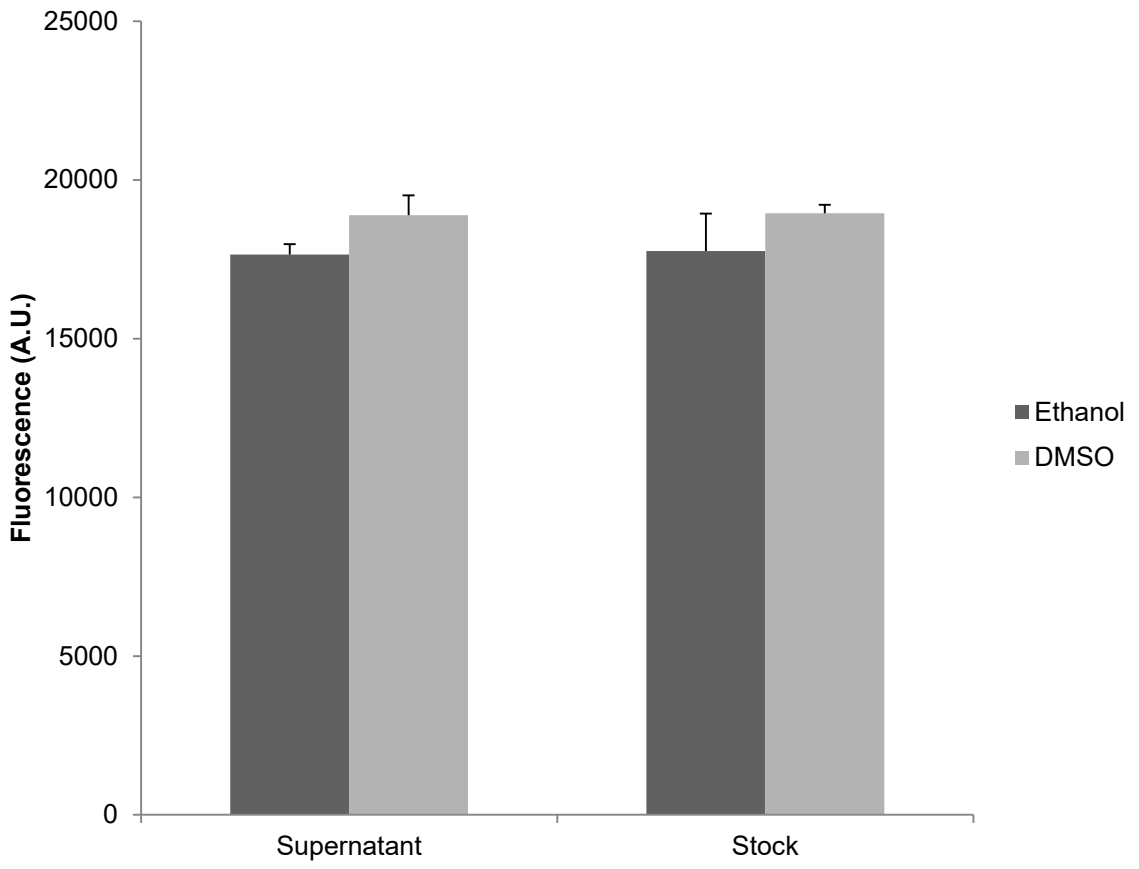

Figure 2.1. Fluorescence measurements of NBD-ceramide loading. The supernatant after loading in ethanol (blue) or DMSO (red) was compared to a stock solution of NBD-ceramide in either solvent.

Fractional Distillation (Evaporative) Method

Rationale

The inability of carbon nanoparticles to load NBD ceramide in pure organic solvents suggests that there are insufficient molecular forces to hold the aliphatic hydrocarbon of ceramide chains to the aromatic surface chemistry of graphene oxide nanoparticles. In fact, the inability of the NBD tag to pi stack with the graphene suggests that in a more hydrophobic environment, the aliphatic chains may interfere with the interaction between graphene and the

NBD tag. However, there is evidence that graphene can bind to aliphatic hydrocarbon chains. Previously we have used the surfactant DSPE-PEG to grant oxidized graphene nanoparticles increased dispersibility in aqueous solution. This surfactant consists of a hydrophilic polyethylene glycol tail conjugated to a distearoyl lipid with a phosphoethanolamine headgroup. In aqueous solution, these stearic acid tails bind to the surface of graphene oxide and are held in place by the hydrophobic interaction between them. In other words, it is more energetically favorable for the aliphatic stearic acid tails to remain bound to the surface of graphene than to disassociate and form micelles. Thus it theoretically possible for ceramide to remain bound to graphene, provided that there is a force to bind it in the first place.

It may be possible to combine these two properties of lipid/graphene interactions to bind ceramide. By gradually shifting the environment from hydrophobic to hydrophilic, it may be possible to force the ceramide to interact with graphene and then hold it there for delivery to a cell, tissue, or organ. Here, we describe such a method using fractional distillation of an ethanol-water mixture. Since ethanol has a lower boiling point than water, it should be possible to remove ethanol selectively from a water-ethanol mixture. By changing a 90:10 ethanol/water mixture to a lower ethanol fraction, it should be possible to remove ethanol without greatly changing the volume of water in the mixture, shifting the environment from hydrophobic and hydrophilic.

Methods

500 μL of a 1 mg/mL solution of O-GNRs in ethanol and 500 μL of a 200 μg/mL solution of C_{16} ceramide in ethanol were added to a round-bottomed flask, along with 8mL of pure ethanol and 1mL of ddH_2O. To perform fractional distillation on the mixture, the flask was

attached to a Buchi Rotavapor R-215 rotary evaporator (Postfach, Switzerland) with the pressure set to 30 kPa and the temperature of the water bath set to 50 °C. The evaporation was allowed to continue until the volume of the liquid was reduced to approximately 1 mL, or 10% of its original volume, which took approximately 30 minutes.

Results/Discussion

Although the evaporation of ethanol from the solution was successful, the mixing of water and ethanol led to an irreversible aggregation of the O-GNRs. Before beginning the distillation procedure, the addition of a water/ethanol mixture to the mixture of ceramide and O-GNRs in ethanol caused the O-GNRs to clump up (Fig. 2.2A). After the distillation was completed, there was even more aggregation present (Fig. 2.2B). A 30 minute bath sonication of the O-GNR solution did not have a significant effect on the aggregation of the O-GNRs (Fig. 2.2C).

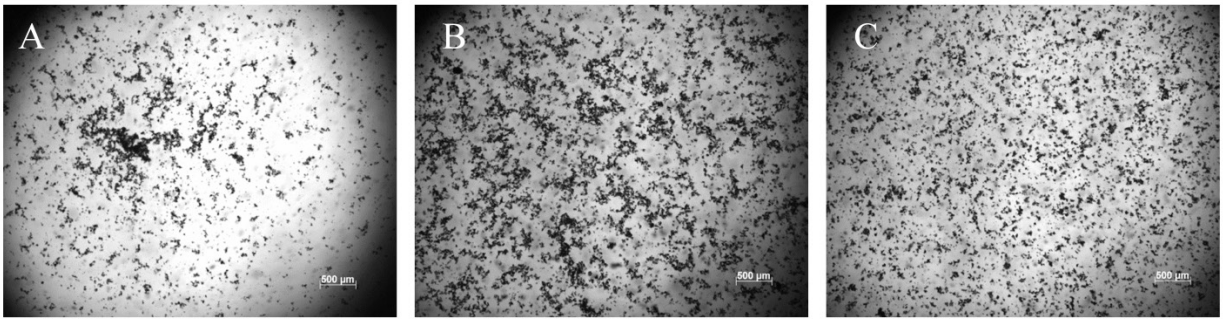

Figure 2.2. Low magnitude images of O-GNRs after loading using the rotary evaporator. Prior to starting the evaporation process, the O-GNRs became aggregated (A). After the loading process, the O-GNRs remained very aggregated (B). Even after 30 minutes of sonication, the O-GNRs did not undergo a reversal of aggregation (C).

This aggregation is a major issue for loading of drugs and other molecules onto O-GNRs. Nanoparticle aggregation greatly reduces the surface area available for ceramide to bind.

Additionally, aggregated nanoparticles can have drastically different biological effects and uptake compared to well-dispersed nanoparticle solutions[5]. Aggregated O-GNRs at very high concentrations do not exhibit significant toxicity while non-aggregated nanoparticles do (Fig. 2.3). There may be ways to control for this effect and successfully load ceramide onto O-GNRs by shifting the environment from hydrophobic to hydrophilic, but the rotary evaporator does not seem to be a good way to accomplish this.

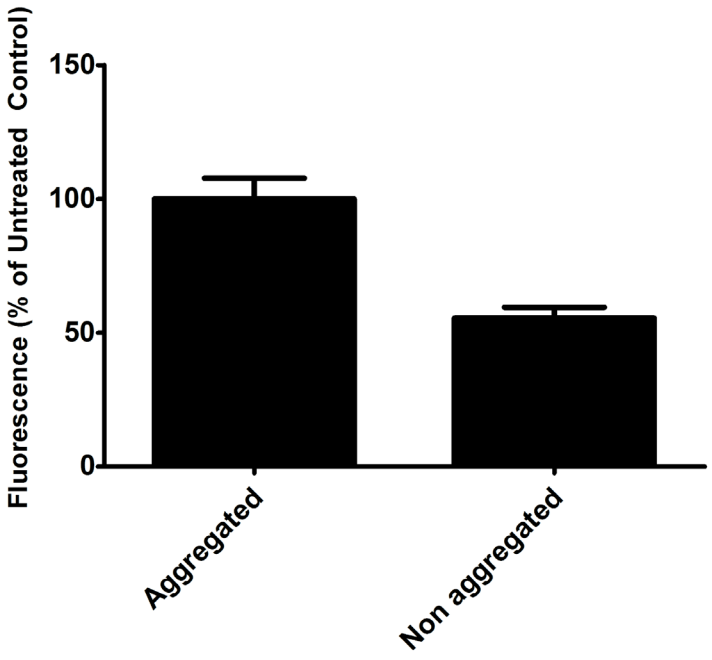

Figure 2.3. Cells treated with 250 μg/mL of aggregated or non-aggregated nanoparticles, showing that aggregated nanoparticles do not have as large an effect on cells as non-aggregated nanoparticles.

Addition of Water by Burette

Rationale

The fundamental issue with the rotary evaporator method was the introduction of water in the initial mixture of ceramide and O-GNRs. However, by approaching the problem from the

other direction - by starting with a mixture of O-GNRs and ceramide in a solution of pure ethanol, and then slowly adding water to the mixture over time - it may help reduce O-GNR aggregation.

Methods

500 μL of a 1 mg/mL solution of O-GNRs in ethanol and 500 μL of a 200 μg/mL solution of C_{16} ceramide in ethanol were added to a 20 mL glass scintillation vial with a PTFE-coated magnetic stir bar and set on a magnetic stir plate with the cap left off. A 10mL burette was fixed over the scintillation vial using a ring stand, and the knob was adjusted so that the opening was barely visible when looking down from the top. After adjustment, 9mL of ddH_2O was added to the burette and the water was allowed to drain completely from the flask (approximately 2 hours).

Results/Discussion

Figure 2.4 shows the aggregate formation of the O-GNRs after the loading process. There is still significant aggregate formation compared to the fractional distillation method. However, this could be attributed to the difficulty in fine-tuning the flow rate. The flow rate of the burette flask is exceedingly difficult to control, with small adjustments of the knob leading to a large difference in flow rates. Furthermore, the large bore of the dropper tube results in large droplet formation, which adds water in larger, discrete volumes. Using a method that allows for smaller drop formation and more precise control over the flow rate may help to prevent aggregation of nanoparticles.

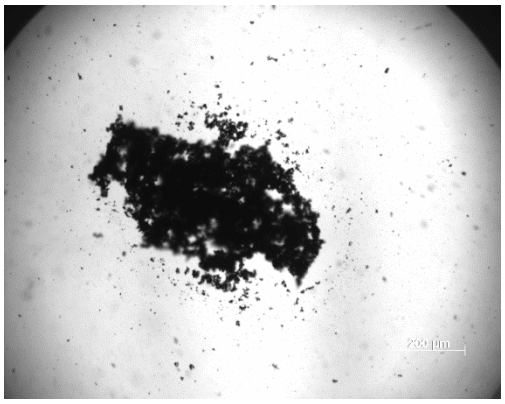

Figure 2.4. Aggregation of O-GNRs after addition of water via burette. Large amounts of aggregation are visible near the center.

Addition of Water by Syringe Pump

Rationale

Although the burette flask did not appreciably reduce O-GNR aggregation, there are other methods for controlled delivery of a fluid to a container. One such method is the syringe pump, which can deliver volumes of a fluid with excellent control over the flow rate. Furthermore, the attachment of small-bore needles to the tips allows for much smaller droplet formation and thus smaller volumes of water added at shorter intervals.

In addition to the syringe pump, a small sonic cleaner was added to the loading process. This sonic cleaner allows a level of sonication that may reduce O-GNR aggregation while also not being forceful enough to interfere with the interaction between ceramide and the O-GNRs.

Methods

500 µL of a 1 mg/mL solution of O-GNRs in ethanol and 500 µL of a 200 µg/mL solution of C_{16} ceramide in ethanol were added to a 20 mL glass scintillation vial with a PTFE-coated magnetic stir bar, covered with parafilm, and placed inside a Cole-Parmer sonic cleaner (Vernon

Hills, Illinois, USA) on top of a magnetic stir plate. A 10 mL syringe connected to a 10" section of plastic tubing and a 25 gauge needle was filled with 9 mL of water and placed on a New Era NE-300 syringe pump (New Era Pump Systems Inc. Farmingdale, NY, USA). The water was added to the scintillation vial over a period of 2 hours.

Two variables were examined: the rate of addition of water, and the length of sonication. For addition rate, sonication was kept constant through the entire loading process. Three addition rates were tested: fast to slow (7 mL/hour for 1 hour to 2 mL/hour for 1 hour), slow to fast (2 mL/hour for 1 hour to 7 mL/hour for 1 hour) and then a constant flow rate (4.5 mL/hour for the entire 2 hours). The best flow rate was determined by aggregate formation and was then used to test variable sonication times from 0 to 2 hours total in 30-minute intervals.

Results/Discussion

Figure 2.5 shows the effect of flow rate on O-GNR aggregation. Aggregation was directly proportional to the flow rate in the first hour, with an addition of 7mL showing the most aggregation (Fig. 2.5A) an addition of 4.5 mL showing smaller amounts of aggregates (Fig. 2.5B) and an addition of 2 mL showing very little aggregation (Fig. 2.5C). As such, a flow rate of 2 mL in the first hour and 7 mL in the second hour was chosen to further examine the effect of sonication on aggregate formation.

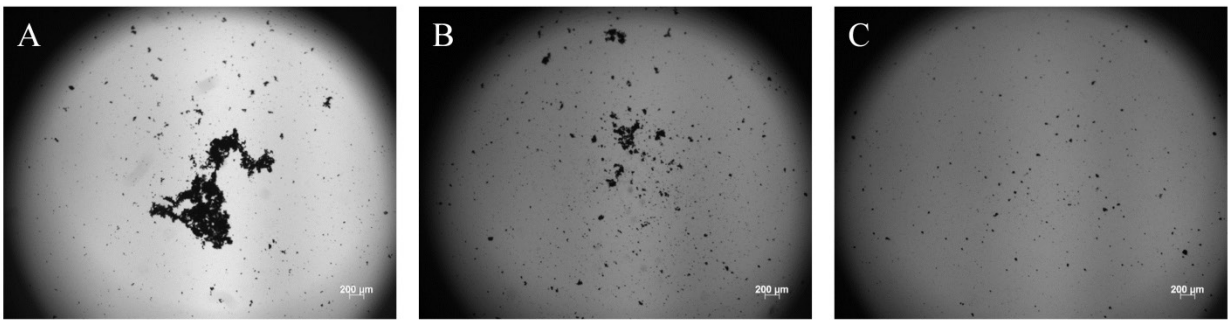

Figure 2.5. Aggregation of O-GNRs after addition of water via syringe pump at 3 different flow rates: (A) fast to slow (7 mL/hour for 1 hour to 2 mL/hour for 1 hour), (B) a constant flow rate (4.5 mL/hour for the entire 2 hours), (C) and slow to fast (2 mL/hour for 1 hour to 7 mL/hour for 1 hour)

Figure 2.6 shows the effect on sonication with a flow rate of 2 mL in the first hour and 7 mL in the second hour. Without sonication, there was a significant amount of aggregation present (Fig. 2.6A). With 30 minutes of sonication (Fig. 2.6B) and 1 hour of sonication (Fig. 2.6C), there was still significant aggregation present, although the aggregation decreased proportionally with the length of sonication. With 1.5 hours of sonication (Fig. 2.6D) and 2 hours of sonication (Fig. 2.6E), there was very little aggregation present, with very little difference between the two durations of sonication. However, given the way sonication heats up the solution during loading, as well as the potential of sonication to knock ceramide off of O-GNRs, a sonication time of 1.5 hours was chosen for the finalized loading process.

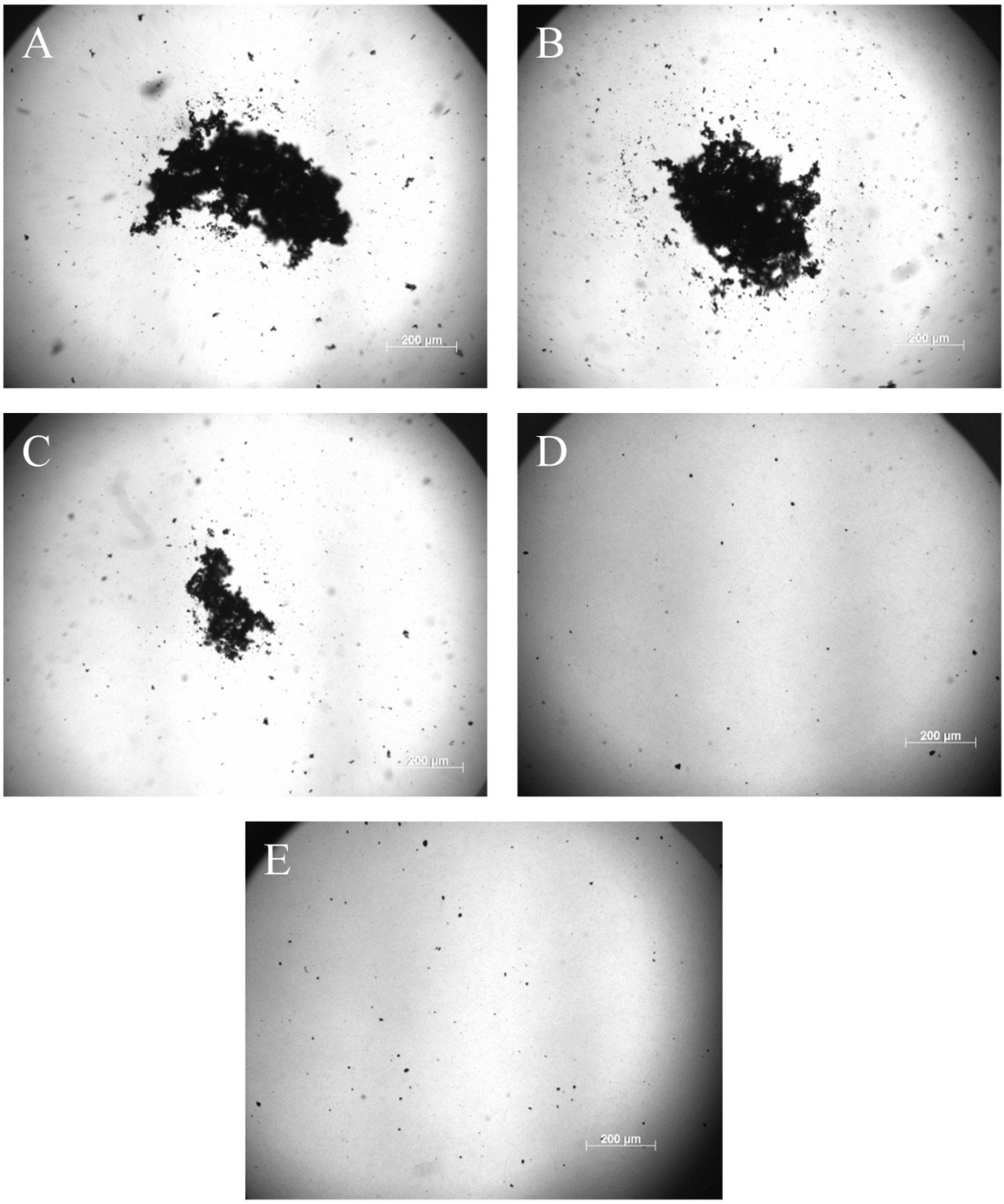

Figure 2.6. Aggregation of O-GNRs after addition of water via syringe pump using a flow rate of 2 mL/hour for 1 hour, and then 7 mL/hour for 1 hour, under varying amounts of sonication. (A) No sonication (B) 30 minutes of sonication (C) 1 hour of sonication (D) 1.5 hours of sonication (E) 2 hours of sonication.

Finalized loading method and quantification

500 µL of a 1 mg/mL solution of O-GNRs in ethanol and 500 µL of a 200 µg/mL solution of C_{16} ceramide in ethanol were added to a 20 mL glass scintillation vial. This mixture was bubbled with nitrogen gas and covered in parafilm to prevent oxidation of ceramide. It was then bath sonicated for 15 minutes to allow interspersion of individual nanoparticles and ceramide molecules.

To this solution, 9mL of double-distilled water were added using a New Era NE-300 syringe pump (New Era Pump Systems Inc. Farmingdale, NY, USA) over a period of two hours under constant mixing. However, the water was not added at a constant rate: for the first hour, water was added at a rate of 2 mL/hr, and for the second hour, water was added at a rate of 7 mL/hr. During the first 1.5 hrs of this loading process, the ceramide/nanoparticle mixture was subjected to mild sonication using a sonic cleaner to prevent the clumping of nanoparticles caused by the addition of water to ethanol. To separate ceramide-loaded nanoparticles from unloaded ceramide, the mixture was centrifuged at 4000 RPM for at least 30 minutes in a 15mL polypropylene conical tube. The supernatant was discarded, and the nanoparticles were washed by resuspension in pure double-distilled water and repeating the centrifugation step, yielding ceramide-loaded O-GNRs.

Samples were prepared for mass spectrometry by first resuspending ceramide-loaded nanoparticles in 100% ethanol and bath-sonicating for 1 hr, to force ceramide to dissociate from the nanoparticles. The mixture was centrifuged at 13000 rpm for 1 hr to ensure all nanoparticles were concentrated at the bottom. 100 µL of the supernatant was extracted for mass spectrometry. 100 µL of the ceramide stock solution used for loading was also analyzed as a basis of

comparison to calculate loading efficiency. Samples were analyzed using a Fison's MD800 Gas Chromatography Mass Spectrometer. The signals generated from samples were correlated to a standard curve to calculate the exact concentration of ceramide.

Results

Mass spectroscopy revealed a loading efficiency of approximately 70% compared to the stock solution for C_{16} ceramide.

Conclusions

We have successfully developed a method that can load significant amounts of ceramide while keeping O-GNR aggregation to a minimum. These ceramide loaded O-GNRs will be tested for their biological effects in cells in future studies.

References

1 Ma, Y. Y., Mou, X. Z., Ding, Y. H., Zou, H. & Huang, D. S. Delivery systems of ceramide in targeted cancer therapy: ceramide alone or in combination with other anti-tumor agents. *Expert opinion on drug delivery*, 1-10, doi:10.1080/17425247.2016.1188803 (2016).

2 Dreyer, D. R., Park, S., Bielawski, C. W. & Ruoff, R. S. The chemistry of graphene oxide. *Chemical Society reviews* **39**, 228-240, doi:10.1039/B917103G (2010).

3 Kosynkin, D. V. *et al.* Longitudinal unzipping of carbon nanotubes to form graphene nanoribbons. *Nature* **458**, 872-876, doi:10.1038/nature07872 (2009).

4 Liu, Z., Robinson, J. T., Sun, X. & Dai, H. PEGylated nanographene oxide for delivery of water-insoluble cancer drugs. *Journal of the American Chemical Society* **130**, 10876-10877, doi:10.1021/ja803688x (2008).

5 Liao, K. H., Lin, Y. S., Macosko, C. W. & Haynes, C. L. Cytotoxicity of graphene oxide and graphene in human erythrocytes and skin fibroblasts. *ACS applied materials & interfaces* **3**, 2607-2615, doi:10.1021/am200428v (2011).

Chapter 3

Oxidized Graphene Nanoparticles as a Delivery System for the Pro-Apoptotic Sphingolipid C_6 Ceramide

Contributions by: Cassandra Suhrland Jean-Philip Truman, Lina M. Obeid, Balaji Sitharaman

Abstract

Ceramide is a type of sphingolipid that has attracted much attention as a possible anticancer agent due to its potent pro-apoptotic effects. However, due to its extreme hydrophobicity, there is currently no clinically approved delivery method for *in vivo* use as a therapeutic agent. To this end, we have developed a novel method for loading the short-chain C_6 ceramide onto oxidized graphene nanoribbons (O-GNRs) and graphene nanoplatelets (GNPs). Mass spectrometry revealed loading efficiencies of 57% and 51.5% for C_6 ceramide onto O-GNRs and GNPs, respectively. The PrestoBlue viability assay revealed that 100 μg/mL of C_6 ceramide-loaded O-GNRs and C_6 ceramide-loaded GNPs reduced HeLa cell viability by ~93% and ~76%, respectively, compared to untreated HeLa cells, while equal concentrations of these nanoparticles without C_6 ceramide did not significantly reduce HeLa cell viability. We confirmed that this cytotoxicity was apoptotic in nature via capase-3 activity Hoescht staining. Using live-cell confocal imaging with the fluorescent NBD-ceramide loaded on O-GNRs, we observed robust uptake into HeLa cells within 30 minutes while NBD-ceramide on its own was uptaken much more rapidly. Transmission electron microscopy confirmed that C_6 ceramide-loaded O-GNRs were entering cells. Taken together, these data show that O-GNRs are a promising delivery agent for ceramide. To our knowledge, this study is the first to use such a loading method.

Introduction

Lipids have long been recognized for their passive roles in cellular metabolism as the main constituent of cell membranes and membrane-bound organelles. However, in recent years there has been a growing appreciation for the active roles certain lipids take in cellular processes. Of particular interest is the group of sphingolipids known as ceramides, which have important roles in many cell signaling processes including cell cycle progression, apoptosis, and autophagy[1-11]. These lipids are composed of sphingosine linked to a fatty acid by an amide bond, and different biological effects on cells depending on the length of the fatty acid chain have been reported[12]. C_{24} ceramide, for example, generally has roles in cell proliferation and survival, while C_{16} ceramide has anti-proliferative effects and is associated with apoptosis[13-19].

Given their interesting biological effects, there is an increased interest in using ceramides for therapeutic applications, such as in the treatment of cancer. The addition of exogenous C_{16} ceramide is capable of sensitizing cancer cells to radiation treatment and chemotherapy, even in cancers previously resistant to these treatments[20]. However, as a lipid, ceramide has extremely limited solubility in aqueous solution and requires the use of a delivery agent to deliver it to cells. Such delivery agents have been sufficient for *in vitro* studies of certain ceramide species but have drawbacks that limit their usefulness for therapeutic applications. For example, although ceramide can be dissolved in organic solvents such as DMSO to enhance their solubility in aqueous solution[21], this could only work for short chain, cell permeable ceramides such as C_2 and C_6 ceramides[22]. Ceramide can also be incorporated into liposomes; however, the synthesis of these liposomes is a complicated and sensitive process. Additionally, other lipids and cofactors are required to form stable liposomes due to ceramide's high packing parameter,

putting an upper limit on the efficiency of ceramide incorporation[23]. Thus, there is a need for better delivery systems for these sphingolipids.

Graphene is a versatile two-dimensional carbon nanostructure that has a number of applications in disciplines ranging from electronics to biology[24-26]. Due to its sp^2 hybridized orbital structure, pristine graphene is very hydrophobic. However, it can be oxidized to a more water-dispersible form while still retaining hydrophobic sp^2 moieties, giving rise to oxidized graphene nanoparticles. These nanoparticles have previously been investigated as a drug delivery platform for anticancer drugs such as doxorubicin since their large surface areas allow for high amounts of drug binding[27,28]. Binding of these drugs is achieved through the pi-stacking phenomenon, a reversible hydrophobic interaction between aromatic rings on graphene and the drug molecules[29].

However, these hydrophobic portions of graphene are also capable of binding non-aromatic hydrophobic molecules; for example, it is possible to increase the dispersibility of graphene oxide in aqueous solution using surfactants such as 1,2-distearoyl-*sn*-glycero-3-phosphoethanolamine-N-[amino(polyethylene glycol)] (DSPE-PEG)[30]. Thus, it is theoretically possible for graphene oxide nanoparticles to bind ceramide given a loading method that facilitates hydrophobic interactions between the two while also being compatible with ceramide's extreme hydrophobicity.

Herein we describe such a method for loading the short-chain C_6 ceramide onto graphene nanoparticles. We demonstrate that by gradually shifting the environment of a ceramide-graphene nanoparticle mixture from hydrophobic to aqueous, we are able to achieve high levels of ceramide loading. Furthermore, we demonstrate that these ceramide-loaded nanoparticles are

able to enter HeLa cells and induce significant toxicity. To our knowledge, this is the first example of bioactive lipids being loaded onto graphene nanoparticles using such a method.

Methods

Materials

C_6-Ceramide and NBD Ceramide (C_6 N-[6-[(7-nitro-2-1,3-benzoxadiazol-4-yl)amino]hexanoyl]-D-erythro-sphingosine) were purchased from Avanti Polar Lipids (Alabaster, AL, USA). DSPE-PEG was purchased from NOF America Corporation (White Plains, NY, USA). All other materials and reagents were purchased from Sigma-Aldrich (St. Louis, MO, USA) unless otherwise noted.

O-GNR and GNP Synthesis

O-GNRs were synthesized from multi-walled carbon nanotubes (MWCNTs) using the longitudinal unzipping method with centrifugation instead of filtration for purification[31]. Briefly, MWCNTs (150mg) were dispersed in 30 mL of concentrated sulfuric acid. After 3 hr, 750mg of potassium permanganate was added and then the mixture was stirred for 1 hr. The mixture was then heated to approximately 60 °C for 1 hr in an oil bath to complete the reaction. It was then allowed to cool to room temperature and was washed with dilute hydrochloric acid. The product was isolated by flocculation using ethanol and ether, followed by centrifugation at 3000 rpm and drying overnight in a vacuum oven.

GNPs were synthesized from graphite flakes using a modified Hummers Method[32].

Atomic Force Microscopy Characterization

Dispersions of O-GNRs and GNPs in ethanol were diluted to 1 μg/mL, and 10 μL of these dispersions were drop cast onto silicon wafers (Ted Pella, Inc.). The samples were

characterized using a V-shaped AFM cantilever of frequency f_c = 145–230, tip radius less than 10 nm, and spring constant k = 20–95 N/m (ACL-10, Applied NanoStructures, Inc., Mountain View, CA, USA). Imaging was performed using a NanoSurf® EasyScan 2 FlexAFM (NanoScience Instruments, Inc., Phoenix, AZ, USA).

Loading of Ceramide onto Carbon Nanoparticles

O-GNRs or GNPs were dispersed in 100% ethanol at a concentration of 1 mg/mL using a bath sonicator. C_6 ceramide was dispersed in 100% ethanol at a concentration of approximately 150 μg/mL. 500 μL of the nanoparticle solution (either O-GNRs or GNPs) and 500 μL of the ceramide solution were added to a 20 mL glass scintillation vial. This mixture was bubbled with nitrogen gas and covered in parafilm to prevent oxidation of ceramide. It was then bath sonicated for 15 minutes to allow interspersion of individual nanoparticles and ceramide molecules.

To this solution, 9mL of double-distilled water were added using a New Era NE-300 syringe pump (New Era Pump Systems Inc. Farmingdale, NY, USA) over a period of two hours under constant mixing. However, the water was not added at a constant rate: for the first hour, water was added at a rate of 2 mL/hr, and for the second hour, water was added at a rate of 7 mL/hr. During the first 1.5 hrs of this loading process, the ceramide/nanoparticle mixture was subjected to mild sonication using a sonic cleaner to prevent the clumping of nanoparticles caused by the addition of water to ethanol. To separate ceramide-loaded nanoparticles from unloaded ceramide, the mixture was centrifuged at 4000 rpm for at least 30 minutes in a 15mL polypropylene conical tube. The supernatant was discarded, and the nanoparticles were washed by resuspension in pure double-distilled water and repeating the centrifugation step, yielding ceramide-loaded nanoparticles.

Quantification of Loading Using Mass Spectrometry

Samples were prepared for mass spectrometry by first resuspending ceramide-loaded nanoparticles in 100% ethanol and bath-sonicating for 1 hr, to force ceramide to dissociate from the nanoparticles. The mixture was centrifuged at 13000 rpm for 1 hr to ensure all nanoparticles were concentrated at the bottom. 100 μL of the supernatant was extracted for mass spectrometry. 100 μL of the ceramide stock solution used for loading was also analyzed as a basis of comparison to calculate loading efficiency. Samples were analyzed using a Fisons MD800 Gas Chromatography Mass Spectrometer. The signals generated from samples were correlated to a standard curve to calculate the exact concentration of ceramide.

Cell Culture

HeLa cervical cancer cells, MDA-MB-231 breast cancer cells, and U87MG glioblastoma cells were obtained from ATCC (Manassas, VA, USA). NIH 3T12 cells were a kind gift from Dr. Laurie Krug. All cells except MDA-MB-231 were grown in Dulbecco's Modified Eagle Medium (DMEM) supplemented with 10% fetal bovine serum and 1% penicillin-streptomycin. MDA-MB-231 were grown in RPMI supplemented with 10% fetal bovine serum and 1% penicillin-streptomycin. Cells were grown at 37 °C in a humidified atmosphere of 5% carbon dioxide.

PrestoBlue Viability and Apoptosis Assays

Cells were seeded in flat-bottomed 96 well plates at a density of 5000 cells/well and were allowed to adhere overnight. Ceramide-loaded nanoparticles (O-GNRs or GNPs) were added to each well at various concentrations ranging from 10-100 μg/mL of nanoparticles. To ensure that any observed decrease in viability compared to untreated cells could not be attributed to the loading process, we repeated the loading process with only nanoparticles and incubated them

with HeLa cells at the highest concentration used (100 μg/mL). After 24 hours, the media was aspirated, and each well was rinsed twice with PBS. A mixture of 10 μL of Presto Blue Viability Reagent (Life Technologies, Grand Island, NY, USA) and 90 μL of DMEM or RPMI with 10% FBS and 1% P/S were added to each well and placed back in the incubator. After 2 hours, the plates were removed, and the fluorescence intensity of each well was measured using a Molecular Devices SpectraMax M2e (Sunnyvale, CA, USA) with an excitation wavelength of 560 nm and an emission wavelength of 590 nm. Lysed cells were used as a positive control, and untreated cells were used as a negative control. The cell viability is expressed as a percent of the lysis control with the formula $\left((I_{test} - I_{blank})/(I_{control} - I_{blank}) \times 100\%\right) - 100\%$, where I_{test} is the fluorescence intensity of cells exposed to ceramide-loaded nanoparticles, $I_{control}$ is the fluorescence intensity of lysed cells, and I_{blank} is the fluorescence intensity from empty wells.

In a separate experiment, the efficacy of ceramide-loaded O-GNRs was compared to free C_6 ceramide in HeLa cells. A stock solution of C_6 ceramide in 100% ethanol or ceramide-loaded O-GNRs in water were diluted in water to concentrations ranging from 2-10 μg/mL of C_6 ceramide. Ethanol diluted in water or O-GNRs alone served as a control for the delivery vehicle. Viability was assessed with PrestoBlue using identical methods as described above.

Apoptosis was assessed at the highest levels of nanoparticles tested using a Biovision Caspase 3 Fluorometric Assay (Biovision, San Francisco, CA). Fluorescence was measured using a Molecular Devices SpectraMax M2e with an excitation of 400nm and an emission of 505nm.

Hoechst Stain for Apoptosis

HeLa cells were seeded at a density of 7.5 x 10^4 cells/mL in 6 well plates and allowed to attach overnight. Ceramide-loaded O-GNRs were added at a concentration of 40 μg/mL for 24 hrs, with non-loaded O-GNRs serving as a control. After 24 hrs, the media was removed and saved. Cells were then rinsed with PBS (which was also saved) and then trypsinized. Detached cells were added together with the removed DMEM and PBS, and centrifuged at 1000 rpm for 5 minutes. The pellet was resuspended in 10% paraformaldehyde until needed. To visualize apoptotic nuclei, the cells were centrifuged and resuspended in a 1% solution of bisBenzimide H 33342 trihydrochloride for 10 minutes. Cells were imaged using a Zeiss Axio Imager M2 (Thornwood, NY, USA) with an excitation wavelength of ~350 nm and emission wavelength of ~460 nm.

Live-Cell Confocal Microscopy of HeLa Cells

To visualize the uptake of ceramide-loaded nanoparticles into cells, we loaded O-GNRs with C_6 ceramide conjugated to 4-Chloro-7-nitrobenzofurazan (NBD-ceramide). HeLa cells were seeded in glass-inset confocal dishes at a density of 7.5 x 10^4 cells/mL with 2 mL per plate and allowed to adhere overnight. The following day, cells were placed in a LiveCell™ stage top incubation platform (Pathology Devices Inc., Westminster, MD, USA) and NBD-ceramide-loaded O-GNRs were added to these plates at a concentration of 40 μg/mL. As a control, cells were also incubated with an equivalent amount of NBD-ceramide in ethanol in a separate experiment. The cells were then imaged using a Leica TCS SP8 Laser Scanning Confocal Microscope System (Buffalo Grove, IL, USA) over a period of one hour at two-minute intervals.

TEM Visualization of Uptake of C6 Ceramide-Loaded O-GNRs

HeLa cells were grown on ACLAR® film (Electron Microscopy Sciences, Hatfield, PA) in 6 well plates at a density of 20000 cells per well and allowed to settle overnight. The

following day, cells were exposed to C_6 ceramide-loaded O-GNRs for one hour. The cells were subsequently fixed with 2.5% glutaraldehyde (Electron Microscopy Sciences, Hatfield, PA) in 0.1 M PBS for 15 minutes at room temperature. The films were then placed in 2% osmium tetroxide in 0.1 M PBS, dehydrated through graded ethanol washes, and embedded using durcupan resin. The embedded specimens were screened for areas with high cell densities, and these areas were cut into 80 nm sections using an Ultracut E microtome (Reichert-Jung, Cambridge, UK), and placed on formvar-coated copper grids. Sections were imaged using a Tecnai Bio Twin G transmission electron microscope (FEI, Hillsboro, OR), at 80 kV. Images were acquired using an XR-60 CCD digital camera system (AMT, Woburn, MA).

Statistical Analysis

Data are presented as mean ± standard deviation for PrestoBlue assays (n = 6). One-way ANOVA was used to make multiple comparisons between groups, and Tukey-Kramer post hoc analysis was used to determine where significant differences occurred. Statistical analysis was performed using a 95% confidence interval ($p < 0.05$) with GraphPad Prism.

Results

AFM Characterization

O-GNRs characterized with AFM had a size range of mainly 50-2500 nm with a high aspect ratio characteristic of carbon nanotubes. Several particles were as long as 8000 nm (Fig. 3.1A). The thickness of these particles ranged from 4-10 nm, indicating that they were several-layers thick. The observed dimensions for GNPs were much smaller in range, mainly between 20 and 500 nm with slightly irregular shapes and aspect ratios closer to one (Fig. 3.1B). The

observed thickness of GNPs was comparable to O-GNRs, with thicknesses ranging between 2 and 12 nm.

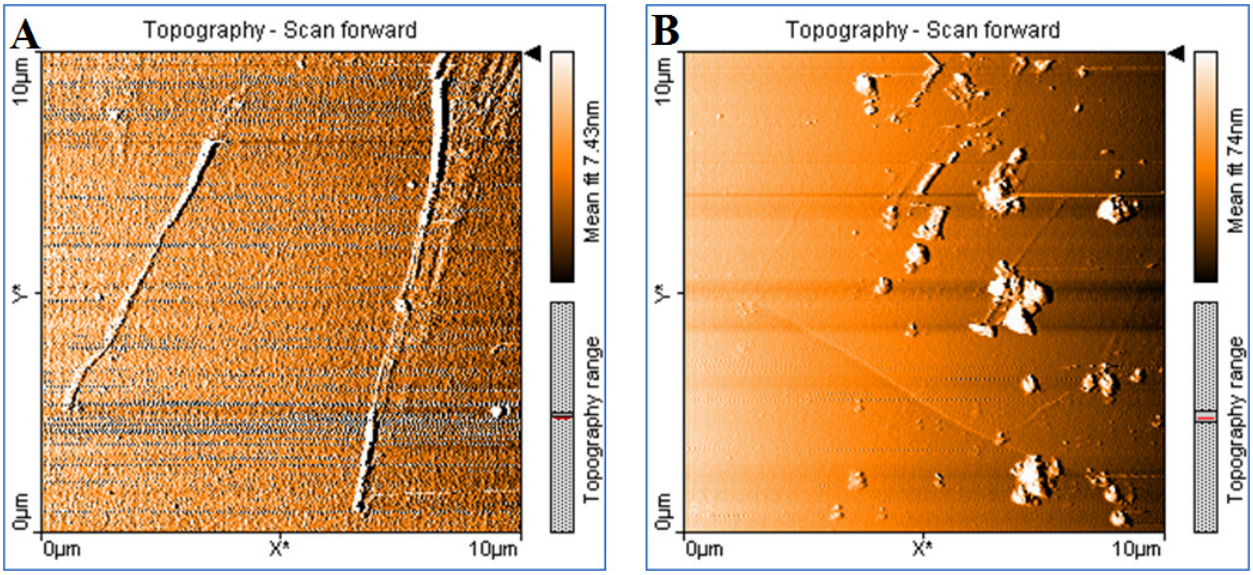

Figure 3.1. Atomic Force Microscopy images of **A)** O-GNRs and **B)** GNPs.

C_6 Ceramide Loading onto Graphene Nanoparticles

Figure 3.2 displays the raw data readout of relative abundances of C_6 ceramide as determined by mass spectrometry. The readout is standardized with the stock solution as 100 (Fig. 3.2A) to which the relative abundances of C_6 ceramide loaded onto O-GNRs (Fig. 3.2B) and GNPs (Fig. 3.2C). Although these raw data show the relative differences of O-GNR and GNP C_6 ceramide loading, the actual concentrations of ceramide found need to be determined from a C_6 standard curve calculated with known concentrations of C_6 ceramide. Using this standard curve, we determined that the loading efficiencies for O-GNRs and GNPs were approximately 57% and 51.5%. On a mass per mass basis, this represents at least a 50% increase in incorporation efficiency compared to C_6 ceramide incorporation into liposomes[23].

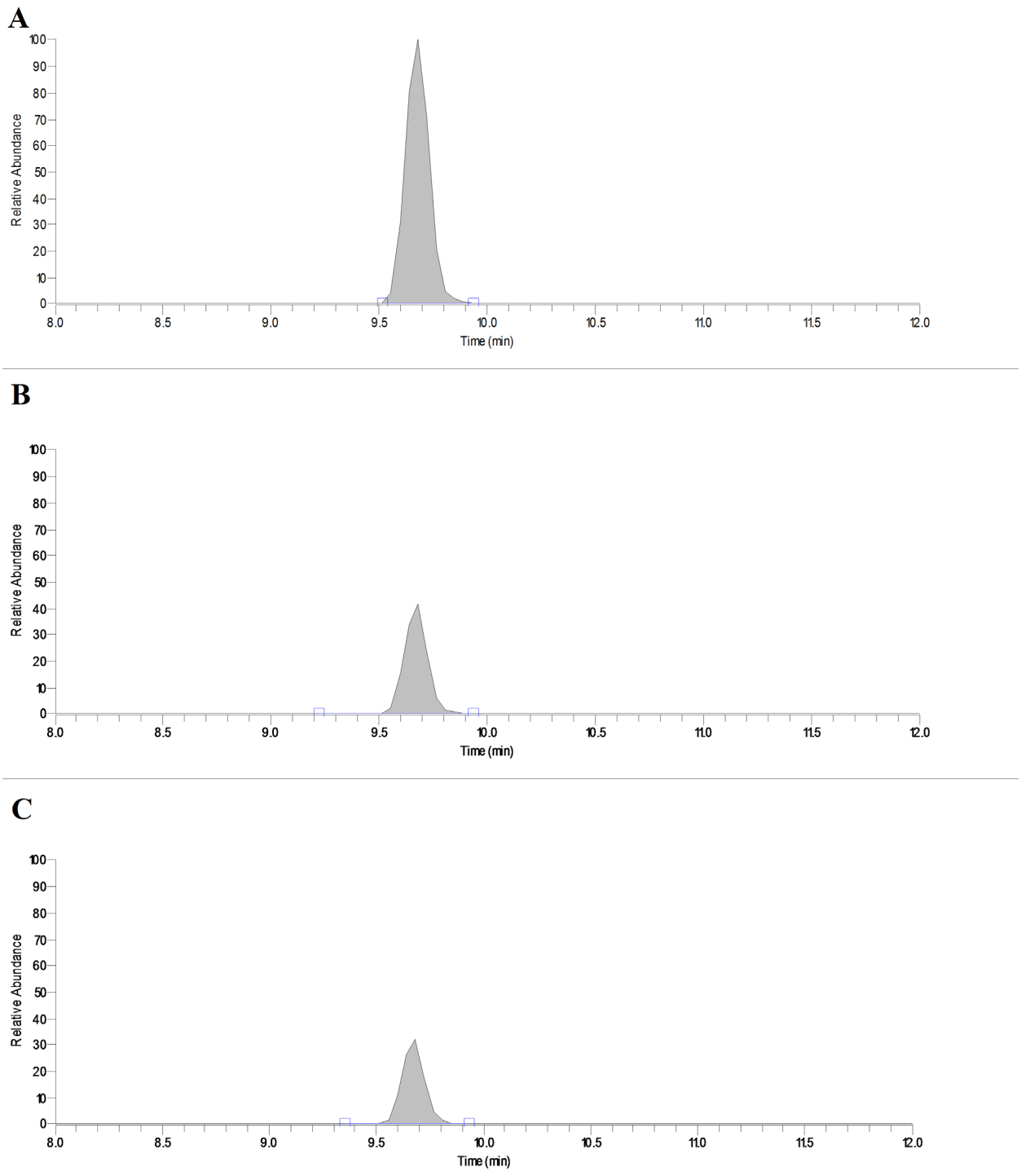

Figure 3.2. Mass spectrometry readouts showing the relative abundance of C_6 ceramide over time for **A)** the C_6 ceramide stock solution **B)** C_6 ceramide loaded onto O-GNRs **C)** and C_6 ceramide loaded onto GNPs.

PrestoBlue Viability and Apoptosis Assays

After determining that our loading method was loading high amounts of ceramide onto nanoparticles, we wanted to determine if our delivery system was capable of toxicity to HeLa cells. PrestoBlue is a resazurin dye that can be reduced by living cells to a form that fluoresces intensely at 590 nm when excited at 560 nm. Thus, the fluorescence measured from this dye is directly related to the level of cell viability in each well. We incubated HeLa cells with concentrations of O-GNRs and GNPs loaded with C_6 ceramide ranging from 10-100 µg/mL of nanoparticles. After 2 hours of incubation with PrestoBlue, we determined that C_6 ceramide-loaded O-GNRs and GNPs were significantly toxic to all concentrations tested (Figs. 3.3A, B). For O-GNRs, 100 µg/mL greatly reduced cell viability, which was only 5.51% more viable than the lysis control. Even at the lowest concentration tested (10 µg/mL), these cells were only 39% more viable than lysed cells (Fig. 3.3A). For GNPs, at the highest concentration of 100 µg/mL tested, cells were only 12.41% more viable than lysed cells, and 60.12% more viable than lysed cells at the lowest concentration tested.

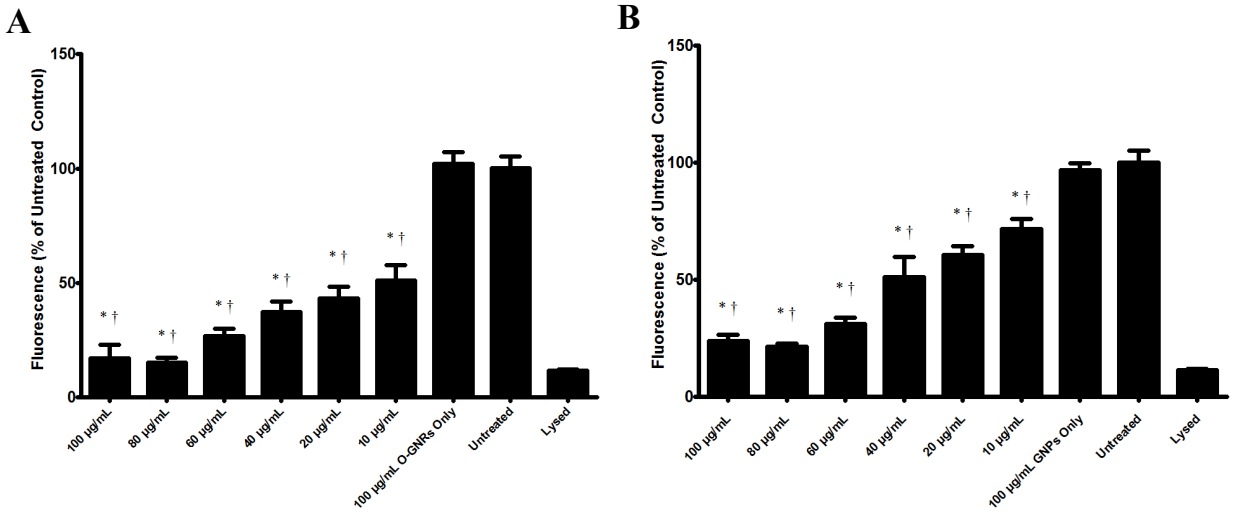

Figure 3.3. Viability of HeLa cells assessed by PrestoBlue after 24hrs of incubation with **A)** C_6 ceramide-loaded O-GNRs or **B)** C_6 ceramide-loaded GNPs. O-GNRs and GNPs not loaded with

C_6 ceramide served as controls. * indicates significant difference from "Untreated." † indicates significant difference from "100 μg/mL O-GNRs/GNPs only."

Since carbon nanoparticles are often combined with agents that increase their dispersibility in aqueous solution, we wanted to see if using such a dispersion agent would have any negative effect on the toxicity of our C_6 ceramide delivery system. Thus, after loading and washing our C_6 ceramide-loaded nanoparticles, we resuspended them in a 1.2 mg/mL solution of DSPE-PEG - which we have previously used with graphene nanoparticles – and repeated our PrestoBlue viability assay. Figures 3.4A and 3.4B show that resuspension in DSPE-PEG did not have a negative impact on the toxicities of C_6 ceramide-loaded O-GNRs and C_6 ceramide-loaded GNPs, respectively. HeLa cells incubated with C_6 ceramide-loaded O-GNRs were only 4.01% and 40.5% more viable than lysed cells at concentrations of 100 μg/mL and 10 μg/mL, respectively, which was very significant compared to the viability of untreated cells, and cells treated with O-GNRs only (Fig. 3.4A). This toxicity was relatively the same compared to cells incubated with C_6 ceramide-loaded O-GNRs not resuspended in DSPE-PEG (Fig. 3.3A). There was a similar result in toxicity for cells incubated with C_6 ceramide-loaded GNPs in DSPE-PEG, with a reduction in viability of 20.82% and 69.61% at concentrations of 100 μg/mL and 10 μg/mL, respectively (Fig. 3.4B).

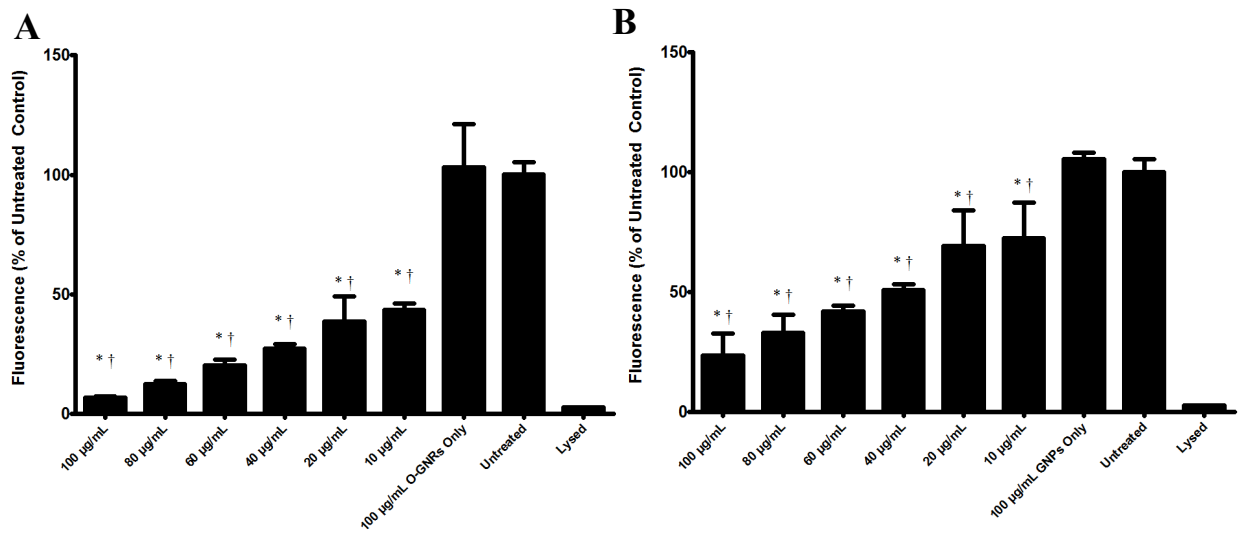

Figure 3.4. Viability of HeLa cells assessed by PrestoBlue after 24hrs of incubation with **A)** C_6 ceramide-loaded O-GNRs resuspended in PEG-DSPE or **B)** C_6 ceramide-loaded GNPs resuspended in PEG-DSPE. O-GNRs and GNPs not loaded with C_6 ceramide served as controls. * indicates significant difference from "Untreated." † indicates significant difference from "100 µg/mL O-GNRs/GNPs only."

We also found that C_6 ceramide-loaded O-GNRs were significantly more toxic than C_6 ceramide in ethanol alone at concentrations of 8, 4, and 2 µg/mL (Fig. 3.5A). At the highest level of toxicity (8 µg/mL), HeLa cell viability was 34.34% greater than lysed cells for C_6 ceramide-loaded O-GNRs, while HeLa cell viability was 55.8% greater than lysed for C_6 ceramide alone (Fig. 3.5A). Apoptosis, as determined by caspase-3 activity, showed that C_6 ceramide-loaded O-GNRs, C_6 ceramide-loaded GNPs, and C_6 ceramide alone had equally high levels of apoptosis (Fig. 3.5B). GNPs and O-GNRs alone did not cause a significant increase in caspase 3 activity (Fig. 3.5B).

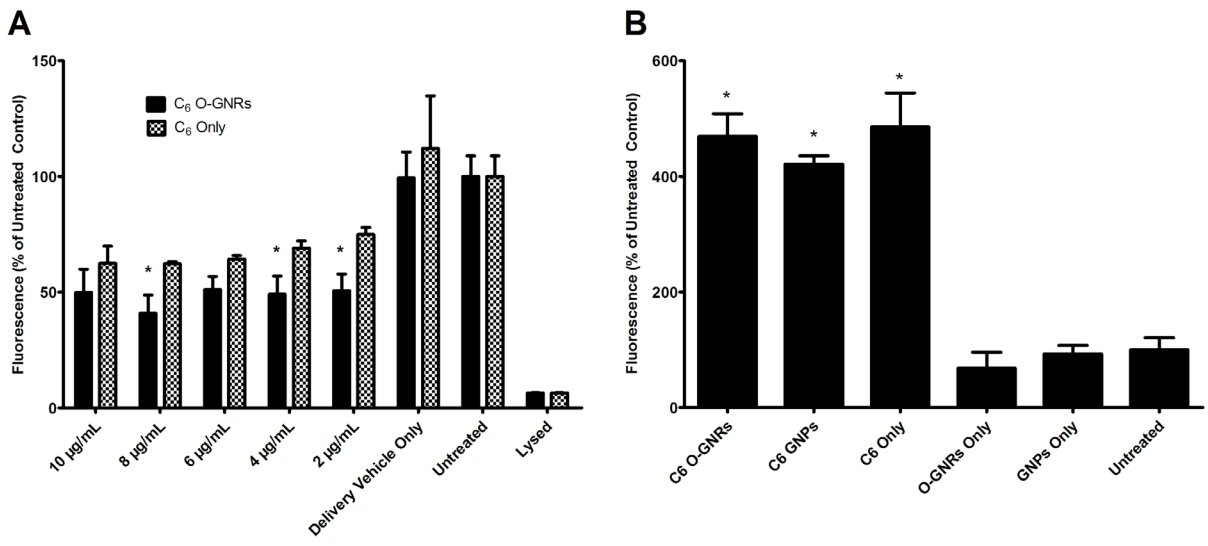

Figure 3.5. A) Viability of HeLa cells assessed by PrestoBlue after 24 hrs of incubation with C_6 ceramide-loaded O-GNRs or C_6 ceramide alone. * indicates significant difference from "C_6 only" at the respective concentration. **B)** Apoptosis level in HeLa cells determined by caspase-3 activity. * indicates difference from "untreated."

We also tested three other cell lines with C_6 ceramide-loaded O-GNRs to see how the performance of this delivery system would compare to the results seen in HeLa cells. U87MG and MDA-MB-231 had similar reductions in viability to HeLa cells, with all C_6 ceramide-loaded O-GNR conditions being significantly less viable than untreated controls (Fig. 3.6A and B). However, NIH-3T12 cells were only significantly different from untreated controls to a concentration of 60 µg/mL (Fig. 3.6 C). This indicates that low levels of C_6 ceramide-loaded O-GNRs were not as toxic to non-cancerous cells as they are to cancer cell lines. C_6 ceramide-loaded O-GNRs were also able to induce high levels of apoptosis in all 3 cell lines tested, as measured by caspase-3 activity (Fig 3.6D).

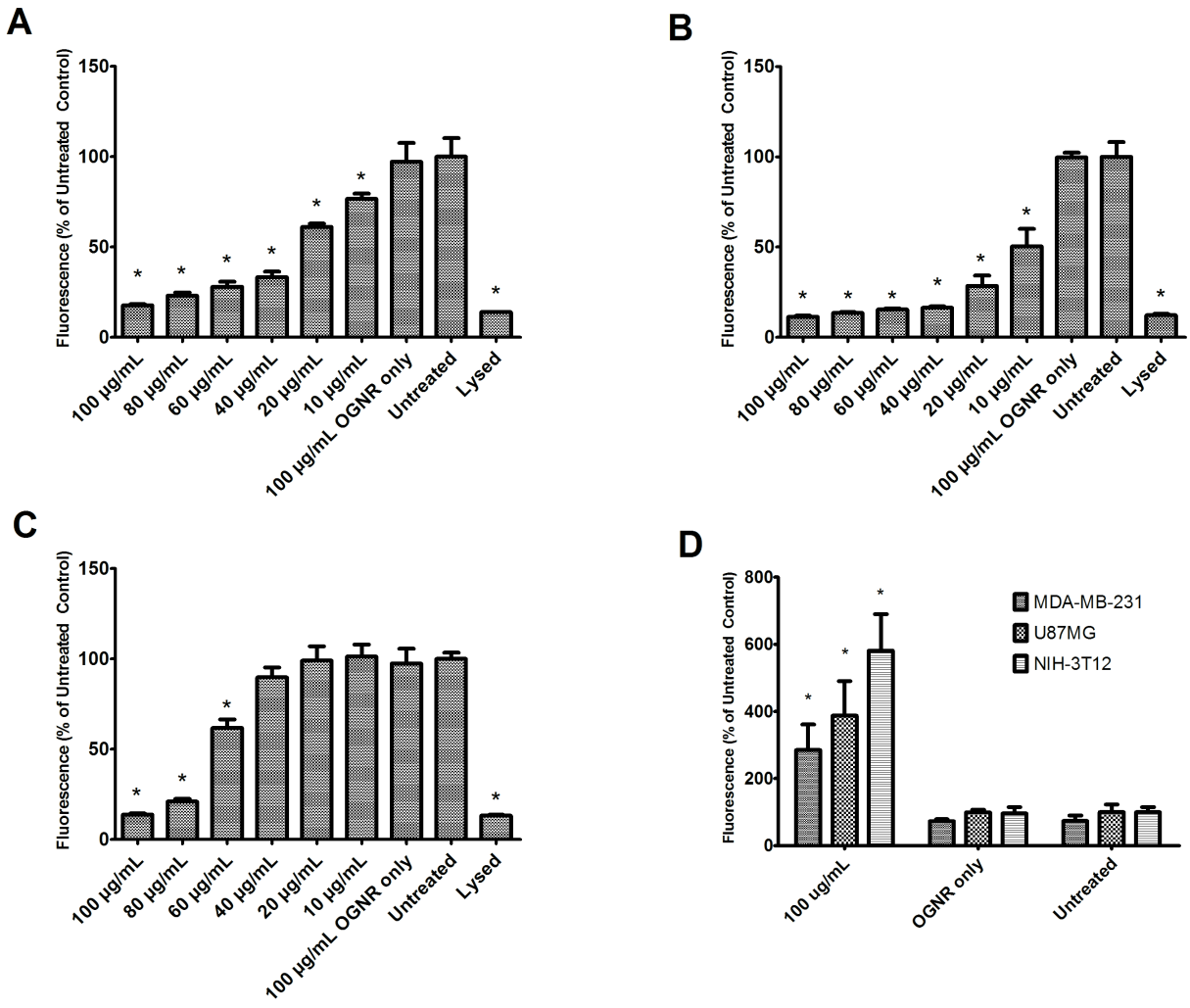

Figure 3.6. Viability of A) U87MG glioblastoma cells B) MDA-MB-231 breast cancer cells C) NIH-3T12 fibroblasts after 24hr of treatment with C_6 ceramide-loaded O-GNRs as determined by Prestoblue. D) Apoptosis of these cell lines after 24 hr of treatment with C_6 ceramide-loaded O-GNRs as determined by caspase-3 activity. "*" indicates significant difference from "untreated" control.

Hoechst Stain for Apoptosis

Although caspase-3 activity revealed that the cell death we observed from our C_6 ceramide-loaded nanoparticles was apoptotic in nature, we wanted further confirmation through direct observation. Hoechst stain binds to DNA, and under UV light, apoptotic cells appear much brighter than their non-apoptotic counterparts as a result of condensed chromatin and nuclear

fragmentation. HeLa cells stained with bisbenzimide displayed bright nuclei (Fig. 3.7A) and nuclear fragmentation (Fig. 3.7B) characteristic of apoptosis. By contrast, HeLa cells exposed to 40 μg/mL O-GNRs did not exhibit any signs of apoptosis (Fig. 3.7C) despite the presence of high levels of O-GNRs on the surface of cells (Fig. 3.7D). This indicates that our C_6 ceramide-loaded O-GNRs, and not unloaded O-GNRs, were inducing significant levels of apoptosis.

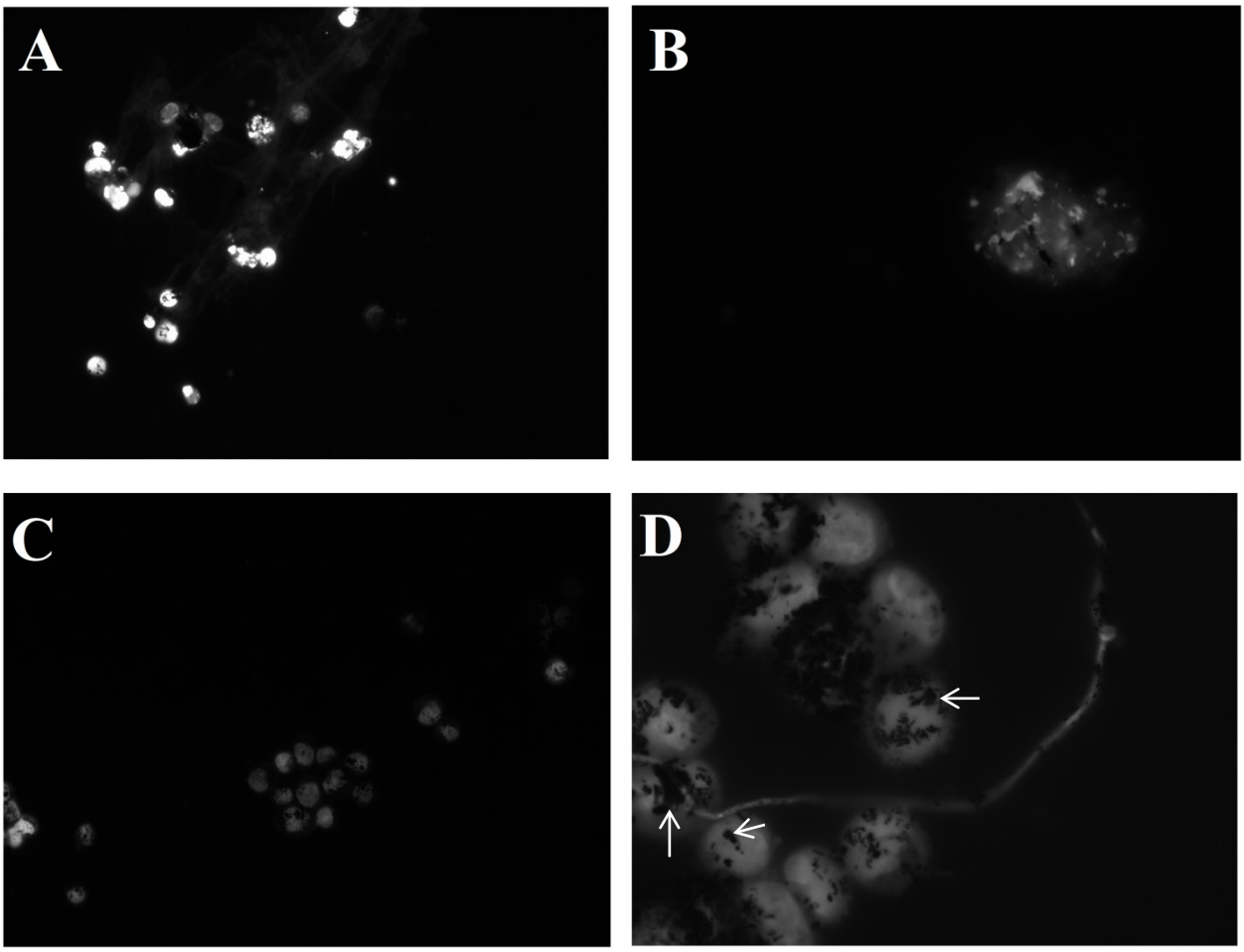

Figure 3.7. Hoechst staining for apoptosis in HeLa cells after 24-hour exposure to C_6 ceramide-loaded O-GNRs (**A, B**) or O-GNRs alone (**C, D**). **A)** Cells exposed to C_6 ceramide-loaded O-GNRs display bright nuclei after 24 hours, indicating apoptosis. **B)** A single cell nucleus displaying fragmentation characteristic of apoptosis after treatment with C_6 ceramide-loaded O-GNRs. **C)** Cells exposed to O-GNRs only do not demonstrate significant levels of apoptosis after 24 hours. **D)** A closer image of cells treated with only O-GNRs shows that these cells come in contact with high numbers of O-GNRs (dark spots, indicated by arrows).

Live-Cell Confocal Microscopy of Fluorescent Ceramide

Figure 3.8 shows time-lapsed images (12-minute intervals) of live HeLa cells incubated with 40 μg/mL NBD ceramide-loaded O-GNRs. Although our prior experiments pointed to C_6 ceramide being the toxic component of our delivery system, it was not clear whether this toxicity was being caused by entry of ceramide into cells, or if there was some other mode of toxicity such as destabilization of the cell membrane that did not require entry of ceramide into the cells. By using the fluorescently-tagged NBD ceramide in our delivery system and combination with live cell imaging, it allows us to determine to which parts of the cells ceramide is localizing. Immediately after the addition of NBD ceramide-loaded O-GNRs, there was no visible fluorescence (Fig. 3.8A) and minimal fluorescence after 12 minutes (Fig. 3.8B). There is some green NBD fluorescence present after 24 minutes, possibly due to some NBD-ceramide on the O-GNRs crystallizing and falling off (Fig. 3.8C). Between 24 and 36 minutes, there is a sudden large increase in fluorescence, with some substructures of cells being visibly highlighted by NBD ceramide (Fig. 3.8D). This sudden increase in fluorescence is possibly related to the uptake of O-GNRs, which are uptaken into HeLa cells in as little as 15 minutes[33]. The intensity of this fluorescence continued to increase after 48 and 60 minutes, indicating that the entry of NBD ceramide into HeLa cells did not diminish over time and possibly continued beyond the one-hour time frame of our study (Figs. 3.8E and F).

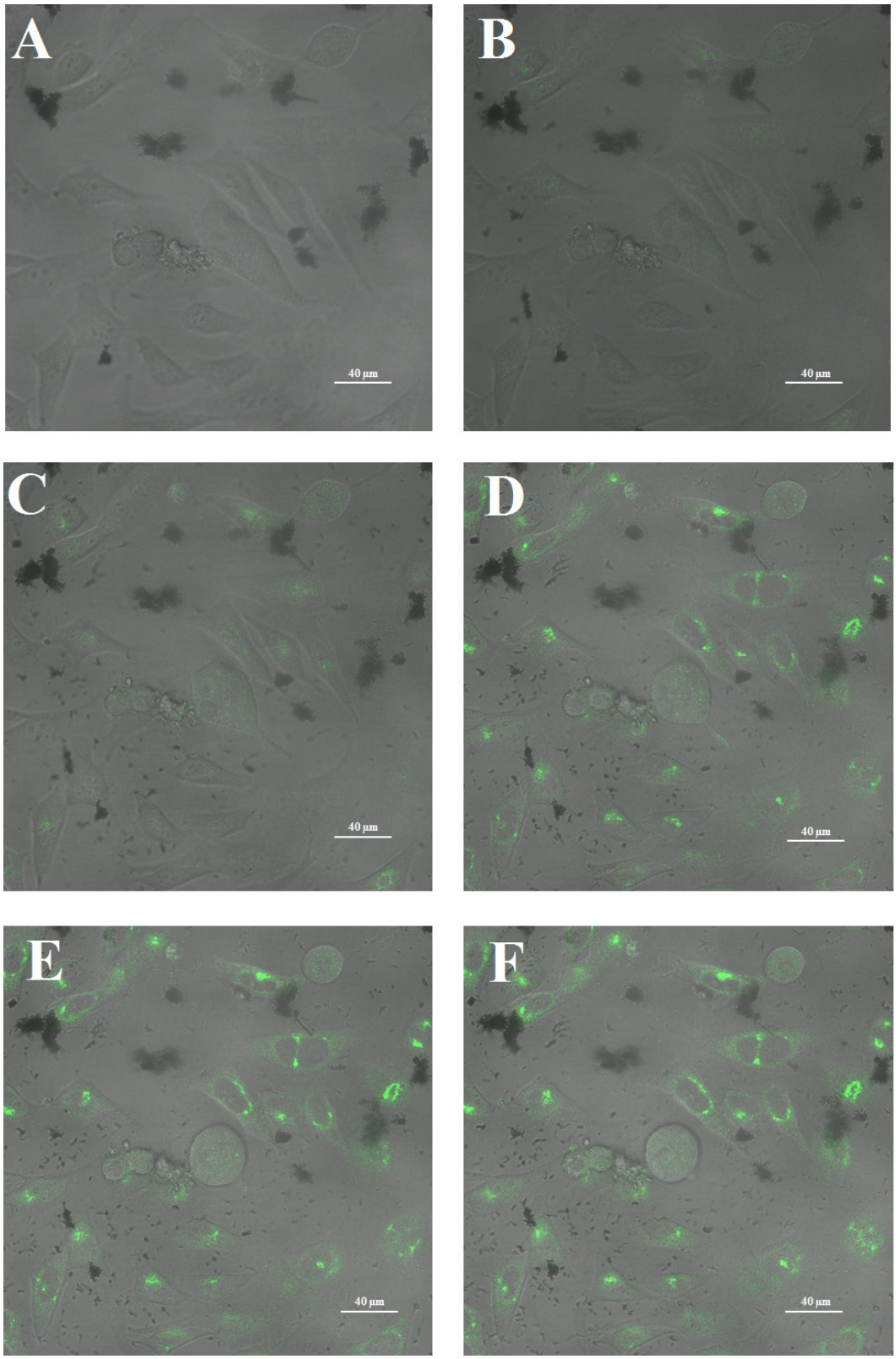
A
40 µm
B
40 µm
C
40 µm
D
40 µm
E
40 µm
F
40 µm

Figure 3.8. Time-lapsed confocal microscopy images of HeLa cells incubated with NBD ceramide loaded O-GNRs **A)** after initial additional of O-GNRs (t = 0 minutes), **B)** after 12 minutes, **C)** after 24 minutes, **D)** after 36 minutes, **E)** after 48 minutes, and **F)** after 60 minutes. There is no fluorescence from ceramide present initially (**A**) and some fluorescence present after 24 minutes have passed (**B and C**). There is a large increase in fluorescence between 24 minutes and 36 minutes, possibly due to the uptake of NDB-ceramide loaded O-GNRs (**D**). This fluorescence does not diminish over time, indicating a non-transient effect (**E and F**).

To see if there was a difference in the uptake between our C_6 ceramide-loaded O-GNRs and C_6 ceramide alone, we performed the same experiment using an equal concentration of NBD-ceramide in ethanol alone. HeLa cells incubated with NBD ceramide alone demonstrated a rapid uptake into HeLa cells. Before addition of NBD ceramide, there was no visible fluorescence (Supp. Fig. 3.1A). However, between the time that the NBD ceramide was added, and we began taking images, there was already a large amount of observable fluorescence (Supp. Fig. 3.1B). Compared to the slower increase in fluorescence seen with NBD-ceramide-loaded O-GNRs, this rapid uptake profile with free NBD ceramide would suggest that NBD ceramide loaded onto O-GNRs is not merely dissociating from the nanoparticles in proximity to cells, but remaining bound to the O-GNRs and being released as the nanoparticles are uptaken by the cells.

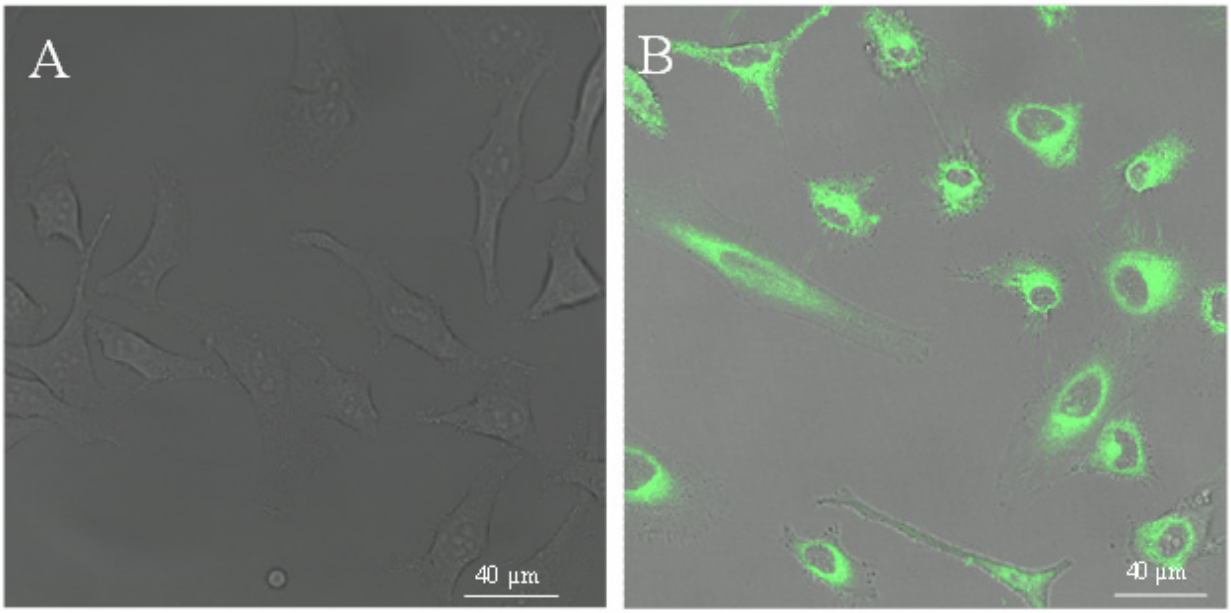

Supplementary Figure 3.1. Live Cell Confocal Microscopy images of HeLa cells (A) prior to addition of NBD-ceramide and (B) after 7 minutes of exposure to NBD ceramide.

TEM of C_6 Ceramide-Loaded O-GNRs Uptake into HeLa Cells

Although there were large aggregates of O-GNRs visible under confocal microscopy (Fig. 3.8), the much smaller particles that would be actually be entering cells and delivering ceramide were not visible from this magnification. Moreover, while we have previously shown uptake of these particles into cells, it was not clear if the loading of ceramide onto O-GNRs were altering the route of entry into cells, or if these nanoribbons were entering cells at all. Figure 3.9 shows TEM images of HeLa cells incubated with C_6 ceramide-loaded O-GNRs for one hour. There was a high degree of uptake of O-GNRs, with many O-GNRs of different shapes and sizes contained within vacuoles visible (Figs. 3.9A and 3.9B). Further examination of other HeLa cells in the samples revealed the uptake process in progress, with the outward blebbing of the cell membrane to surround the O-GNRs clearly visible (Figs. 3.9C and 3.9D, white arrows). This uptake modality of O-GNRs is similar to the macropinocytotic-like process previously observed

in HeLa cells[34,35]. As such, it does not seem that loading ceramide onto O-GNRs affects their entry into HeLa cells.

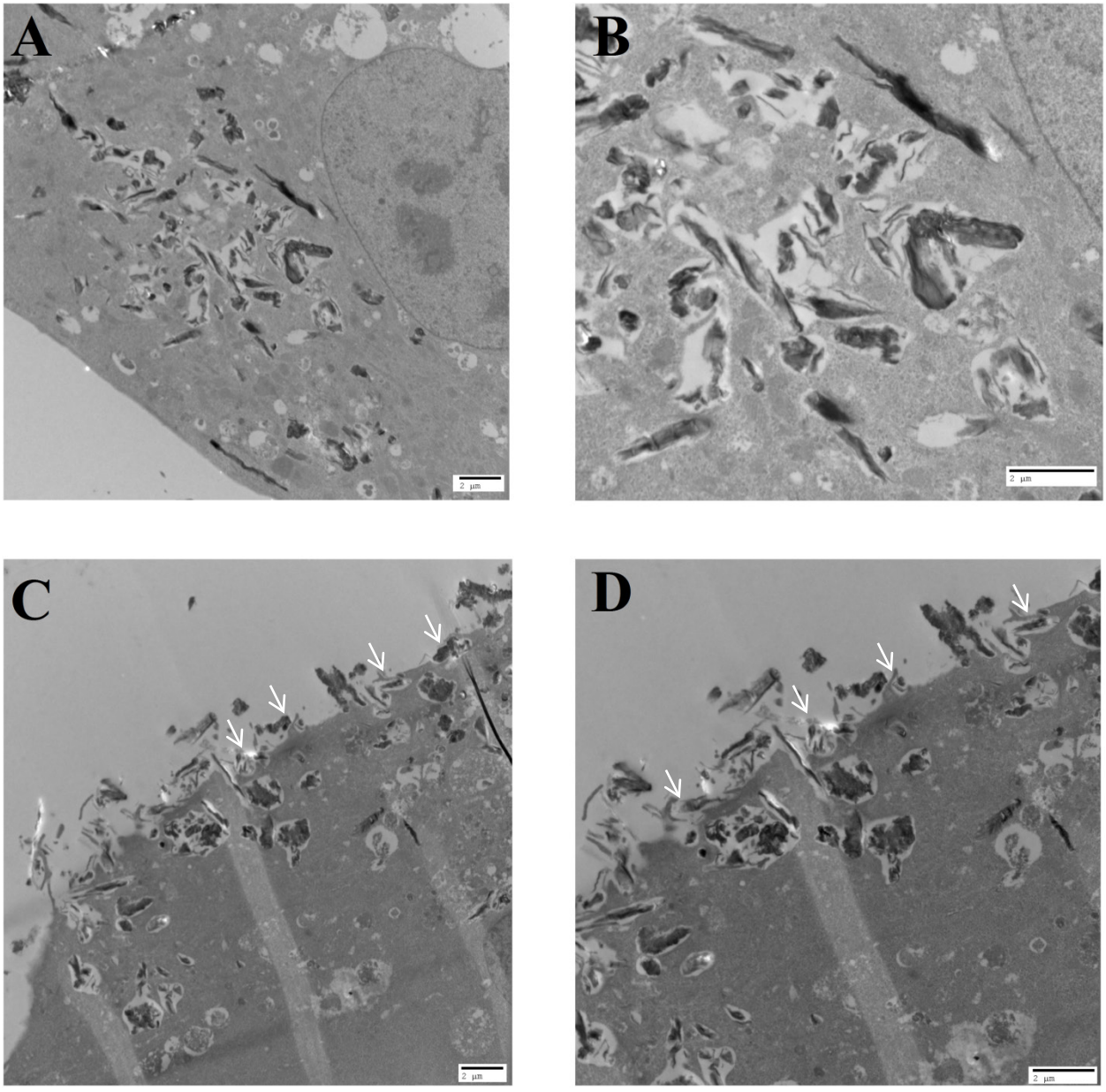

Figure 3.9. Transmission electron microscopy images of HeLa cells incubated with C_6 ceramide-loaded O-GNRs after one hour. **A)** After one hour, there are many O-GNRs present in

the cells contained in vacuoles. **B)** A zoomed-in perspective shows O-GNRs of different sizes and shapes in these vacuoles. **C)** Uptake of O-GNRs into HeLa cells shows the same macropinocytotic-like features found in previous studies (indicated by arrows). **D)** A closer view reveals the blebbing of the cell membrane around the O-GNRs characteristic of the macropinocytotic-like process previously found, indicating that loading of ceramide onto O-GNRs does not significantly alter the process by which these particles enter cells.

Discussion

Ceramide represents an untapped therapeutic target for cancer research and treatment. Despite its potent pro-apoptotic effects, there is currently no clinically-approved *in vivo* method of delivering ceramide. To this end, we have developed a method for loading the short-chain C_6 ceramide onto graphene nanoparticles.

There has been previous work studying the interaction between lipids and graphene nanoparticles. For example, Okamoto *et al.* were able to form lipid bilayers on GNPs[36]. However, the procedure required formation of these liposomes prior to loading onto GNPs. There was also a study by Hirtz *et al.* that used dip-pen nanolithography (DPN) to deposit phospholipids in a spatially controlled manner to form specific patterns of lipid bilayers, which did not require pre-formation of liposomes[37]. However, as the authors note, the "ink" for "writing" lipids onto the surface of graphene is not compatible with all lipids, and given the hydration method used to load phospholipids, it is most likely not compatible with the substantially more hydrophobic sphingolipids. In both cases, the purpose of the research was to form a supported lipid bilayer more for studying lipid bilayer mechanics than directly therapeutic goals. By comparison, our method does not rely on any specific formulation or manipulation of lipids themselves but achieves an interface between graphene and ceramide by bulk hydrophobicity. Moreover, although we have only tested ceramide, the theoretical basis for our

loading method could allow for other combinations of lipids to be loaded onto graphene nanoparticles.

We found that O-GNRs were able to load more C_6 ceramide than GNPs, representing a difference in loading efficiencies of approximately 6.5% (Fig. 3.2). However, the reason for this observed difference is not entirely clear. We have previously determined that O-GNRs actually show increased oxidation and decreased the prevalence of the hydrophobic sp^2 carbon structure characteristic of pristine graphene compared to GNPs[38]. This conflicts with our theoretical basis for the loading process; since the GNPs have less oxidation overall, they should be outperforming O-GNRs regarding ceramide loading efficiency. However, the explanation may lie in the different synthesis methods for GNPs and O-GNRs. O-GNRs are formed by the longitudinal unzipping of carbon nanotubes using concentrated acids and potassium permanganate, and the inside surface of innermost layer forms one of the outer surface of O-GNRs. This surface is relatively "protected" from the oxidizing conditions, and may not undergo extensive modification. By contrast, GNPs are synthesized by the oxidation and exfoliation of graphite flakes, and both surfaces are more evenly exposed to acids. In other words, although O-GNRs undergo more oxidation overall, this oxidation may be concentrated along the outer surface and edges of the nanoparticles, leaving a greater number of hydrophobic pockets on the inner surface and allowing more ceramide to bind.

This difference in loading is also reflected in viability as determined by PrestoBlue, where C_6 ceramide-loaded O-GNRs generally reduced HeLa cell viability more than C_6 ceramide-loaded GNPs. Although the toxicity of both systems was relatively the same at highest dose of 100 μg/mL, O-GNRs maintained higher toxicity all the way to the lowest dose of 10 μg/mL (Fig. 3.3). This same trend continued even when C_6 ceramide-loaded nanoparticles were

resuspended in DSPE-PEG (Fig. 3.4). Although this difference in cytotoxicity between the two types of nanoparticles could be partly due to the differences in loading, this could also possibly due to the selective uptake property of O-GNRs[34]. We have recently determined that O-GNRs are uptaken by cells through activation of EGFR and that this process is enhanced in cells that have an integrated HPV genome and express the viral E5 protein[35]. Since HeLa cells express both EGFR and E5[39], it is possible that at least the part of the difference between O-GNRs and GNPs in cytotoxicity is attributable to the enhanced uptake of O-GNRs, especially at lower concentrations. This is supported by the uptake of O-GNRs observed via TEM, which showed a significant number of visible nanoparticles taken up by HeLa cells (Fig. 3.9).

Although exogenous ceramide is not normally soluble in aqueous solution, it can be delivered *in vitro* to cells if it is first dissolved in an organic solvent such as ethanol. Upon delivery to the cell, ceramide tends to localize mostly in endosomes, particularly lysosomes[40]. Using live-cell confocal imaging of NBD-ceramide uptake into HeLa cells, we observed significant fluorescence in HeLa cells in as little as 24 minutes after delivery, and a large increase in fluorescence between the 24 minute and 36-minute time points (Fig 3.8C and D). However, while the fluorescence at 24 minutes is more generalized and even throughout parts of the cells, at 36 minutes there are endosomes exhibiting fluorescence (Fig. 3.8D). One possible explanation for this phenomenon is related to the macropinocytotic-like mechanism by which O-GNRs enter cells. Since we have previously confirmed that O-GNRs are uptaken by HeLa cells in as little as 15 minutes[33], this specific increase in fluorescence may correspond to a bulk uptake of O-GNRs loaded with NBD-ceramide, with a subsequent bulk release of NBD-ceramide from O-GNRs inside the macropinosome during its relatively rapid (2 - 4 minutes) maturation

process[41]. However, it is unclear what exactly what triggers the release of ceramide from the O-GNRs.

Conclusions

We have developed a quick, easy, and reliable method for the loading of ceramide onto oxidized graphene nanoparticles. Furthermore, we have demonstrated that these ceramide-loaded nanoparticles can induce apoptosis in HeLa cells and that the uptake of these nanoparticles occurs rapidly. This research represents a first step in realizing the goal of a therapeutic ceramide cancer treatment using graphene nanoparticles as a delivery system.

Acknowledgements

We would like to thank Susan Van Horn and the Central Microscopy Facility at Stony Brook University for her assistance with TEM. We would like to that Izolda Mileva and the Lipidomics Facility at Stony Brook University for her help with mass spectrometry.

References

1 Phillips, D. C. & Griffiths, H. R. Ceramide induces a loss in cytosolic peroxide levels in mononuclear cells. *Biochem J* **375**, 567-579, doi:10.1042/BJ20030693 (2003).

2 Lee, J. Y., Bielawska, A. E. & Obeid, L. M. Regulation of cyclin-dependent kinase 2 activity by ceramide. *Experimental cell research* **261**, 303-311, doi:10.1006/excr.2000.5028 (2000).

3 Phillips, D. C., Allen, K. & Griffiths, H. R. Synthetic ceramides induce growth arrest or apoptosis by altering cellular redox status. *Archives of biochemistry and biophysics* **407**, 15-24 (2002).

4 Lee, J. Y., Leonhardt, L. G. & Obeid, L. M. Cell-cycle-dependent changes in ceramide levels preceding retinoblastoma protein dephosphorylation in G2/M. *Biochem J* **334 (Pt 2)**, 457-461 (1998).

5 Pattingre, S., Bauvy, C., Levade, T., Levine, B. & Codogno, P. Ceramide-induced autophagy: To junk or to protect cells? *Autophagy* **5**, 558-560 (2009).

6 Schaefer, J. T., Barthlen, W. & Schweizer, P. Ceramide induces apoptosis in neuroblastoma cell cultures resistant to CD95 (Fas/APO-1)-mediated apoptosis. *Journal of pediatric surgery* **35**, 473-479 (2000).

7 Smyth, M. J., Obeid, L. M. & Hannun, Y. A. Ceramide: a novel lipid mediator of apoptosis. *Advances in pharmacology (San Diego, Calif.)* **41**, 133-154 (1997).

8 Wagenknecht, B., Roth, W., Gulbins, E., Wolburg, H. & Weller, M. C2-ceramide signaling in glioma cells: synergistic enhancement of CD95-mediated, caspase-dependent apoptosis. *Cell Death Differ* **8**, 595-602, doi:10.1038/sj.cdd.4400848 (2001).

9 Yoon, G. *et al.* Ceramide increases Fas-mediated apoptosis in glioblastoma cells through FLIP down-regulation. *Journal of neuro-oncology* **60**, 135-141 (2002).

10 Dumitru, C. A. & Gulbins, E. TRAIL activates acid sphingomyelinase via a redox mechanism and releases ceramide to trigger apoptosis. *Oncogene* **25**, 5612-5625, doi:10.1038/sj.onc.1209568 (2006).

11 Cuvillier, O. *et al.* Sphingosine generation, cytochrome c release, and activation of caspase-7 in doxorubicin-induced apoptosis of MCF7 breast adenocarcinoma cells. *Cell Death Differ* **8**, 162-171, doi:10.1038/sj.cdd.4400793 (2001).

12 Stiban, J., Tidhar, R. & Futerman, A. H. Ceramide synthases: roles in cell physiology and signaling. *Advances in experimental medicine and biology* **688**, 60-71 (2010).

13 Nirala, N. K. *et al.* Survival response to increased ceramide involves metabolic adaptation through novel regulators of glycolysis and lipolysis. *PLoS genetics* **9**, e1003556, doi:10.1371/journal.pgen.1003556 (2013).

14 Mesicek, J. *et al.* Ceramide synthases 2, 5, and 6 confer distinct roles in radiation-induced apoptosis in HeLa cells. *Cellular signalling* **22**, 1300-1307, doi:10.1016/j.cellsig.2010.04.006 (2010).

15 Osawa, Y. *et al.* Roles for C16-ceramide and sphingosine 1-phosphate in regulating hepatocyte apoptosis in response to tumor necrosis factor-alpha. *The Journal of biological chemistry* **280**, 27879-27887, doi:10.1074/jbc.M503002200 (2005).

16 Thomas, R. L., Jr., Matsko, C. M., Lotze, M. T. & Amoscato, A. A. Mass spectrometric identification of increased C16 ceramide levels during apoptosis. *The Journal of biological chemistry* **274**, 30580-30588 (1999).

17 Eto, M. *et al.* C16 ceramide accumulates following androgen ablation in LNCaP prostate cancer cells. *The Prostate* **57**, 66-79, doi:10.1002/pros.10275 (2003).

18 Eto, M., Bennouna, J., Hunter, O. C., Lotze, M. T. & Amoscato, A. A. Importance of C16 ceramide accumulation during apoptosis in prostate cancer cells. *International journal of urology : official journal of the Japanese Urological Association* **13**, 148-156, doi:10.1111/j.1442-2042.2006.01249.x (2006).

19 Aflaki, E. *et al.* C16 ceramide is crucial for triacylglycerol-induced apoptosis in macrophages. *Cell death & disease* **3**, e280, doi:10.1038/cddis.2012.17 (2012).

20 Paschall, A. V. *et al.* Ceramide targets xIAP and cIAP1 to sensitize metastatic colon and breast cancer cells to apoptosis induction to suppress tumor progression. *BMC cancer* **14**, 24, doi:10.1186/1471-2407-14-24 (2014).

21 Radin, N. S. Killing cancer cells by poly-drug elevation of ceramide levels: a hypothesis whose time has come? *European journal of biochemistry / FEBS* **268**, 193-204 (2001).

22 Mei, J., Wang, C. N., O'Brien, L. & Brindley, D. N. Cell-permeable ceramides increase basal glucose incorporation into triacylglycerols but decrease the stimulation by insulin in 3T3-L1 adipocytes. *International journal of obesity and related metabolic disorders : journal of the International Association for the Study of Obesity* **27**, 31-39, doi:10.1038/sj.ijo.0802183 (2003).

23 Khazanov, E., Priev, A., Shillemans, J. P. & Barenholz, Y. Physicochemical and biological characterization of ceramide-containing liposomes: paving the way to ceramide therapeutic application. *Langmuir : the ACS journal of surfaces and colloids* **24**, 6965-6980, doi:10.1021/la800207z (2008).

24 Liu, W. *et al.* Large scale pattern graphene electrode for high performance in transparent organic single crystal field-effect transistors. *ACS nano* **4**, 3927-3932, doi:10.1021/nn100728p (2010).

25 Lin, Y. M. *et al.* Wafer-scale graphene integrated circuit. *Science* **332**, 1294-1297, doi:10.1126/science.1204428 (2011).

26 Huang, P. *et al.* Folic Acid-conjugated Graphene Oxide loaded with Photosensitizers for Targeting Photodynamic Therapy. *Theranostics* **1**, 240-250 (2011).

27 Sun, X. *et al.* Nano-Graphene Oxide for Cellular Imaging and Drug Delivery. *Nano Res* **1**, 203-212, doi:10.1007/s12274-008-8021-8 (2008).

28 Koninti, R. K., Sengupta, A., Gavvala, K., Ballav, N. & Hazra, P. Loading of an anti-cancer drug onto graphene oxide and subsequent release to DNA/RNA: a direct optical detection. *Nanoscale* **6**, 2937-2944, doi:10.1039/c3nr06081k (2014).

29 Zhang, L., Xia, J., Zhao, Q., Liu, L. & Zhang, Z. Functional graphene oxide as a nanocarrier for controlled loading and targeted delivery of mixed anticancer drugs. *Small* **6**, 537-544, doi:10.1002/smll.200901680 (2010).

30 Chowdhury, S. M. *et al.* Graphene nanoribbons as a drug delivery agent for lucanthone mediated therapy of glioblastoma multiforme. *Nanomedicine : nanotechnology, biology, and medicine*, doi:10.1016/j.nano.2014.08.001 (2014).

31 Kosynkin, D. V. *et al.* Longitudinal unzipping of carbon nanotubes to form graphene nanoribbons. *Nature* **458**, 872-876, doi:10.1038/nature07872 (2009).

32 Hummers Jr, W. S. & Offeman, R. E. Preparation of graphitic oxide. *Journal of the American Chemical Society* **80**, 1339-1339 (1958).

33 Mullick Chowdhury, S., Manepalli, P. & Sitharaman, B. Graphene nanoribbons elicit cell specific uptake and delivery via activation of epidermal growth factor receptor enhanced by human papillomavirus E5 protein. *Acta biomaterialia* **10**, 4494-4504, doi:10.1016/j.actbio.2014.06.030 (2014).

34 Mullick Chowdhury, S. *et al.* Cell specific cytotoxicity and uptake of graphene nanoribbons. *Biomaterials* **34**, 283-293, doi:10.1016/j.biomaterials.2012.09.057 (2013).

35 Mullick Chowdhury, S., Manepalli, P. & Sitharaman, B. Graphene nanoribbons elicit cell specific uptake and delivery via activation of epidermal growth factor receptor enhanced by human papillomavirus E5 protein. *Acta biomaterialia*, doi:10.1016/j.actbio.2014.06.030 (2014).

36 Okamoto, Y. *et al.* Fabrication of Supported Lipid Bilayer on Graphene Oxide. *J Phys Conf Ser* **352**, doi:Artn 012017

Doi 10.1088/1742-6596/352/1/012017 (2012).

37 Hirtz, M., Oikonomou, A., Georgiou, T., Fuchs, H. & Vijayaraghavan, A. Multiplexed biomimetic lipid membranes on graphene by dip-pen nanolithography. *Nat Commun* **4**, doi:Artn 2591

Doi 10.1038/Ncomms3591 (2013).

38 Talukdar, Y., Rashkow, J. T., Lalwani, G., Kanakia, S. & Sitharaman, B. The effects of graphene nanostructures on mesenchymal stem cells. *Biomaterials* **35**, 4863-4877, doi:10.1016/j.biomaterials.2014.02.054 (2014).

39 Samama, B. *et al.* HPV DNA detection by in situ hybridization with catalyzed signal amplification on thin-layer cervical smears. *The journal of histochemistry and cytochemistry : official journal of the Histochemistry Society* **50**, 1417-1420 (2002).

40 Shabbits, J. A. & Mayer, L. D. Intracellular delivery of ceramide lipids via liposomes enhances apoptosis in vitro. *Biochimica et biophysica acta* **1612**, 98-106 (2003).

41 Racoosin, E. L. & Swanson, J. A. Macropinosome maturation and fusion with tubular lysosomes in macrophages. *The Journal of cell biology* **121**, 1011-1020 (1993).

Chapter 4

Oxidized Graphene Nanoribbons Protect HeLa Cells from UV-Induced Apoptosis Through Buffering of Reactive Oxygen Species

Contribution by: Cassandra Suhrland, Balaji Sitharaman

Abstract

Here we report the use of oxidized graphene nanoribbons (O-GNRs) derived from carbon nanotubes to protect HeLa cells from apoptosis induced by ultraviolet (UV) radiation. We find that O-GNRs added to cells after exposure to UV radiation were able to protect these cells from a loss in viability down to a concentration of 5 μg/mL. However, oxidized graphene nanoplatelets (GNPs) derived from graphite were not able to protect HeLa cells from UV-induced viability loss at any concentration. This property of O-GNRs was further supported by a reduction in apoptosis determined by caspase-3 activity. We determined that this could be explained in part by the buffering of reactive oxygen species generated from UV radiation. Taken together, these data indicate that O-GNRs may be able to partially protect cells from UV-induced damage at nontoxic concentrations.

Introduction

Graphene oxide is a two-dimensional nanoparticle with many biomedical applications in disciplines such as drug delivery, gene delivery, and biosensing[1-7]. It is comprised largely of carbon, but also many oxygen-containing functional groups. These oxygen-containing groups are chemically active, and it has previously been shown that they are capable of buffering reactive oxygen species (ROS) and preventing radiation-induced cell death[8]. Given that graphene oxide nanoparticles can differ greatly in their chemical properties depending on the starting material they were synthesized from[9], it is possible that nanoparticles synthesized from different starting materials may have differential effects on the efficacy of treatments such as ultraviolet (UV) radiation treatment. Here we show that oxidized graphene nanoribbons (O-GNRs) derived from carbon nanotubes can protect HeLa cells from UV-induced apoptosis, whereas oxidized graphene nanoplatelets (GNPs) are not.

Methods

All reagents were purchased from (Sigma-Aldrich St. Louis, MO, USA) unless otherwise noted. O-GNRs were synthesized from multi-walled carbon nanotubes (MWCNTs) using the longitudinal unzipping method with centrifugation instead of filtration for purification[10]. Briefly, MWCNTs (150mg) were dispersed in 30 mL of concentrated sulfuric acid. After 3 hr, 750mg of potassium permanganate was added and then the mixture was stirred for 1 hr. The mixture was then heated to approximately 60 °C for 1 hr in an oil bath to complete the reaction. It was then allowed to cool to room temperature and was washed with dilute hydrochloric acid. The product was isolated by flocculation using ethanol and ether, followed by centrifugation at 3000 rpm and drying overnight in a vacuum oven. GNPs were synthesized from graphite flakes using a modified Hummers Method[11].

HeLa cells were obtained from ATCC (Manassas, VA, USA). Cells were grown in Dulbecco's Modified Eagle Medium (DMEM) supplemented with 10% fetal bovine serum and 1% penicillin-streptomycin. Cells were grown at 37 °C in a humidified atmosphere of 5% carbon dioxide. For assays, cells were seeded in flat-bottomed 96 well plates at a density of 5000 cells/well and were allowed to adhere overnight. Cells were then exposed to ultraviolet (UV) radiation at 40 mJ/cm^2 using a Stratagene Stratalinker. Carbon nanoparticles (O-GNRs or GNPs) were added to each well at various concentrations ranging from 5-50 μg/mL of nanoparticles.

For viability determined by PrestoBlue, the media was aspirated after 24 hours, and each well was rinsed twice with PBS. A mixture of 10 μL of Presto Blue Viability Reagent (Life Technologies, Grand Island, NY, USA) and 90 μL of DMEM with 10% FBS and 1% P/S were added to each well and placed back in the incubator. After 2 hours, the plates were removed, and the fluorescence intensity of each well was measured using a Molecular Devices SpectraMax

M2e (Sunnyvale, CA, USA) with an excitation wavelength of 560 nm and an emission wavelength of 590 nm. The cell viability is expressed as a percent of the untreated control with the formula $\left((I_{test} - I_{blank})/(I_{control} - I_{blank}) \times 100\%\right)$, where I_{test} is the fluorescence intensity of cells exposed to UV and/or nanoparticles, $I_{control}$ is the fluorescence intensity of untreated cells, and I_{blank} is the fluorescence intensity from empty wells.

Caspase-3 activity was determined using a Biovision caspase-3 fluorometric assay kit. Briefly, 24 hours after exposure to UV radiation, media was aspirated, and wells were gently rinsed with PBS. After this, lysis buffer was added to each well, and the plates were incubated on ice for 10 minutes. After this, the assay reagents were added to each well, and the plates were placed back in 37°C. After 1 hour, the plates were removed, and the fluorescence intensity of each well was measured using a Molecular Devices SpectraMax M2e with an excitation wavelength of 400 nm and an emission wavelength of 505 nm. The caspase-3 activity is expressed as a percent of the untreated control with the formula $\left((I_{test} - I_{blank})/(I_{control} - I_{blank}) \times 100\%\right)$ where I_{test} is the fluorescence intensity of cells exposed to UV and/or nanoparticles, $I_{control}$ is the fluorescence intensity of untreated cells, and I_{blank} is the fluorescence intensity from empty wells.

ROS activity was measured using fluorescent ROS detector 2',7' –dichlorofluorescein diacetate (DCFDA). Cells were preincubated with 50 µg/mL O-GNRs for 4 hours and rinsed twice prior to irradiation. 100 µL of PBS was left in the wells while the cells were irradiated. 30 minutes after irradiation, DCFDA in PBS was added to the cells at a final concentration of 25 µM. After 1 hour, DCFDA fluorescence was measured at an excitation of 485 nm and an emission of 520 nm using a Molecular Devices SpectraMax M2e.

Results

Figure 4.1 shows the PrestoBlue viability of HeLa cells after exposure to 40 mJ/cm^2 of UV radiation and subsequent incubation with varying levels of O-GNRs and GNPs for 24 hours, normalized to untreated cells. At the maximum concentration of O-GNRs tested (50 μg/mL) the viability of cells exposed to UV radiation was 103.6% of the untreated control, while cells exposed to UV without nanoparticles were only 62.79% as viable as untreated cells. O-GNRs were able to significantly protect HeLa cells from UV-induced viability loss down to the lowest concentration tested of 5 μg/mL, being 79.0% as viable as untreated cells. However, GNPs were not able to protect HeLa cells from UV-induced viability loss at any concentration, with no significant difference between cells treated with GNPs and cells exposed to UV without nanoparticles. The nanoparticles themselves had no significant effect on cell viability in the absence of UV radiation.

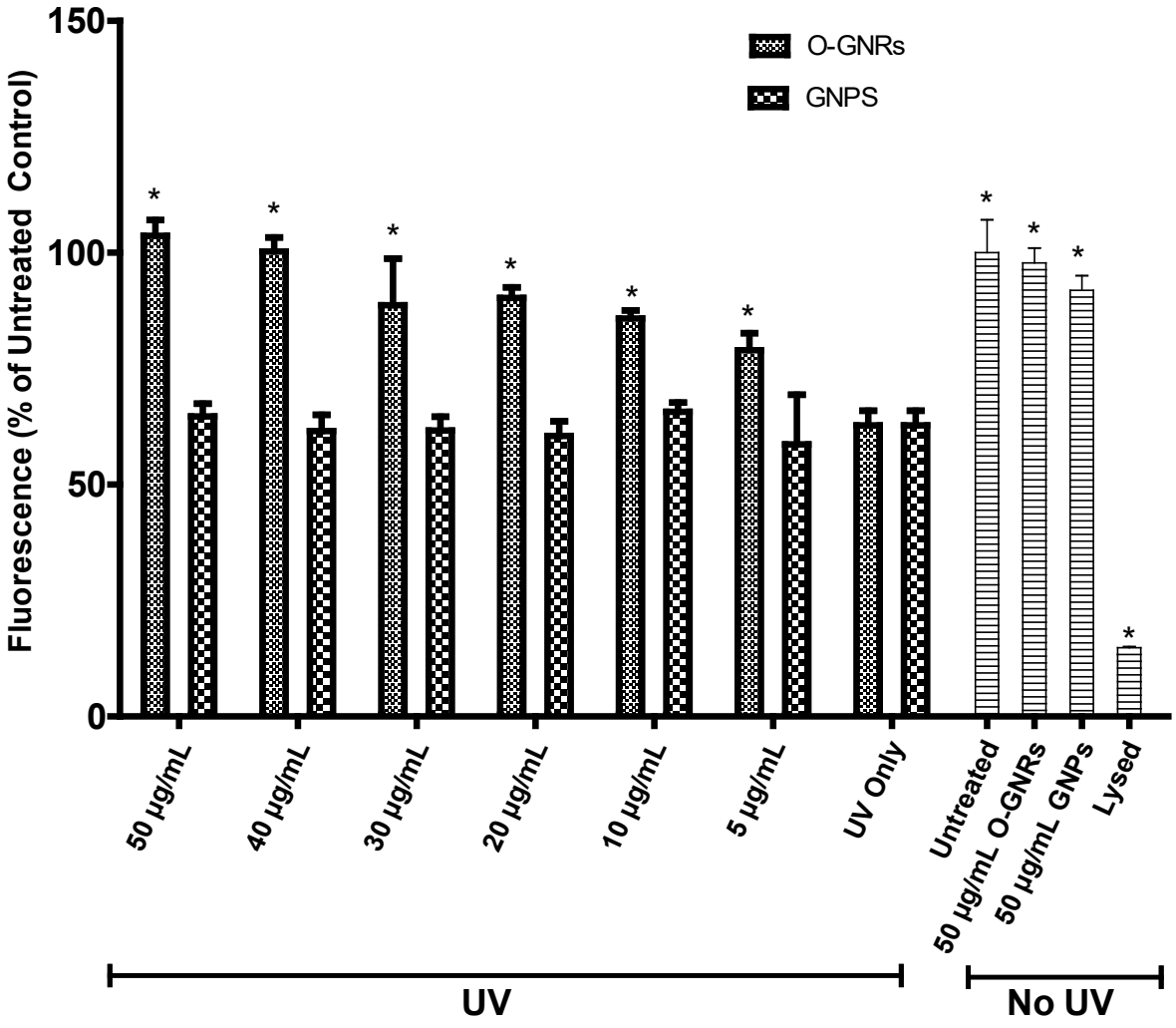

Figure 4.1. Viability of HeLa cells after treatment with UV and/or nanoparticles. Cells exposed to UV were treated with varying concentrations of O-GNRs or GNPs from 5 to 50 µg/mL, or only exposed to UV. Cells not exposed to UV, the max concentrations of O-GNRs or GNPs, or lysed served as controls. * Indicates significant difference from "UV Only."

Because UV induces cell death through apoptosis[12-15], we wanted to determine if O-GNRs were increasing the viability of UV-exposed HeLa cells through apoptosis. Figure 4.2 shows the caspase-3 activity of HeLa cells treated with UV radiation and/or O-GNRs after 24

hours, normalized to the untreated control. The caspase activity of cells exposed to UV without O-GNRs was 1144% of the untreated control, indicating high levels of apoptosis. However, cells treated with 50 μg/mL O-GNRs after UV exposure only showed 145.1% caspase activity of the untreated control, which was not significantly different from the untreated control. Cells exposed only to O-GNRs also did not show a significant increase in caspase-3 activity.

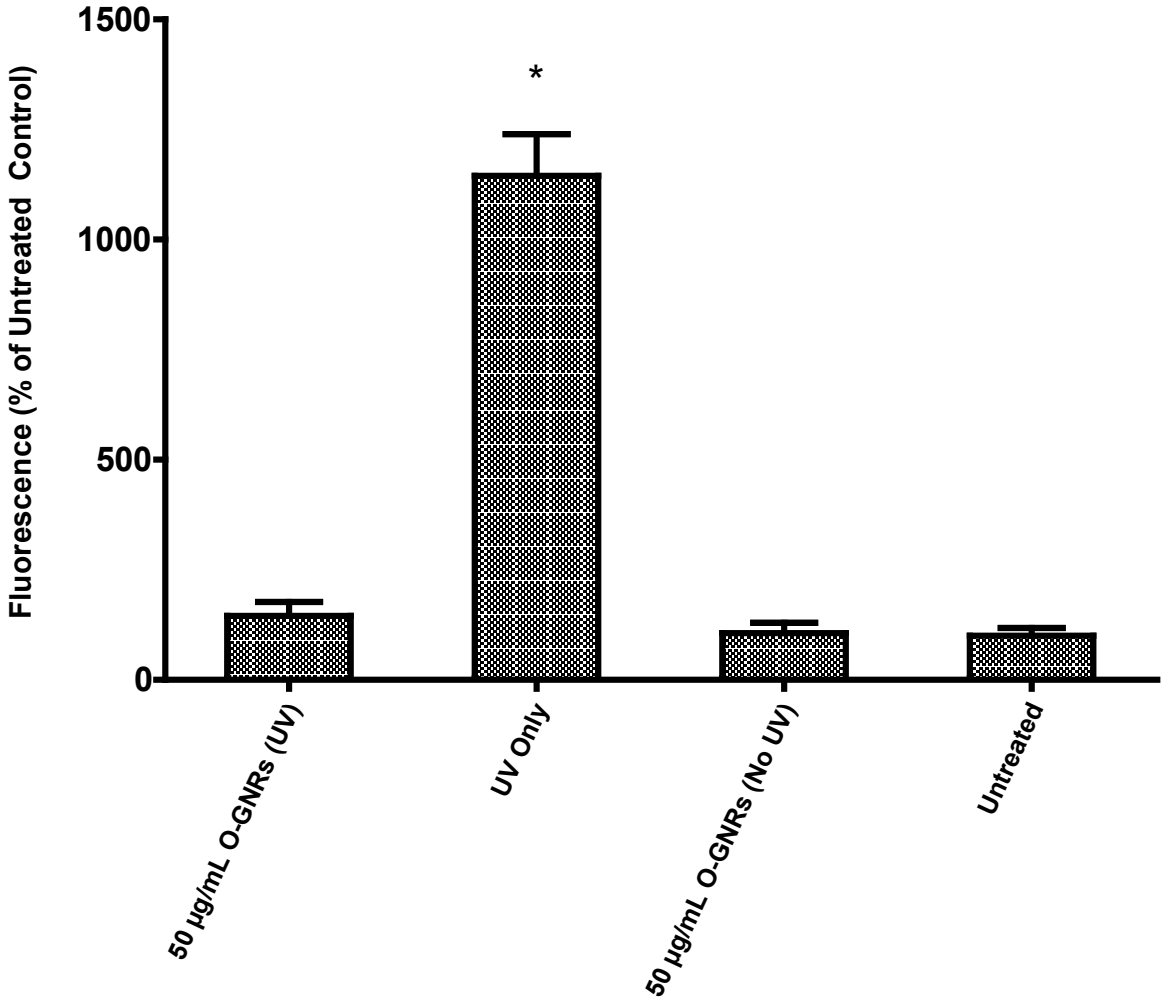

Figure 4.2. Caspase-3 activity after exposure to UV and/or 50 μg/mL O-GNRs, or no treatment. * indicates significant difference from "Untreated."

We also wanted to determine if this protection from UV-induced apoptosis could be attributed to the buffering of ROS as previously demonstrated. Figure 4.3 shows the fluorescence of DCFDA of cells exposed to UV or no UV and O-GNRs or no O-GNRs. Cells exposed to UV but preincubated with O-GNRs showed 293.8% the ROS activity of the untreated sample, which was significantly different from the cells treated only with UV, which showed 411.7% the ROS activity of the untreated cells. The O-GNRs themselves had some activation of DCFDA, with 193.9% the ROS activity as the untreated cells. However, despite this activation of DCFDA, cells treated with UV and O-GNRs demonstrated significantly less ROS generation compared to cells treated with only O-GNRs, indicating that protective effect of O-GNRs on HeLa cells could be partially explained by the buffering of ROS.

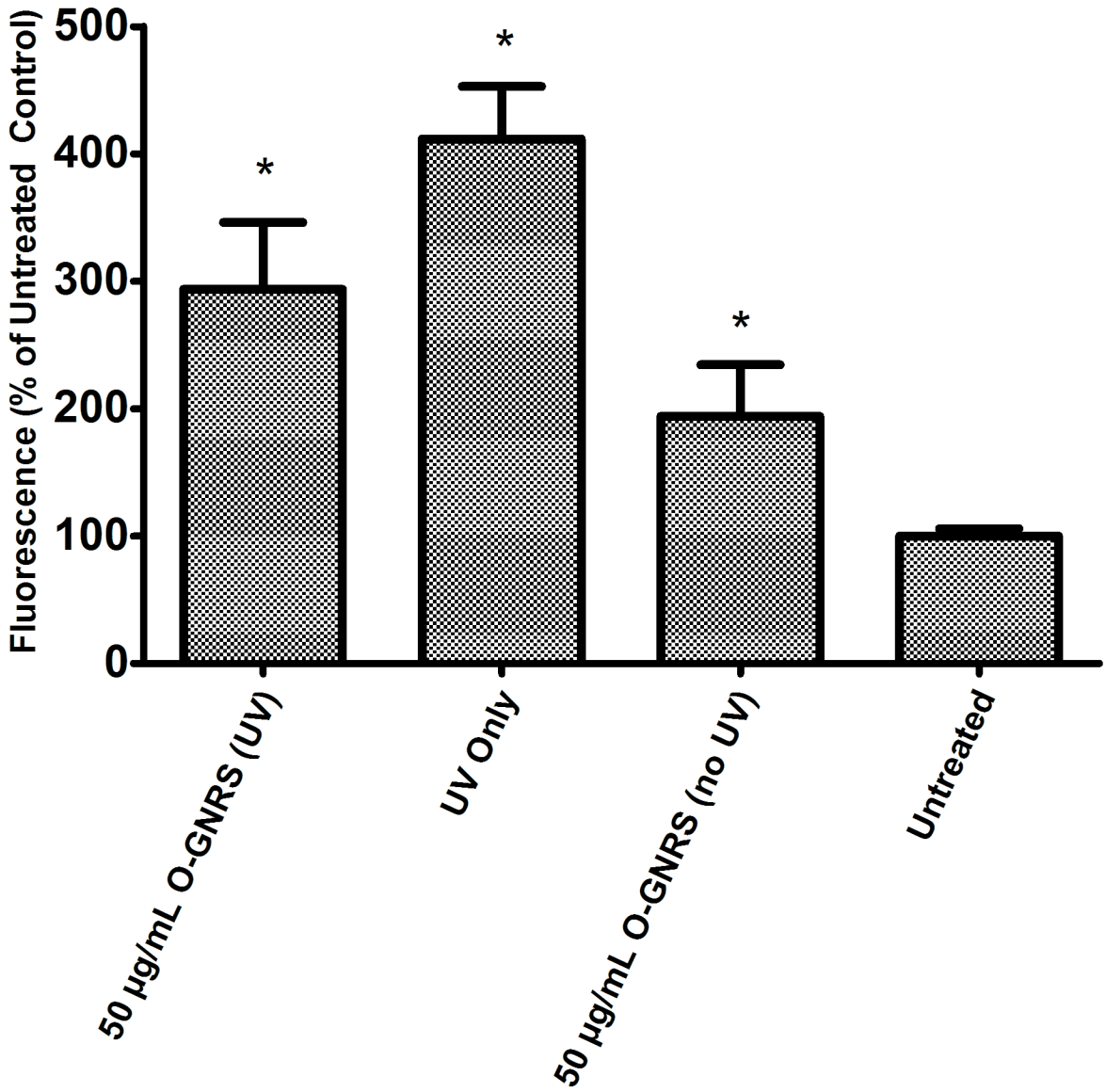

Figure 4.3. ROS activity determined by DCFDA fluorescence. "*" indicates significant difference from "Untreated control.

Discussion

ROS generation is a crucial part of UV-induced apoptosis[16-20]. Previous studies have indicated that the oxygen-containing side groups of graphene oxide, such as carboxyl and hydroxyl groups, can act as antioxidants to quench free radicals such as ROS[21]. The previous study demonstrating the protective effects of graphene oxide on cells (fibroblasts) from X-ray irradiation (which also stimulates apoptosis through the production of ROS[8]) preincubated graphene oxide nanoparticles for 24 hours similarly low concentrations.

However, the study only looked at graphene oxide derived from one starting material. Our current data suggest that not only could graphene oxide nanoparticles be administered after exposure to radiation and offer a protective effect, but also that the potency of this protective effect could be drastically affected by the starting material used to produce GO nanoparticles. However, since GNPs are not as highly oxidized as O-GNRs[9], it is also possible that the starting material is not as large a factor as the final degree of oxidation. This should be tested in a future study by comparing the protective effects of graphene oxide nanoparticles produced by different methods and with different degrees of oxidation.

The data presented here also have implications for other types of treatment that use graphene oxide as a delivery system. Anticancer drugs such as doxorubicin can rely on ROS generation as a way to induce apoptosis[22-24]. Previous studies have examined the use of graphene oxide nanoparticles as a delivery system for drugs such as doxorubicin, seemingly without any issues arising from ROS buffering[6]. However, it may be possible to increase the efficacy of such treatments by optimizing the properties of the graphene oxide used. This kind of optimization may also give a needed edge to treatments that otherwise fail due to the ROS buffering effect overwhelming the effects of the treatment.

Conclusions

We have shown that O-GNRs derived from carbon nanotubes are able to protect HeLa cells from UV-induced apoptosis through the buffering of ROS. We have also shown that GNPs derived from the oxidation of graphite were not able to protect HeLa cells from UV-induced apoptosis at all. Taken together, these data indicate that the starting material and degree of oxidation for graphene oxide nanoparticles should be taken into consideration for applications that involve ROS generation.

References

1 Lu, C. H., Yang, H. H., Zhu, C. L., Chen, X. & Chen, G. N. A graphene platform for sensing biomolecules. *Angewandte Chemie (International ed. in English)* **48**, 4785-4787, doi:10.1002/anie.200901479 (2009).

2 Hu, W. *et al.* Graphene-Based Antibacterial Paper. *ACS nano* **4**, 4317-4323, doi:10.1021/nn101097v (2010).

3 Wang, Y. *et al.* Aptamer/graphene oxide nanocomplex for in situ molecular probing in living cells. *Journal of the American Chemical Society* **132**, 9274-9276, doi:10.1021/ja103169v (2010).

4 Song, Y., Chen, Y., Feng, L., Ren, J. & Qu, X. Selective and quantitative cancer cell detection using target-directed functionalized graphene and its synergetic peroxidase-like activity. *Chemical communications (Cambridge, England)* **47**, 4436-4438, doi:10.1039/c0cc05533f (2011).

5 Feng, L., Zhang, S. & Liu, Z. Graphene based gene transfection. *Nanoscale* **3**, 1252-1257, doi:10.1039/c0nr00680g (2011).

6 Yang, X. *et al.* High-Efficiency Loading and Controlled Release of Doxorubicin Hydrochloride on Graphene Oxide. *The Journal of Physical Chemistry C* **112**, 17554-17558, doi:10.1021/jp806751k (2008).

7 Zhang, L., Xia, J., Zhao, Q., Liu, L. & Zhang, Z. Functional graphene oxide as a nanocarrier for controlled loading and targeted delivery of mixed anticancer drugs. *Small* **6**, 537-544, doi:10.1002/smll.200901680 (2010).

8 Qiao, Y., Zhang, P., Wang, C., Ma, L. & Su, M. Reducing X-Ray Induced Oxidative Damages in Fibroblasts with Graphene Oxide. *Nanomaterials (Basel)* **4**, 522-534, doi:10.3390/nano4020522 (2014).

9 Talukdar, Y., Rashkow, J. T., Lalwani, G., Kanakia, S. & Sitharaman, B. The effects of graphene nanostructures on mesenchymal stem cells. *Biomaterials* **35**, 4863-4877, doi:10.1016/j.biomaterials.2014.02.054 (2014).

10 Kosynkin, D. V. *et al.* Longitudinal unzipping of carbon nanotubes to form graphene nanoribbons. *Nature* **458**, 872-876, doi:10.1038/nature07872 (2009).

11 Hummers Jr, W. S. & Offeman, R. E. Preparation of graphitic oxide. *Journal of the American Chemical Society* **80**, 1339-1339 (1958).

12 Martin, S. J. & Cotter, T. G. Ultraviolet B irradiation of human leukaemia HL-60 cells in vitro induces apoptosis. *Int J Radiat Biol* **59**, 1001-1016 (1991).

13 Bender, K., Gottlicher, M., Whiteside, S., Rahmsdorf, H. J. & Herrlich, P. Sequential DNA damage-independent and -dependent activation of NF-kappaB by UV. *EMBO J* **17**, 5170-5181, doi:10.1093/emboj/17.17.5170 (1998).

14 Aragane, Y. *et al.* Ultraviolet light induces apoptosis via direct activation of CD95 (Fas/APO-1) independently of its ligand CD95L. *The Journal of cell biology* **140**, 171-182 (1998).

15 Simon, M. M., Aragane, Y., Schwarz, A., Luger, T. A. & Schwarz, T. UVB light induces nuclear factor kappa B (NF kappa B) activity independently from chromosomal DNA damage in cell-free cytosolic extracts. *J Invest Dermatol* **102**, 422-427 (1994).

16 Farber, J. L. Mechanisms of cell injury by activated oxygen species. *Environ Health Perspect* **102 Suppl 10**, 17-24 (1994).

17 Masaki, H., Sakaki, S., Atsumi, T. & Sakurai, H. Active-oxygen scavenging activity of plant extracts. *Biol Pharm Bull* **18**, 162-166 (1995).

18 Peus, D. *et al.* UVB activates ERK1/2 and p38 signaling pathways via reactive oxygen species in cultured keratinocytes. *J Invest Dermatol* **112**, 751-756, doi:10.1046/j.1523-1747.1999.00584.x (1999).

19 Tyrrell, R. M. Ultraviolet radiation and free radical damage to skin. *Biochem Soc Symp* **61**, 47-53 (1995).

20 Kulms, D., Zeise, E., Poppelmann, B. & Schwarz, T. DNA damage, death receptor activation and reactive oxygen species contribute to ultraviolet radiation-induced apoptosis in an essential and independent way. *Oncogene* **21**, 5844-5851, doi:10.1038/sj.onc.1205743 (2002).

21 Qiu, Y. *et al.* Antioxidant chemistry of graphene-based materials and its role in oxidation protection technology. *Nanoscale* **6**, 11744-11755, doi:10.1039/c4nr03275f (2014).

22 Kim, S. Y. *et al.* Doxorubicin-induced reactive oxygen species generation and intracellular Ca2+ increase are reciprocally modulated in rat cardiomyocytes. *Experimental & molecular medicine* **38**, 535-545, doi:10.1038/emm.2006.63 (2006).

23 Tsang, W. P., Chau, S. P. Y., Kong, S. K., Fung, K. P. & Kwok, T. T. Reactive oxygen species mediate doxorubicin induced p53-independent apoptosis. *Life sciences* **73**, 2047-2058, doi:http://dx.doi.org/10.1016/S0024-3205(03)00566-6 (2003).

24 Wang, Z., Wang, J., Xie, R., Liu, R. & Lu, Y. Mitochondria-derived reactive oxygen species play an important role in Doxorubicin-induced platelet apoptosis. *International journal of molecular sciences* **16**, 11087-11100, doi:10.3390/ijms160511087 (2015).

Chapter 5

Delivery of Long Chain C_{16} and C_{24} in HeLa Cells Using Oxidized Graphene Nanoribbons

Contributions by: Cassandra Suhrland, Jean-Philip Truman, Lina M. Obeid, Balaji Sitharaman

Abstract

The bioactive sphingolipid ceramide has many important roles in cell signaling processes, particularly in signaling programmed cell death in cancer. However, ceramide levels are often impaired in multi-drug resistant (MDR) and radiation-resistant cancers due to the dysregulation of ceramide metabolism. Restoration of ceramide levels through external delivery represents a potential therapeutic target for the treatment of resistant cancers. However, as a lipid ceramide is extremely hydrophobic and requires a delivery system to enter cells. Here we report the development of a method to load significant amounts of the long chain C_{16} and C_{24} ceramides onto oxidized graphene nanoribbons (O-GNRs) derived from carbon nanotubes. Using O-GNRs as a delivery for these ceramides, we were able to induce significant biological effects in HeLa cells in conjunction with C_6 ceramide and ultraviolet radiation treatment. However, we found that O-GNRs themselves exert significant biological effects and can interfere with the actions of these ceramides and ultraviolet treatment. Loading of ceramides onto O-GNRs did not have a significant effect on the entry of the nanoparticles together. Despite the need for further improvement, these data represent an important first step in the development of O-GNRs as a delivery system for long chain ceramides.

Introduction

Sphingolipids comprise a broad group of lipids with many different functions and activities[1,2]. The backbone of these lipids is sphinganine, a long chain fatty acid with hydroxyl groups and an amino group. This sphingoid base can be acylated at the amine group, and with a subsequent introduction of a 4,5 trans double bond, yield ceramide[2]. Of all the sphingolipids, ceramide has been revealed as one of the most biologically active, with important roles in a number of processes including cell growth and proliferation, cell senescence, differentiation, apoptosis, necrosis, and autophagy[3-9]. Apoptosis specifically has been shown to have many ceramide-dependent mechanisms in both the extrinsic pathway mediated by death ligands[10-21] and the intrinsic pathway mediated by mitochondrial outer membrane permeabilization (MOMP)[22-29]. It has also been shown to be an important part of the metabolism of many types of cancers[30]. Many anticancer drugs such as doxorubicin have been shown to induce apoptosis in part through ceramide accumulation[30-32]. Conversely, many cancers exhibit low ceramide levels and impaired ceramide metabolism through the depletion of ceramide by overexpression of ceramide-metabolizing enzymes such as ceramidases and glucosylceramide synthase[15,33-46]. Therefore, the restoration of ceramide levels through external delivery may represent a potential therapeutic target for the restoration of ceramide levels.

However, as a lipid ceramide is extremely hydrophobic, and requires a delivery system. There has been much work devoted to the development of delivery methods for ceramide. Many of these methods have centered around the use of the short-chain C_6 ceramide, a synthetic ceramide analog which is a potent inducer of apoptosis[47]. One of the more common methods of short chain ceramide delivery is liposomes, which incorporate C_6 ceramide or other short chain ceramides into constructs containing other co-factors[4,48,49]. However, when introduced into an

aqueous environment ceramide rapid releases from the liposomes, limiting their systemic delivery[50]. Other methods of short chain ceramide delivery have been attempted, such as calcium phosphate nanocomposites[51], thermally sensitive dendritic nanoparticles[52], polyethyleneoxide-modified-polyepsilon-caprolactone nanoparticles[53,54] and carbon nanotubes[55]. As of yet, no method has been clinically approved for the therapeutic delivery of ceramide, and it remains to be seen whether these methods can translate into therapeutic treatments.

There has been considerably less attention has been devoted to the long chain ceramides such as C_{16} and C_{24} ceramide, which are the endogenous ceramides that mediate biological signaling processes. Unlike their short-chain counterparts, which can be dissolved in an organic solvent and added to cell media to enter cells, long chain ceramides cannot form micelles in aqueous solution and require a delivery system to be able to enter cells in significant quantities[56]. It is most likely this reason that there are very few delivery methods for long chain ceramides, despite their potent effects[57-59]. There are *in vitro* methods such as the dodecane-ethanol system and cholesteryl phosphocholine, which can deliver C_{16} ceramide into cells with considerable effiiciency[60,61]. They are valuable research tools, but it is not clear that they could be translated into therapeutic delivery methods. Currently, the only system with therapeutic potential is liposomes. Success with long chain ceramide liposomes has been mixed, with the uptake of these liposomes sensitive to formulation and cell type[48]. There have also been some successes with liposomes containing modified long chain ceramides to sensitize cancer cells to other treatments[62]. However, in general, liposome synthesis can be a tedious and error-prone process. Despite what potential liposomes may hold, the therapeutic potential of externally-delivered long chain ceramides is overshadowed by the lack of methods to deliver it *in vitro* and *in vivo*.

Graphene oxide is a two-dimensional carbon nanostructure that has been explored for many biomedical applications[63-71]. One of graphene oxide's features that make it desirable from a biomedical perspective is the combination of hydrophobic and hydrophilic regions. Pristine graphene is comprised entirely of carbon atoms in sp^2 arrangement, making it very hydrophobic. The oxidation of graphene introduces many 'defects' in this structure which disrupts the aromatic groups with oxygen-containing groups such as carboxyls and hydroxyls[72,73]. However, some of these aromatic groups remain, giving rise to amphiphilic molecules that have hydrophobic groups while retaining their aqueous dispersibility. This important feature of graphene oxide has been previously exploited in the past for the delivery of hydrophobic anticancer drugs through the 'pi-stacking' phenomenon between aromatic groups[74-78]. It has also been shown that aliphatic hydrocarbons are capable of binding to these hydrophobic regions. The surfactant 1,2-distearoyl-*sn*-glycero-3-phosphoethanolamine-N-[amino(polyethylene glycol)] (DSPE-PEG) has been used to increase the dispersibility of graphene oxide nanoparticles in aqueous solution, based on the principle that the lipid moiety DSPE binds to the hydrophobic regions of graphene while the PEG moiety extends out into solution lending increased solubility[79-81]. Thus it is possible for an extremely hydrophobic molecule like long chain ceramides to bind to these hydrophobic regions.

Here we describe a method for loading C_{16} and C_{24} ceramides onto oxidized graphene nanoribbons (O-GNRs) derived from carbon nanotubes. Using this facile method we were able to load a high amount of each ceramide onto O-GNRs. We tested the ability of our ceramide loaded O-GNRs to sensitize (C_{16}) or protect (C_{24}) HeLa cells from the pro-apoptotic stressors of C_6 ceramide and ultraviolet (UV) radiation. We found that the O-GNRs themselves have a number of significant biological effects that interfere with the ability of long chain ceramides to sensitize or protect HeLa cells from pro-apoptotic stressors. However, we found that ceramide-loaded O-

GNRs had significantly different effects on cell viability and apoptosis compared to O-GNRs alone. We also found that loading ceramide onto O-GNRs did not have a significant effect on the ability of these nanoparticles to enter HeLa cells.

Methods

Materials

C_{24} and C_{16} ceramide and C_{12} NBD ceramide (N-[12-[(7-nitro-2-1,3-benzoxadiazol-4-yl)amino]dodecanoyl]-D-erythro-sphingosine) were purchased from Avanti Polar Lipids (Alabaster, AL, USA) and Cayman Chemical (Ann Arbor, Michigan, USA). DSPE-PEG was purchased from NOF America Corporation (White Plains, NY, USA). All other materials and reagents were purchased from Sigma-Aldrich (St. Louis, MO, USA) unless otherwise noted.

O-GNR Synthesis

O-GNRs were synthesized using multi-walled carbon nanotubes (MWCNTs) and the longitudinal unzipping method, purified by centrifugation instead of filtration[73]. Briefly, MWCNTs (150mg) were dispersed in a volume of 30 mL of concentrated sulfuric acid. After 3 hr, 750mg of potassium permanganate ($KmNO_4$) was added and then the mixture was stirred for 1 hr. Then using an oil bath, the mixture was then heated to approximately 60 °C for 1 hr to complete the reaction. It was then washed with dilute hydrochloric acid after being allowed to cool to room temperature. The product was isolated by flocculation using ethanol and ether, followed by centrifugation at 3000 rpm and drying overnight in a vacuum oven.

Loading of Ceramide onto Carbon Nanoparticles

Stock solutions of O-GNRs and PEG-DSPE were dispersed in 100% ethanol at a concentration of 1 mg/mL, while C_{24} and C_{16} ceramide were dispersed in 100% ethanol at a concentration of 2 mg/mL using a bath sonicator. 100 μL of the ceramide stock solution and 200μL of the PEG-DSPE and O-GNR solutions were added to a 20 mL glass scintillation vial, and the volume was made to 1 mL using 100% ethanol. This mixture was bubbled with nitrogen

gas and covered in parafilm to prevent oxidation of ceramide. It was then bath sonicated for 15 minutes to allow interspersion of individual nanoparticles and ceramide molecules.

To this solution, 9mL of double-distilled water were added using a New Era NE-300 syringe pump (New Era Pump Systems Inc. Farmingdale, NY, USA) over a period of one hour under constant sonication. To separate ceramide-loaded nanoparticles from unloaded ceramide, the mixture was centrifuged at 13000 rpm for at least 30 minutes. The supernatant was discarded, and the nanoparticles were washed by resuspension in pure double-distilled water and repeating the centrifugation step, yielding ceramide-loaded nanoparticles. For sham controls, C_{16} or C_{24} ceramide underwent the loading process without any nanoparticles (volume replaced by 100% ethanol). For O-GNR controls, O-GNRs underwent the loading process without ceramide (volume replaced by 100% ethanol).

Quantification of Loading Using Mass Spectrometry

Sample preparation for mass spectrometry was carried out by first resuspending ceramide-loaded nanoparticles in 100% ethanol and bath-sonicating for 1 hr under nitrogen gas, to force ceramide to dissociate from the nanoparticles. The mixture was centrifuged at 13000 rpm for 1 hr to ensure all nanoparticles were concentrated at the bottom. 100 μL of the supernatant was extracted for mass spectrometry. 100 μL of the ceramide stock solution used for loading was also analyzed as a basis of comparison to calculate loading efficiency. Samples were analyzed using a Fisons MD800 Gas Chromatography Mass Spectrometer. The signals generated from samples were correlated to a standard curve to calculate the exact concentration of ceramide.

Particle Size Measurement

To see the effect of the loading method on nanoparticle aggregation, the size distribution of ceramide-O-GNR complexes was measured using a ZetaView Particlemetrix (Mebane, NC, USA). 100 μL of each sample was diluted in approximately 13 mL of water and loaded into a 5mL syringe. 3 to 4 mL of sample was injected into the device, and 1600-2000 particles were measured over the course of approximately 30 seconds.

Cell Culture

HeLa cells were obtained from ATCC (Manassas, VA, USA). Cells were grown in Dulbecco's Modified Eagle Medium (DMEM) supplemented with 10% fetal bovine serum and 1% penicillin-streptomycin. Cells were grown at 37 °C in a humidified atmosphere of 5% carbon dioxide.

Viability and Apoptosis Assays

To assess the ability of C_{24} ceramide to prevent damage to cells, and C_{16} ceramide to sensitize cells to other treatments, HeLa cells were seeded in flat-bottomed 96 well plates at a density of 5000 cells/well and were allowed to adhere overnight. For cell assays, plates were either subjected to treatment with free C_6 ceramide (25μM) or UV irradiation (40 mJ/cm^2). Immediately following C_6 ceramide treatment or UV irradiation, C_{16} and C_{24} ceramide-loaded O-GNRs were added to each well at various concentrations ranging from 5-40 μg/mL of nanoparticles. After 24 hours, the media was aspirated, and each well was rinsed twice with PBS. A mixture of 10 μL of Presto Blue Viability Reagent (Life Technologies, Grand Island, NY, USA) and 90 μL of DMEM with 10% FBS and 1% P/S were added to each well and placed back in the incubator. After 2 hours, the plates were removed, and the fluorescence intensity of each well was measured using a Molecular Devices SpectraMax M2e (Sunnyvale, CA, USA) with an excitation wavelength of 560 nm and an emission wavelength of 590 nm. Lysed cells were used

as a positive control, and untreated cells were used as a negative control. The cell viability is expressed as a percent of the lysis control with the formula $\left((I_{test} - I_{blank})/(I_{control} - I_{blank}) \times 100\%\right) - 100\%$, where I_{test} is the fluorescence intensity of cells exposed to ceramide-loaded nanoparticles, $I_{control}$ is the fluorescence intensity of lysed cells, and I_{blank} is the fluorescence intensity from empty wells.

Apoptosis was assessed at the highest levels of nanoparticles tested using a Biovision Caspase 3 Fluorometric Assay (Biovision, San Francisco, CA). Fluorescence was measured using a Molecular Devices SpectraMax M2e with an excitation of 400nm and an emission of 505nm.

Mass Spectrometry Quantification of Uptake

HeLa cells were seeded in 24 well plates at a density of $5x10^4$ cells/well and allowed to adhere overnight. O-GNRs or C_{16}/C_{24} ceramide-loaded O-GNRs were then added to wells at a concentration of 40 μg/mL of nanoparticles for 24 hr. Untreated cells served as a baseline to compare to O-GNRs and ceramide-loaded O-GNRs. To extract lipids, cells were trypsinized and centrifuged down. Cells were resuspended in 2mL of extraction buffer (15:85 v:v 70% isopropanol:ethyl acetate) vortexed for 15 seconds and spun down at 13000 rpm for 30 minutes at 4°C. The supernatant was collected, and this procedure was repeated once more. To see how much C_{16} and C_{24} ceramide was removed as part of the extraction procedure, C_{16} and C_{24} ceramide-loaded O-GNRs were added to 15 mL conical tubes in an equivalent volume of media and incubated at 4 °C for 24 hours, and subjected to an identical procedure for extraction. Sphingolipid content was measured in each sample using a Fisons MD800 Gas Chromatography Mass Spectrometer.

Confocal Microscopy

C_{12} NBD ceramide was loaded onto O-GNRs using the same procedure as C_{24} and C_{16} ceramide. HeLa cells were seeded in glass-inset confocal dishes at a density of 7.5 x 10^4 cells/mL with 2 mL per plate and allowed to adhere overnight. Cells were treated with either 5 μM fluorescent C_{12} NBD ceramide or an equivalent amount of fluorescent C_{12} NBD ceramide loaded on O-GNRs for 2 hours and imaged using a Leica TCS SP8 Laser Scanning Confocal Microscope System (Buffalo Grove, IL, USA). Cells were pretreated with inhibitors of O-GNR uptake Dynasore and Gefitinib, endosome disruptor Desipramine, or no additional treatment for 30 minutes prior to the addition of ceramide or ceramide-loaded O-GNRs.

TEM

HeLa cells were grown on ACLAR® film (Electron Microscopy Sciences, Hatfield, PA) in 6 well plates at a density of 20000 cells per well and allowed to settle overnight. The following day, cells were exposed to C_{24} or C_{16} ceramide-loaded O-GNRs for 24 hours. The cells were subsequently fixed with 2.5% glutaraldehyde (Electron Microscopy Sciences, Hatfield, PA) in 0.1 M PBS for 15 minutes at room temperature. The films were then placed in 2% osmium tetroxide in 0.1 M PBS, dehydrated through graded ethanol washes, and embedded using durcupan resin. The embedded specimens were screened for areas with high cell densities, and these areas were cut into 80 nm sections using an Ultracut E microtome (Reichert-Jung, Cambridge, UK), and placed on formvar-coated copper grids. Sections were imaged using a Tecnai Bio Twin G transmission electron microscope (FEI, Hillsboro, OR), at 80 kV. Images were acquired using an XR-60 CCD digital camera system (AMT, Woburn, MA).

Statistical Analysis

Data are presented as mean ± standard deviation for PrestoBlue and Caspase assays (n = 6). One-way ANOVA was used to make multiple comparisons between groups, and Tukey-Kramer post hoc analysis was used to determine where significant differences occurred. Statistical analysis was performed using a 95% confidence interval ($p < 0.05$) with GraphPad Prism.

Results

Ceramide Loading on O-GNRs

The loading of C_{16} ceramide onto O-GNRs as determined by mass spectrometry was 61.47% of the initial concentration in the pre-loading solution. The loading of C_{24} ceramide onto O-GNRs was 48.76% of the initial concentration in the pre-loading solution, indicating a high level of loading for both types of ceramide.

O-GNR particle aggregation

Figure 5.1 shows the particle size aggregation data for O-GNRs before and after loading with ceramide. Prior to loading, the average size of O-GNRs was 88.0 nm ±50.2 nm, with 10% of particles smaller than 24.8 nm, 50% smaller than 82.9 nm, and 90% smaller than 143.2 nm (Figure 5.1B). After loading O-GNRs with PEG-DSPE but no ceramide, the average size of O-GNRs was 85.7 nm ± 63.1 nm, with 10% of particles smaller than 16.2 nm, 50% smaller than 75.2 nm, and 90% smaller than 165.9 nm (Figure 5.1B). After loading C_{16} ceramide with PEG-DSPE, the average size of O-GNRs was 85.7 nm ± 63.1 nm, with 10% of particles smaller than 15.5 nm, 50% smaller than 72.1 nm, and 90% smaller than 158.3 nm (Figure 5.1C). After loading C_{24} ceramide with PEG-DSPE, the average size of O-GNRs was 83.8 nm ± 58.1 nm, with 10% of particles smaller than 16.7 nm, 50% smaller than 73.2 nm, and 90% smaller than 156.3 nm (Figure 5.1D).

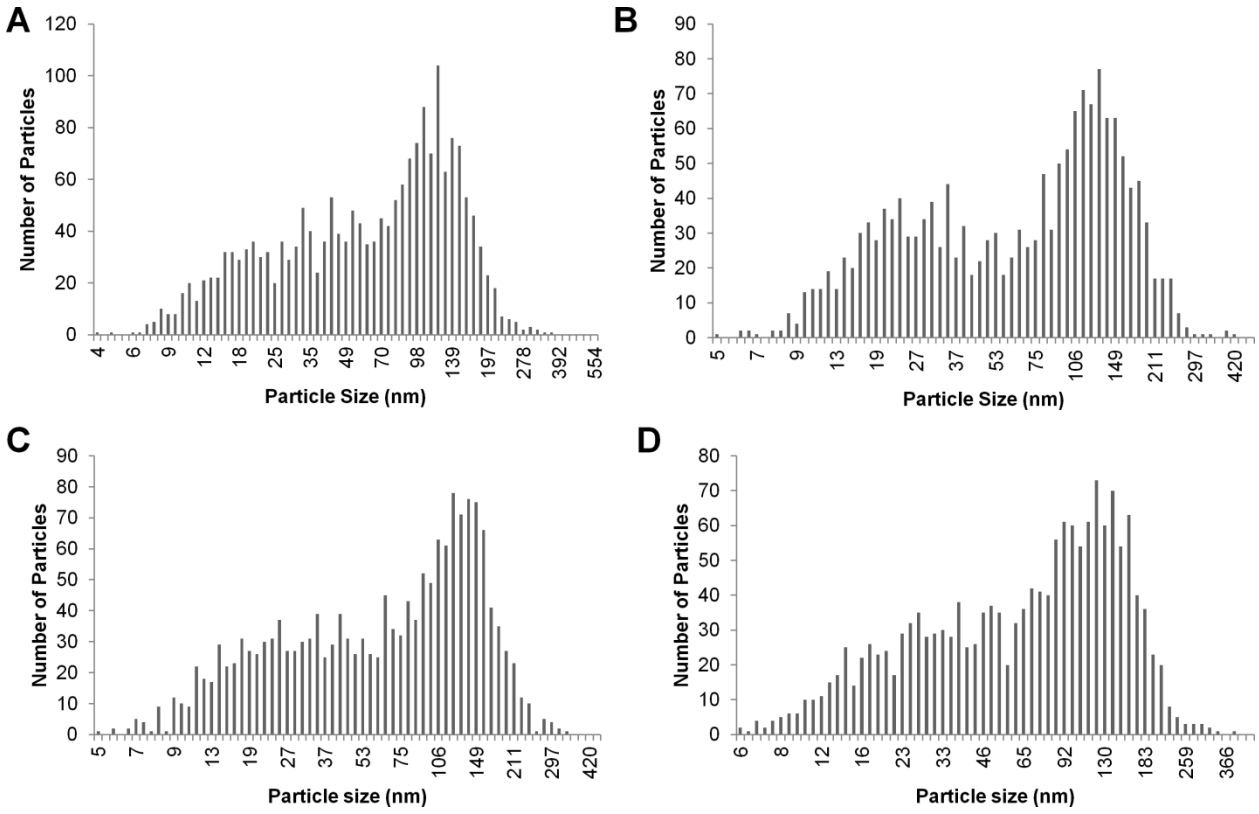

Figure 5.1 The number of O-GNRs counted at different sizes A) prior to the loading process B) loaded with PEG-DSPE but no ceramide C) loaded with PEG-DSPE and C_{16} ceramide D) loaded with PEG-DSPE and C_{24} ceramide.

Quantification of Ceramide Uptake into HeLa cells

In order to determine how much ceramide was getting into cells, we measured the total content of several sphingolipid species in untreated cells, cells treated with O-GNRs, cells treated with C_{16} ceramide-loaded O-GNRs, cells treated with C_{24} ceramide-loaded O-GNRs, and a sham group consisting of C_{16} and C_{24} ceramide-loaded O-GNRs in an equivalent volume of media for an equivalent amount of time, and subjected to the same extraction procedure. Table 5.1 shows the total amount of sphingosine, dihydrosphingosine, sphingosine-1 phosphate, C_{16} ceramide, and C_{24} ceramide for each group. For the group treated with C_{16} ceramide, there were 47.74 ± 26.42 pmol of C_{16} ceramide detected in the sample, compared to an amount below the

detection threshold for the untreated group. There was also 59.97 ± 47.95 pmol of C_{16} ceramide detected from the sham control, indicating a high background with a large degree of variation as well. However, for the C_{24} ceramide and O-GNR groups, there were also 7.43 ± 0.34 and 10.26 ± 3.22 pmol of C_{16} ceramide detected as well, despite no extra C_{16} ceramide being externally delivered.

For C_{24} ceramide there was a similar pattern. The amount of C_{24} ceramide present in the C_{24} ceramide group was 17.46 ± 9.20 pmol of C_{24} ceramide compared to 1.17 ± 1.53 pmol of C_{24} ceramide in the untreated control. There was a very large background from the sham control of 90.09 ±11.39 pmol of C_{24} ceramide. There was also significantly more C_{24} ceramide in the C_{16} ceramide group than in the untreated group, with 4.77 ±0.85 pmol of C_{24} ceramide detected. There was roughly an equivalent amount of C_{24} ceramide in the O-GNR group compared to the untreated group, with 1.40 ± 1.32 pmol of C_{24} ceramide in the O-GNR group. There was also sphingosine and sphingosine-1 phosphate detected in the sham group, but this can be attributed to background from the serum in the media used.

Table 5.1 **Sphingolipid quantification in HeLa cells or sham control**

Group (n=3)		Lipid Quantified (pmol/total sample)				
		Sph	dhSph	Sph-1P	C_{16}	C_{24}
C_{16}	Mean	7.10	2.95	2.21	42.74	4.77
	Std Dev.	±0.10	±0.26	±0.41	±26.42	±0.85
C_{24}	Mean	6.700	1.43	1.72	7.43	17.46
	Std Dev.	±0.60	±0.10	±0.18	±0.34	±9.20
Untreated	Mean	0.43	0.0	1.47	0.0	1.17
	Std Dev.	±0.09	±0.0	±0.20	±0.0	±1.53
O-GNR	Mean	7.62	2.28	1.28	10.26	1.40
Only	Std Dev.	±0.38	±0.29	±0.12	±3.22	±1.32
Sham	Mean	0.58	0.0	0.75	59.97	90.09
	Std Dev.	±0.16	±0.0	±0.03	±47.95	±11.39

(Sph - Sphingosine, dhSph - dihydrosphingosine, Sph-1P - Sphingosine-1 Phosphate)

Viability and Apoptosis with Combinational Therapies

Prestoblue is a resazurin-based reagent that has weak fluorescence in its base, inactive form. When incubated with cells, the dye is then processed by cells to a highly fluorescent form, and so the level of fluorescence detected in each well roughly corresponds to the viability of cells in that well. Figure 5.2 shows the viability of cells subjected to the pro-apoptotic stresses of ultraviolet radiation in combinational treatment with either C_{16} or C_{24} ceramide. UV and C_6

ceramide experiments were conducted together as part of one large experiment with the same controls, and statistical analysis was carried out as one large group. However, UV and C_6 ceramide, and C_{24} and C_{16} ceramide results are displayed in separate graphs for the sake of clarity (Fig. 5.2).

Cells treated with 40 μg/mL C_{24} ceramide-loaded O-GNRs and UV radiation were significantly more viable than the untreated control, with 118.12% of the untreated control (Fig. 5.2A). At 20 μg/mL there was no difference, and at 5 μg/mL cells were only 70.68% as viable as the untreated control. In contrast, no level of O-GNR treatment was significantly higher than the untreated control, but at 5 μg/mL cells were only 74.5% as viable as the untreated control. Cells treated with C_{24} ceramide-loaded O-GNRs or O-GNRs but no UV were significantly higher than the untreated control, with 136.08% and 125.43% the viability of the untreated control, respectively (Fig. 5.2A). The sham C_{24} ceramide treatment (C_{24} ceramide sent through the loading process with no O-GNRs) with UV was not significantly different from the group treated with only UV (Fig. 5.2A).

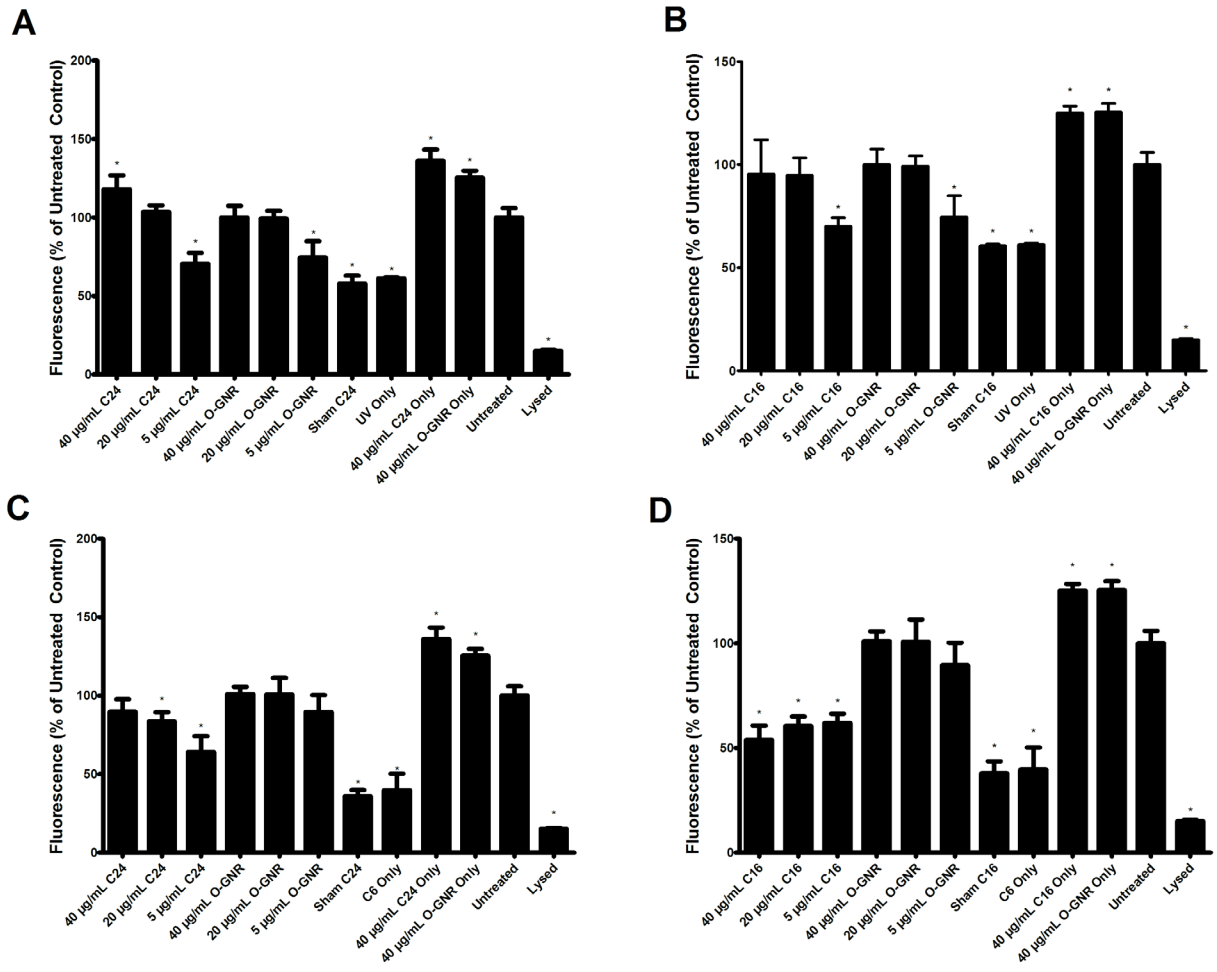

Figure 5.2. Viability of HeLa cells assessed by Prestoblue. Cells were treated with either UV (A, B) or C_6 ceramide (C, D). Following treatment, cells were incubated with C_{24} ceramide (A, C) and C_{16} ceramide (B, D) for 24 hours. O-GNRs without ceramide sent through the loading process were used as a control. Ceramides without nanoparticles sent through loading process (sham) were also used as controls. * indicates significant difference from "Untreated."

Cells treated with C_{16} ceramide-loaded O-GNRs and UV radiation were not significantly different at 40 and 20 µg/mL but were only 70.14% as viable as untreated cells at 5 µg/mL (Fig 5.2B). Cells treated with only O-GNRs followed the same pattern, with no difference at 40 and 20 µg/mL but 74.51% the viability of the untreated control at 5 µg/mL (Fig. 5.2B). Cells treated

with C_{16} ceramide-loaded O-GNRs were significantly more viable than the untreated control at 125.14% of the untreated control, (Fig. 5.2B). The sham C_{16} ceramide treatment (C_{16} ceramide sent through the loading process with no O-GNRs) with UV was not significantly different from cells treated with only UV (Fig. 5.2B).

Cells treated with C_{24} ceramide-loaded O-GNRs and free C_6 ceramide were not significantly different at 40 μg/mL, but were only 83.72% and 64.14% as viable as untreated cells (Fig. 5.2C). However, between individual trials of this experiment, this pattern was not consistent. Cells treated with O-GNRs and C_6 ceramide were not significantly different from the untreated control at any concentration (Fig. 5.2C). Cells treated with the sham C_{24} ceramide condition and C_6 ceramide were not significantly different from cells treated with C_6 ceramide alone (Fig. 5.2C).

Cells treated with C_{16} ceramide-loaded O-GNRs and C_6 ceramide were significantly different from the untreated control at all concentrations tested, with 53.84% the viability of the untreated control at 40 μg/mL (Fig. 5.2D). Cells treated with the sham C_{16} ceramide control and C_6 ceramide were not significantly different from cells treated with C_6 ceramide only (Fig. 5.2D).

The apoptosis assay relies on the use of a DEVD-based substrate to measure caspase-3 activity. The substrate is weakly fluorescent until the DEVD moiety is processed by caspase-3 to a highly fluorescent form, with the fluorescence measured at 400/505 nm excitation/emission wavelengths corresponding to caspase-3 activity. Figure 5.3 shows the relative amount of caspase activity of cells treated with UV or C_6 ceramide plus C_{16} or C_{24} ceramide-loaded O-GNRs at the highest concentration tested of 40 μg/mL. Cells treated with C_6 ceramide showed

the highest level of apoptosis, with 432.66% the fluorescence of the untreated control (Fig. 5.3A). Of the cells treated with nanoparticles, cells treated with C_{24} ceramide-loaded O-GNRs showed the highest level of apoptosis, with 257.84% the fluorescence of the untreated control (Fig. 5.3A). However, this was not significantly different from cells treated with C_{16} ceramide-loaded O-GNRs or O-GNRs only (Fig 5.3A). Cells treated with UV radiation only had 420.01% the fluorescence of the untreated control (Fig. 5.3B). However, the fluorescence of cells treated with nanoparticles with or without ceramide were not significantly different from the untreated control at any concentration tested (Fig. 5.3B).

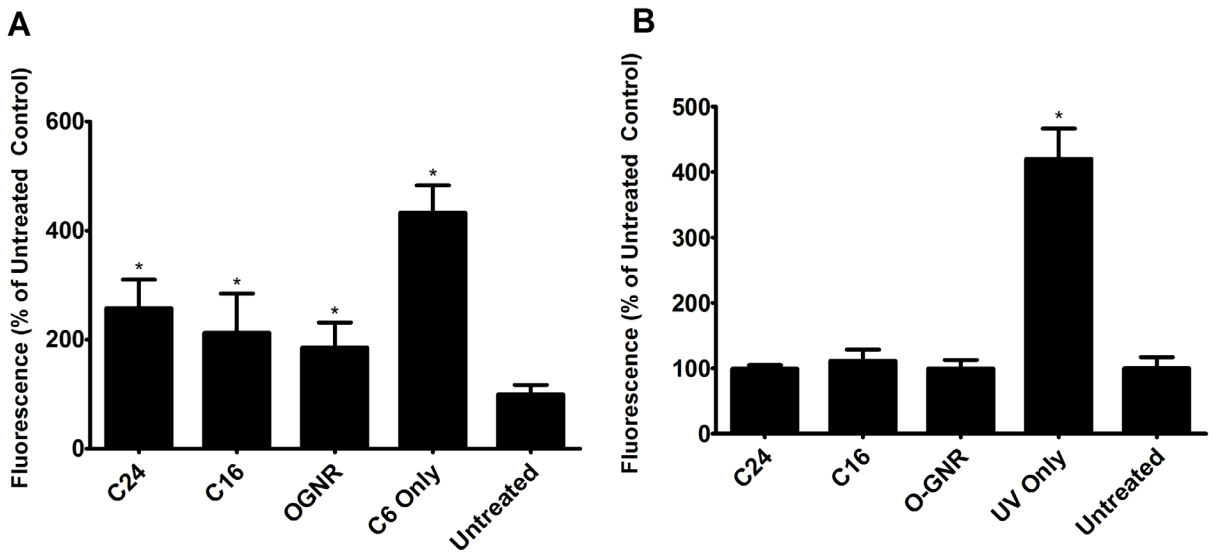

Figure 5.3. Apoptosis of HeLa cells assessed by Capase-3 activity. Cells were treated with either C_6 ceramide (A) or UV (B). Following treatment, cells were incubated with C_{24} ceramide and C_{16} ceramide for 24 hours. O-GNRs without ceramide sent through the loading process were used as a control. * indicates significant difference from "Untreated."

Uptake Inhibitor Effects on Apoptosis and Viability

Because C_{16} and C_{24} ceramides are native components of cellular membranes, we wanted to determine if they had an effect on the entry of O-GNRs into cells. We have previously

established that O-GNRs are uptaken into HeLa cells via a macropinocytotic-like, dynamin-dependent mechanism that relies on activation of epidermal growth factor receptor (EGFR)[80]. This was determined using 4 different inhibitors of specific uptake pathways at non-lethal concentrations: the dynamin inhibitor dynasore, the EGFR inhibitor gefitinib, the macropinocytosis inhibitor ethylisopropylamiloride (EIPA), and the caveolae-mediated endocytosis inhibitor filipin. Here we repeated the experiment using our ceramide-loaded O-GNRs in conjunction with the same uptake inhibitors pretreated for 30 minutes prior to other treatments, with viability and apoptosis measured by Prestoblue and caspase-3 activity, respectively. We measured C_6 ceramide with only C_{16} ceramide-loaded O-GNRs and UV with only C_{24} ceramide-loaded O-GNRs because these were the only conditions tested that showed consistent differences between ceramide loaded O-GNRs and O-GNRs without ceramide (Fig. 5.2). Cells were tested with a high and low concentration of each inhibitor (for dynasore Hi = 80 μM, Lo = 40 μM; for Gefitinib Hi = 1 μM, Lo = 0.5 μM; for EIPA Hi = 0.5 mM, Lo = 0.25 mM; for Filipin, Hi = 3 μg/mL, Lo = 2 μg/mL).

Figure 5.4 shows the effects of uptake inhibitor on C_{16} ceramide-loaded O-GNRs in conjunction with C_6 ceramide and C_{24} ceramide-loaded O-GNRs in conjunction with UV irradiation, as measured by Prestoblue. C_{16} ceramide-loaded O-GNRs with C_6 ceramide and inhibitors showed decreased viability compared to the untreated control for dynasore, gefitinib, and EIPA at both concentrations (percent of untreated control at high concentration: 56.11% for dynasore, 60.55% for gefitinib, 51.95% for EIPA) and were also not significantly different from the C_6 ceramide control without uptake inhibitor (Fig. 5.4A and B). The exception was filipin, which was not significantly different from the untreated control at either concentration tested and was significantly different from the C_6 ceramide only control; there was also no difference

between C_6 ceramide only and C_6 ceramide with filipin, although with filipin was substantially higher than without (Fig. 5.4B). There was also no significant effect of the uptake inhibitor on the reduction in viability of C_6 ceramide without O-GNRs (Fig. 4.5 A and B). O-GNRs without C_{16} ceramide had a similar reduction in viability compared to those with C_{16} ceramide (Fig. 5.4A and B).

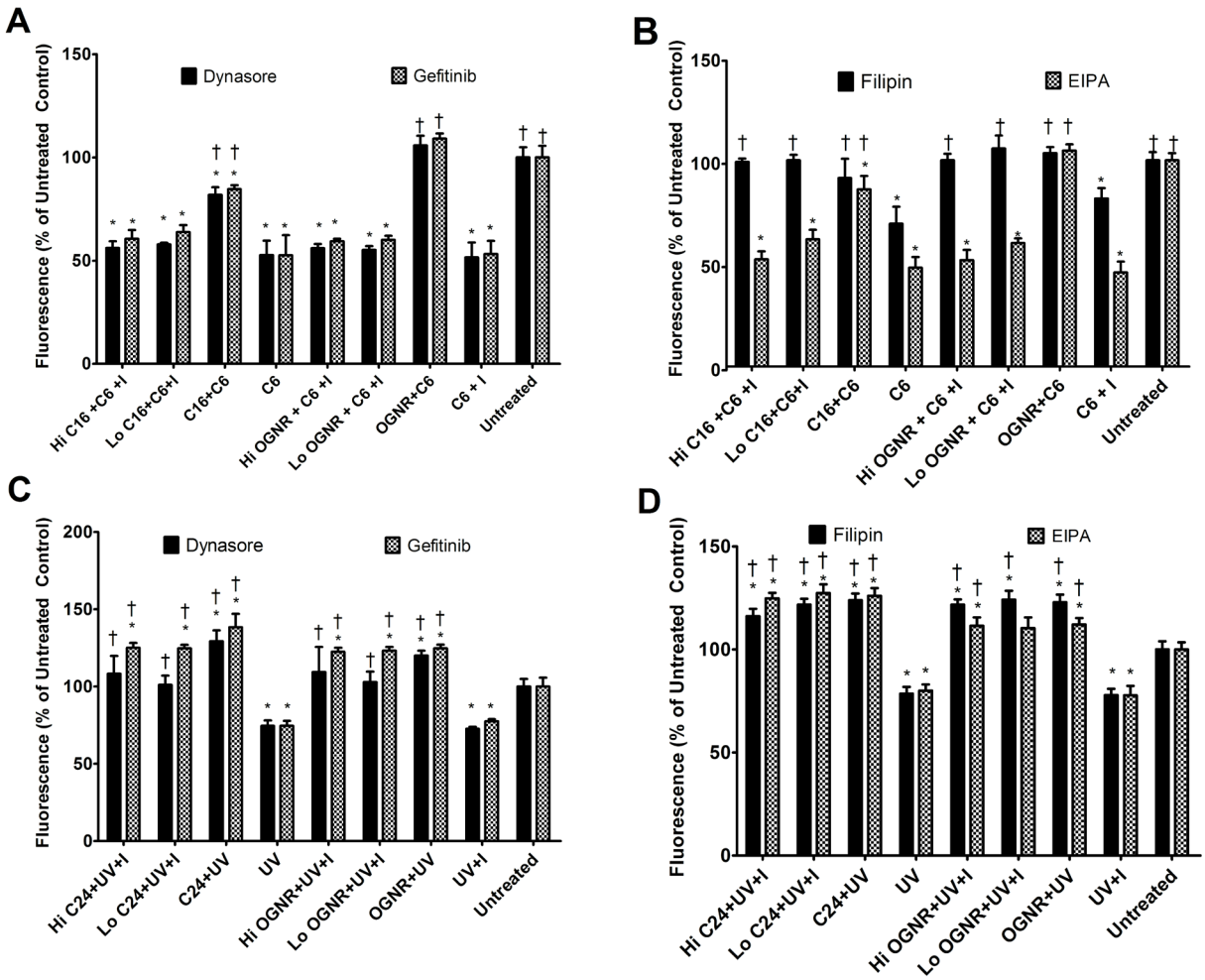

Figure 5.4. Effects of uptake inhibitors (I) on the viability of HeLa cells treated with C_6 ceramide and C_{16} ceramide loaded O-GNRs (A, B) or UV irradiation and C_{24} ceramide loaded O-GNRs (C, D) as measured by Prestoblue. Dynasore, gefitinib, and EIPA showed significant

decreases in viability on cells treated with C_{16} ceramide-loaded O-GNRs and C_6 ceramide (A, B). Filipin showed a significant increase in cells treated with C_{16} ceramide-loaded O-GNRs and C_6 ceramide (B). For C_{24} ceramide treatment, dynasore lowered the viability of UV-irradiated cells with C_{24} ceramide-loaded O-GNRs (C) while treatment with gefitinib, filipin, and EIPA showed no significant effect (C, D). * indicates significant difference from "Untreated" and † indicates significant difference from "C_6" (A, B) or "UV" (C, D). For High and Low concentrations: for dynasore Hi = 80 µM, Lo = 40 µM; for Gefitinib Hi = 1 µM, Lo = 0.5 µM; for EIPA Hi = 0.5 mM, Lo = 0.25 mM; for Filipin, Hi = 3 µg/mL, Lo = 2 µg/mL.

For C_{24} ceramide-loaded O-GNRs in conjunction with UV radiation, the only uptake inhibitor to show significant decrease in viability between C_{24} ceramide-loaded O-GNRs with or without the inhibitor was dynasore, which had 101.11% the viability of the untreated control with dynasore and 129.29% the viability of the untreated control without dynasore (Fig. 5.4C). This was true of O-GNRs without C_{24} ceramide as well, which had a viability of 102.86% of the untreated control with dynasore and 120.04% the viability of the untreated control without dynasore (Fig. 5.4C). None of the uptake inhibitors showed a significant effect on cells treated with only UV (4.4C and D).

Figure 5.5 shows the effects of uptake inhibitors (Higher concentration tested) on apoptosis as measured by caspase activity for C_6 ceramide and C_{16} ceramide-loaded O-GNRs, or UV irradiation and C_{24} ceramide. For cells treated with C_6 ceramide and C_{16} ceramide-loaded O-GNRs, cells treated with dynasore and EIPA showed an increase in apoptosis compared to the condition without inhibitors (475.4% compared to 303.5% for dynasore, 492.19% compared to 289.6% for EIPA), filipin showed a decrease (100.62% compared to 172.07%), and gefitinib showed no change overall (Fig. 5.5A). For cells treated with ceramide loaded O-GNRs and UV irradiation, none of the uptake inhibitors had any effect on apoptosis between any of the condition tested (Fig. 5.5 B).

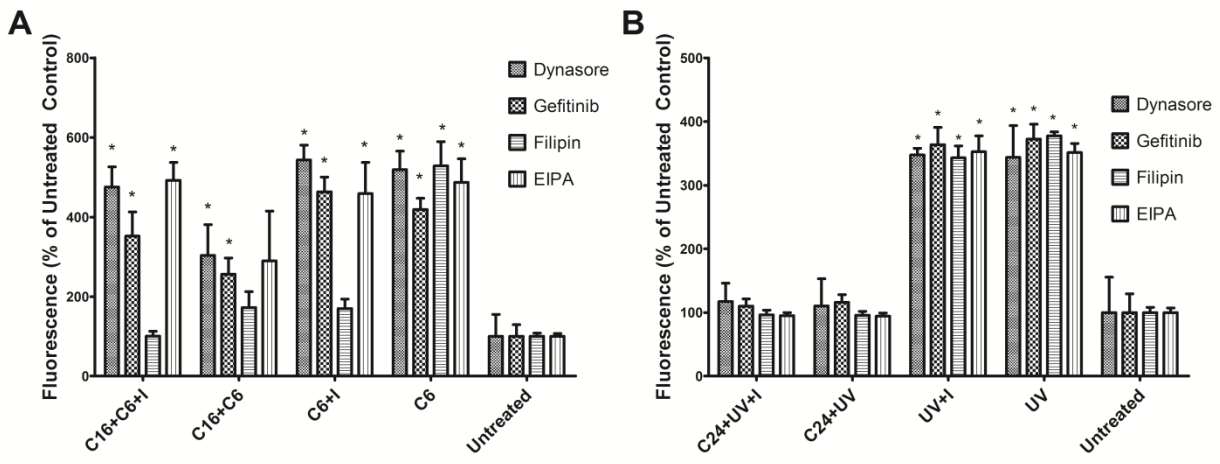

Figure 5.5. Effects of uptake inhibitors on apoptosis induced by C_{16} ceramide loaded O-GNRs and C_6 ceramide (A) or C_{24} ceramide loaded O-GNRs and UV irradiation (B). For cells treated with C_{16} ceramide-loaded O-GNRs and C_6 ceramide, dynasore and EIPA treatment led to an increase in apoptosis, filipin led to a decrease in apoptosis, and gefitinib had no significant effect (A). For cells treated with C_{24} ceramide-loaded O-GNRs and UV, no inhibitor had an effect on the level of apoptosis observed (B). * indicates significant difference from "Untreated." Concentration of inhibitors: dynasore = 80 μM, Gefitinib = 1 μM, EIPA = 0.5 mM, Filipin, = 3 μg/mL.

Confocal Microscopy with C_{12} NBD Ceramide

To visualize the uptake of ceramide into cells, we used the medium chain ceramide C_{12} tagged with the fluorescent NBD marker. We compared C_{12} NBD loaded O-GNRs to C_{12} delivered by ethanol. We also tested the uptake inhibitors dynasore and gefitinib in conjunction with these treatments to see if there would be an effect on the entry of C_{12} NBD loaded O-GNRs into HeLa cells. We also tested the endosome disruptor desipramine[82] to see if it would have a significant effect on the localization of C_{12} NBD loaded O-GNRs. Figure 5.6 shows the uptake of C_{12} NBD loaded O-GNRs or C_{12} NBD ceramide alone into HeLa cells after 2 hours. Cells treated with C_{12} NBD alone showed somewhat higher fluorescence overall (Fig. 5.6 A), with C_{12} NBD loaded O-GNRs showing more localization to endosomes (Fig. 5.6 E). With pre-treatment with the uptake inhibitors dynasore and gefitinib, there was a significant drop in the fluorescence

of cells treated with C_{12} NBD loaded O-GNRs (Fig. 5.6 B and C). However, cells pre-treated with these uptake inhibitors and subsequent treatment with C_{12} NBD ceramide alone saw no significant decrease in fluorescence, indicating that they had no effect on its entry into HeLa cells when not loaded onto O-GNRs (Fig. 5.6 F and G). When cells were pretreated with 15μM of the endosome disruptor desipramine , there was no significant effect on cells treated with C_{12} NBD loaded O-GNRs (Fig. 5.6 D). However, there was a marked effect on cells treated with C_{12} NBD alone, with fluorescence spreading evenly throughout the cell, indicating the release of C_{12} NBD ceramide from endosomes (Fig. 5.6 H).

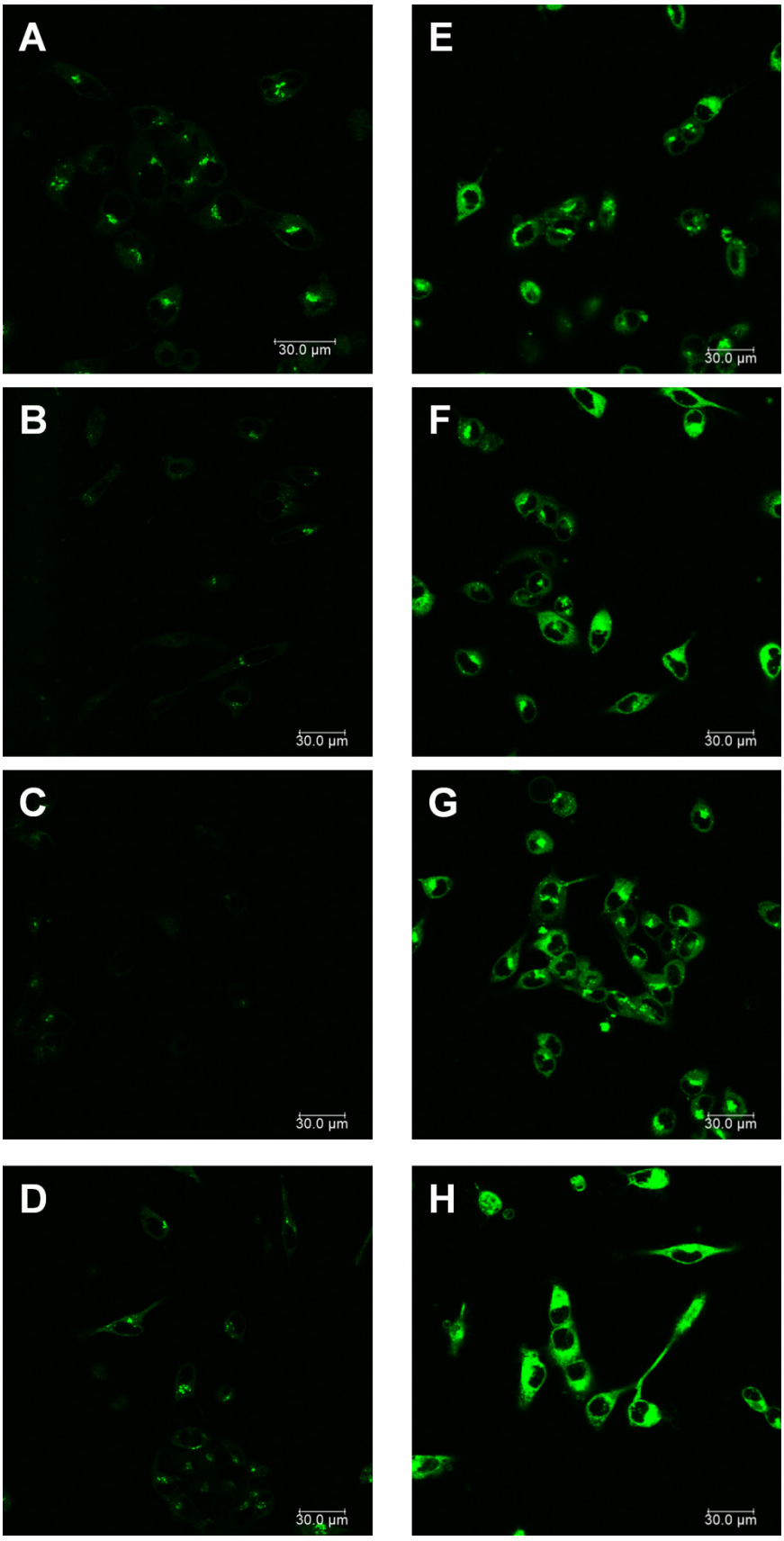
A
30.0 µm
E
30.0 µm
B
30.0 µm
F
30.0 µm
C
30.0 µm
G
30.0 µm
D
30.0 µm
H
30.0 µm

Figure 5.6. Confocal Microscopy images of HeLa cells treated with fluorescent C_{12} NBD ceramide loaded onto O-GNRs (A-D) or fluorescent C_{12} NBD ceramide only (E-H). Ceramide loaded onto O-GNRs (A) shows ceramide more localized to endosomes after 2 hours than free ceramide (E). Cells treated with Dynasore and ceramide-loaded O-GNRs (B) and Gefitinib and ceramide-loaded O-GNRs (C) show significantly less fluorescence than cells not treated with inhibitors of O-GNR uptake (A). However, cells treated with Dynasore and free ceramide (F) and Gefitinib and free ceramide (G) show no difference than cells treated with free ceramide alone (E). Cells treated with free ceramide and endosome disruptor desipramine (H) show significantly less endosome localization than cells treated with free ceramide only (E). However, cells treated with desipramine and ceramide-loaded O-GNRs (D) show no difference in endosome localization compared to cells treated with ceramide-loaded O-GNRs only (A).

TEM of Ceramide Loaded O-GNR Uptake

To determine that ceramide loaded O-GNRs were being uptaken into cells, we obtained transmission electron microscopy images of HeLa cells incubated with C_{16} and C_{24} ceramide-loaded O-GNRs after 24 hours. Figure 5.7 shows the uptake of C_{16} and C_{24} ceramide-loaded O-GNRs into HeLa cells. Both C_{16} ceramide-loaded O-GNRs (Fig. 5.7 A and C) and C_{24} ceramide -loaded O-GNRs (Fig. 5.7 B and D) showed high levels of uptake after 24 hr. There is also evidence of the outward "blebbing" of the membrane characteristic of the mechanism by which O-GNRs get uptaken into cells[80] (Fig. 5.7 A and C, indicated by arrows). There is the indication of O-GNRs being contained within endosome as large voids around them.

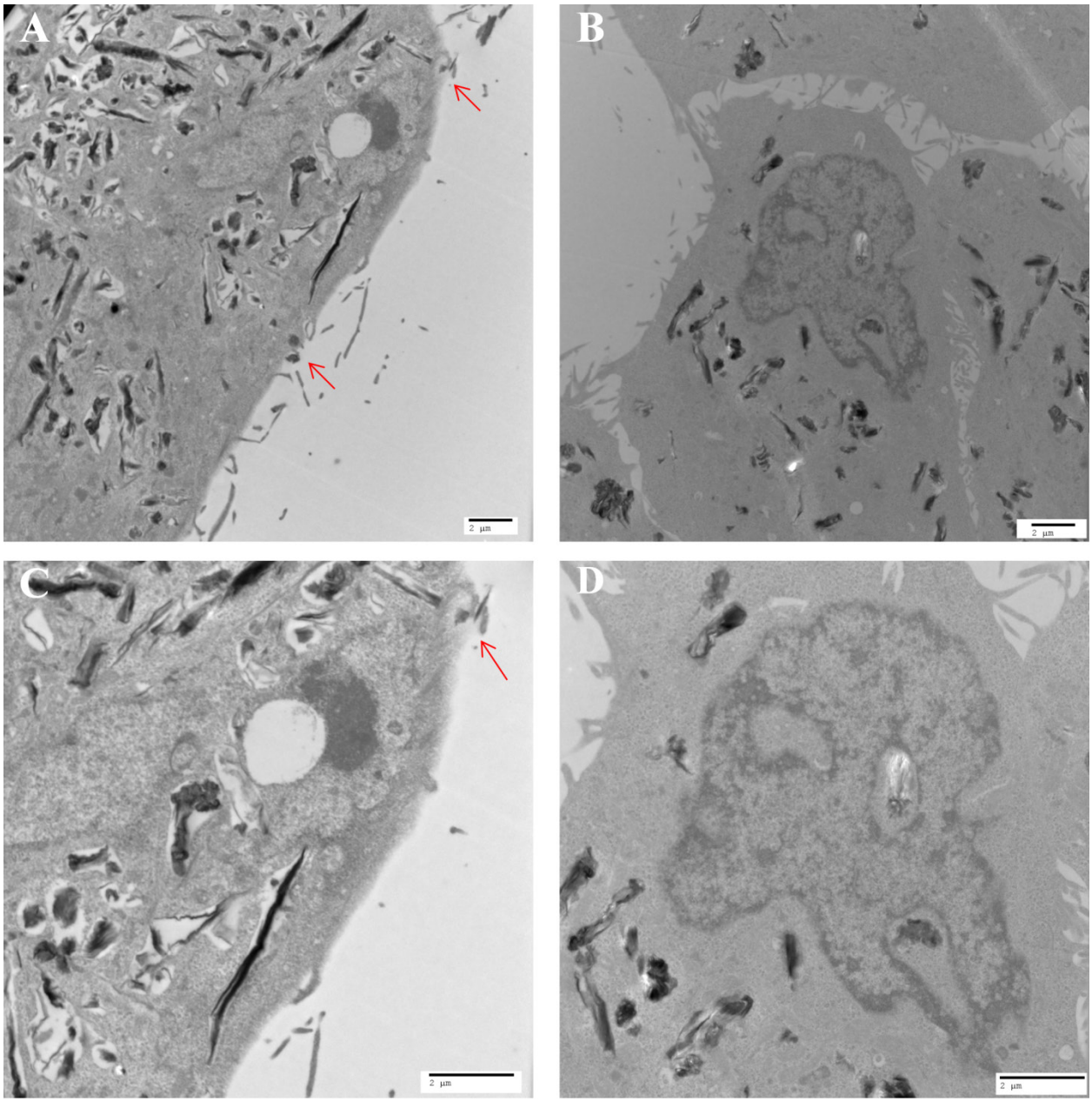

Figure 5.7. Transmission electron microscopy images of HeLa cells incubated with ceramide loaded O-GNRs after 24 hr. Both C_{16} ceramide-loaded O-GNRs (A, C) and C_{24} ceramide-loaded O-GNRs (B, D) show high degrees of nanoparticle uptake. There is also evidence of membrane "blebbing" (arrows) associated with the uptake mechanism (A, C). Zoomed-in views of these regions of interest (C, D) also show O-GNRs localized to endosomes.

Discussion

Since the discovery of its bioactive properties over two decades ago[83], there has been great interest in developing ceramide for therapeutic purposes. However, much of this focus has been on the short-chain ceramide analogs such as C_6 ceramide, which have seen several different approaches to deliver it to cancer cells and induce apoptosis[4,47-49,51,84,85]. There has been considerably less attention devoted to the longer chain ceramides in the realm of therapeutic delivery, mostly due to the difficulties associated with these ceramides in aqueous solution. To this end, we have developed a method to load the long chain ceramides C_{16} and C_{24} ceramide onto O-GNRs.

The loading of C_{16} and C_{24} ceramides onto O-GNRs was 61.47% and 48.76%, respectively. This loading was calculated on a mass per mass basis, whereas the loading efficiency for liposomes is often compared on a mole per mole basis. As there is a large degree of size variation between individual O-GNR nanoparticles (Fig. 5.1), there is not necessarily a way to accurately calculate a molar concentration. However, the mass/mass basis of ceramide loading onto O-GNRs was comparable to the mole/mole basis of C_{16} ceramide into liposomes by Shabbits et al. who developed liposomes containing 50% molar ration of C_{16} ceramide along with 50% cholesteryl hemisuccinate[48].

C_{16} and C_{24} ceramide were selected for this study because of their specific biological effects. C_{16} ceramide has generally been shown to have pro-apoptotic effects, while C_{24} ceramide has been shown to have pro-survival effects[86-92]. In HeLa cells specifically, a shift from C_{24} ceramide to C_{16} ceramide has been shown to increase susceptibility to apoptosis[93]. Given these specific effects, we wanted to test our C_{16} and C_{24} ceramide-loaded O-GNRs to see if we could replicate this effects through external delivery along with the pro-apoptotic stressors C_6

ceramide and UV irradiation. We were able to significantly replicate these effects to a certain degree, although there are some caveats. We found that C_{16} ceramide-loaded O-GNRs were able to induce a greater degree of apoptosis in conjunction with C_6 ceramide than O-GNRs alone, and we also found that C_{24} ceramide-loaded O-GNRs were able to protect cells from UV radiation better than O-GNRs alone (Fig. 5.2). However, C_6 ceramide treatment alone was better than in conjunction with our C_{16} ceramide-loaded O-GNRs, and we found that we were not able to use our C_{16} ceramide-loaded O-GNRs to sensitize HeLa cells to UV irradiation at all, despite much previous evidence showing that externally delivered C_{16} ceramide is capable of sensitizing cells to radiation[57,59] (Fig 5.2). This is probably not related to the ceramides having different biological effects than previously reported, but rather the O-GNRs themselves.

Graphene oxide nanoparticles have a large number of oxygen containing functional groups. It has been previously demonstrated that graphene oxide nanoparticles can act as anti-oxidants and allow the buffering of reaction oxygen species (ROS)[94]. ROS is an important cell signaling mechanism that has largely pro-apoptotic effects and has been shown to be an important mediator of both UV and C_6 ceramide-induced apoptosis[95-98]. In this case, we have demonstrated that O-GNRs alone are capable of rescuing HeLa cells from the pro-apoptotic stressors of UV irradiation and C_6 ceramide (Fig. 5.2, 5.3). However, the effects of O-GNRs on HeLa cells may not be limited just to buffering of ROS.

Through the quantification of several sphingolipid species after treatment with O-GNRs and ceramide loaded O-GNRs, we found that O-GNRs had a significant effect on sphingolipid metabolism on their own (Table 5.1). O-GNRs induced a 17.7 fold increase in the levels of sphingosine compared to the untreated control, which is relevant for two reasons. The first has to do with how sphingolipids are synthesized. All sphingolipids are first synthesized via the *de*

novo pathway, one of three pathways for ceramide synthesis[99]. Although many complex sphingolipids contain a 4,5 trans double bond in the sphingoid backbone, this step does not occur until the conversion of dihydroceramide into ceramide by ceramide desaturase. As of yet, there have been no mammalian 'dihydrosphingosine desaturase' enzymes elucidated, meaning that all sphingosine is generated through the degradation of ceramide by ceramidases. Thus high sphingosine levels may indicate that O-GNRs are increasing the activity of ceramidases, which has been linked to apoptosis resistance[42,43]. The second reason why high sphingosine levels are relevant is due to the possible metabolic fates of sphingosine. Although it can be converted back to ceramide through the salvage pathway[99], it can also be phosphorylated to sphingosine-1 phosphate, a sphingolipid with many pro-survival effects[100]. However, we also measured sphingosine-1 phosphate levels but found that cells treated with O-GNRs did not have significantly higher levels compared to the untreated control (Table 5.1).

Through the quantification of lipids, we also found that we were significantly increasing the levels of C_{16} and C_{24} ceramides compared to untreated cells (Table 5.1). We also found that there was a high degree of 'background' from the sham control, which was higher than the ceramide quantified for both ceramides, although it was not significant in the case of C_{16} ceramide (Table 5.1). There was a high degree of variability, however, and this was a measure of the maximum possible background. In both cases, there was an extremely large difference between how much ceramide was detected, and was theoretically put in each sample. The detected amount of ceramide was on the order of picomoles, while the loading results would suggest that the amount of ceramide was on the order of micromoles, a difference of several orders of magnitude. This may indicate that there is poor release of ceramide from the nanoparticles. One possible explanation is that the O-GNRs may be aggregating around ceramide

during the loading process, and once inside cells, are not releasing ceramide, keeping it trapped between 'sandwiched' layers of O-GNRs. Aggregation induced by the mixing of water and ethanol was a major obstacle in the development of this loading method, and the particle size data presented here may indicate that this is occurring on a microscopic level. There was a small decrease in the number of small particles and a slight increase in the number of large particles after loading O-GNRs compared to prior to loading (Fig. 5.1). This may indicate that some of the smaller particles are combining with larger particles to form even larger aggregates, and trapping the ceramide between them in the process. However this difference between before and after loading was not large, and since the method used measures particle size only indirectly, it is unlikely that these results are significant enough for this explanation.

We also wanted to determine if the loading of ceramide onto O-GNRs would have a significant effect on their entry into cells. Previously we determined that O-GNRs have a macropinocytotic-like, dynamin-dependent mechanism that relies on activation of EGFR[80]. Because ceramides are important components of cellular membranes, we wanted to determine if loading ceramides onto O-GNRs would have an effect on their uptake. We used the same uptake inhibitors in conjunction with our ceramide loaded O-GNRs to determine if disrupting the uptake of our ceramide loaded O-GNRs would change their effects on HeLa cell viability and apoptosis. For C_6 ceramide treatment in conjunction with our C_{16} ceramide-loaded O-GNRs, we found a decrease in viability with dynasore, gefitinib, and EIPA, the three inhibitors which were previously found to inhibit O-GNR entry into HeLa cells (Fig. 5.4A and B)[80]. We also found that dynasore and EIPA caused an increase in apoptosis. Given the apparent protective effects of O-GNRs against C_6 ceramide-induced apoptosis, these results would be consistent with these inhibitors having the same ability to block the entry of O-GNRs into cells, indicating no

significant change from previous results[80]. The exception is filipin, which was previously not shown to have an effect on O-GNR uptake, but here was shown to have the opposite effects of the other inhibitors (Fig. 5.4 B, Fig. 5.5). However, this could be explained by previous data showing that filipin can inhibit the uptake of C_6 ceramide[101], making it likely that this effect was related to the blocking of ceramide uptake rather than O-GNR uptake. The uptake inhibitor data for cells treated with C_{24} ceramide-loaded O-GNRs and UV irradiation showed a similar pattern, with the effects of dynasore consistent with blocking the protective effect of O-GNRs on UV-induced apoptosis (Fig. 5.4C and D). TEM data also confirmed no significant change in the uptake of O-GNRs due to ceramide loading, with high levels of O-GNRs visible in HeLa cells as well as the "blebbing" of the membrane related to the uptake mechanism of O-GNRs (Fig 5.7).

Based on the data that the entry of O-GNRs was not disrupted due to ceramide loading, we wanted to determine the fate of ceramides once they actually entered cells. For this, we used the medium chain ceramide analog C_{12} ceramide with the fluorescent tag NBD. Although not as hydrophobic as its long-chain counterparts, C_{12} ceramide cannot enter cells as easily as short chain ceramides such as C_6 ceramide[102]. We found that C_{12} NBD loaded O-GNRs and free C_{12} had a similar uptake pattern into cells, with much of the ceramide localized to endosomes (Fig 5.7 A and E). However, we found that when uptake inhibitors were introduced, there were stark differences in uptake, with dynasore and gefitinib-treated cells showing a marked decrease in fluorescence from C_{12} NBD loaded O-GNRs (Fig 5.7 B and C) while there was no effect on free C_{12} NBD ceramide (Fig. 5.7 F and G). This indicates that the fluorescence present in cells treated with ceramide loaded O-GNRs was due specifically to the uptake of O-GNRs and not due to ceramide coming off the O-GNRs and entering cells as free ceramide. We also found that the endosome disruptor desipramine was able to release free ceramide from endosomes (Fig. 5.7 H)

while there was no effect on the endosome localization of ceramide when it was delivered via O-GNRs (Fig. 5.7 D). This may indicate that ceramide from O-GNRs may have a difficult time escaping from endosomes, which may also contribute to the decreased efficacy of C_{16} ceramide-loaded O-GNRs in inducing apoptosis.

Conclusions

We have developed a facile method for the loading of long-chain ceramides onto O-GNRs, which are able to deliver these ceramides to cells and exert significant biological effects. However, these O-GNRs themselves have significant biological effects on cells and reduce the overall combinatorial effect between the long chain ceramides and UV or C_6 ceramide treatment. Despite these limitations, O-GNRs are a promising method for the therapeutic delivery of long chain ceramides. However, before this goal can be realized, a substantial amount of optimization of these particles for use with ceramide is needed.

Acknowledgements

We would like to thank Susan Van Horn and the Central Microscopy Facility at Stony Brook University for her assistance with TEM. We would like to thank Izolda Mileva and the Lipidomics Facility for her help with mass spectrometry.

References

1 Gault, C. R., Obeid, L. M. & Hannun, Y. A. An overview of sphingolipid metabolism: from synthesis to breakdown. *Advances in experimental medicine and biology* **688**, 1-23 (2010).

2 Hannun, Y. A., Luberto, C. & Argraves, K. M. Enzymes of sphingolipid metabolism: from modular to integrative signaling. *Biochemistry* **40**, 4893-4903 (2001).

3 Adam, D., Heinrich, M., Kabelitz, D. & Schutze, S. Ceramide: does it matter for T cells? *Trends in immunology* **23**, 1-4 (2002).

4 Zou, P., Stern, S. T. & Sun, D. PLGA/liposome hybrid nanoparticles for short-chain ceramide delivery. *Pharmaceutical research* **31**, 684-693, doi:10.1007/s11095-013-1190-5 (2014).

5 Okazaki, T., Bell, R. M. & Hannun, Y. A. Sphingomyelin turnover induced by vitamin D3 in HL-60 cells. Role in cell differentiation. *The Journal of biological chemistry* **264**, 19076-19080 (1989).

6 Venable, M. E., Lee, J. Y., Smyth, M. J., Bielawska, A. & Obeid, L. M. Role of ceramide in cellular senescence. *The Journal of biological chemistry* **270**, 30701-30708 (1995).

7 Hetz, C. A. *et al.* Caspase-dependent initiation of apoptosis and necrosis by the Fas receptor in lymphoid cells: onset of necrosis is associated with delayed ceramide increase. *Journal of cell science* **115**, 4671-4683 (2002).

8 Obeid, L. M., Linardic, C. M., Karolak, L. A. & Hannun, Y. A. Programmed cell death induced by ceramide. *Science* **259**, 1769-1771 (1993).

9 Pattingre, S., Bauvy, C., Levade, T., Levine, B. & Codogno, P. Ceramide-induced autophagy: To junk or to protect cells? *Autophagy* **5**, 558-560 (2009).

10 White-Gilbertson, S. *et al.* Ceramide synthase 6 modulates TRAIL sensitivity and nuclear translocation of active caspase 3 in colon cancer cells. *Oncogene* **28**, 1132-1141, doi:10.1038/onc.2008.468 (2009).

11 Nam, S. Y., Amoscato, A. A. & Lee, Y. J. Low glucose-enhanced TRAIL cytotoxicity is mediated through the ceramide-Akt-FLIP pathway. *Oncogene* **21**, 337-346, doi:10.1038/sj.onc.1205068 (2002).

12 Dumitru, C. A. & Gulbins, E. TRAIL activates acid sphingomyelinase via a redox mechanism and releases ceramide to trigger apoptosis. *Oncogene* **25**, 5612-5625, doi:10.1038/sj.onc.1209568 (2006).

13 Brenner, B. *et al.* Fas/CD95/Apo-I activates the acidic sphingomyelinase via caspases. *Cell Death Differ* **5**, 29-37, doi:10.1038/sj.cdd.4400307 (1998).

14 Cremesti, A. *et al.* Ceramide enables fas to cap and kill. *The Journal of biological chemistry* **276**, 23954-23961, doi:10.1074/jbc.M101866200 (2001).

15 Elojeimy, S. *et al.* Role of Acid Ceramidase in Resistance to FasL: Therapeutic Approaches Based on Acid Ceramidase Inhibitors and FasL Gene Therapy. *Molecular therapy : the journal of the American Society of Gene Therapy* **15**, 1259-1263 (2007).

16 Huang, S. T., Yang, R. C., Chen, M. Y. & Pang, J. H. Phyllanthus urinaria induces the Fas receptor/ligand expression and ceramide-mediated apoptosis in HL-60 cells. *Life sciences* **75**, 339-351, doi:10.1016/j.lfs.2003.12.013 (2004).

17 Yoon, G. *et al.* Ceramide increases Fas-mediated apoptosis in glioblastoma cells through FLIP down-regulation. *Journal of neuro-oncology* **60**, 135-141 (2002).

18 Donato, N. J. & Klostergaard, J. Distinct stress and cell destruction pathways are engaged by TNF and ceramide during apoptosis of MCF-7 cells. *Experimental cell research* **294**, 523-533, doi:10.1016/j.yexcr.2003.11.021 (2004).

19 Higuchi, M., Singh, S., Jaffrezou, J. P. & Aggarwal, B. B. Acidic sphingomyelinase-generated ceramide is needed but not sufficient for TNF-induced apoptosis and nuclear factor-kappa B activation. *Journal of immunology (Baltimore, Md. : 1950)* **157**, 297-304 (1996).

20 Karasavvas, N. & Zakeri, Z. Relationships of apoptotic signaling mediated by ceramide and TNF-alpha in U937 cells. *Cell Death Differ* **6**, 115-123, doi:10.1038/sj.cdd.4400482 (1999).

21 Sawada, M. *et al.* Molecular mechanisms of TNF-alpha-induced ceramide formation in human glioma cells: P53-mediated oxidant stress-dependent and -independent pathways. *Cell Death Differ* **11**, 997-1008, doi:10.1038/sj.cdd.4401438 (2004).

22 Babiychuk, E. B. *et al.* The targeting of plasmalemmal ceramide to mitochondria during apoptosis. *PloS one* **6**, e23706, doi:10.1371/journal.pone.0023706 (2011).

23 Bionda, C., Portoukalian, J., Schmitt, D., Rodriguez-Lafrasse, C. & Ardail, D. Subcellular compartmentalization of ceramide metabolism: MAM (mitochondria-associated membrane) and/or mitochondria? *Biochem J* **382**, 527-533, doi:10.1042/bj20031819 (2004).

24 Birbes, H., El Bawab, S., Hannun, Y. A. & Obeid, L. M. Selective hydrolysis of a mitochondrial pool of sphingomyelin induces apoptosis. *FASEB journal : official publication of the Federation of American Societies for Experimental Biology* **15**, 2669-2679, doi:10.1096/fj.01-0539com (2001).

25 Yuan, H., Williams, S. D., Adachi, S., Oltersdorf, T. & Gottlieb, R. A. Cytochrome c dissociation and release from mitochondria by truncated Bid and ceramide. *Mitochondrion* **2**, 237-244, doi:10.1016/s1567-7249(02)00106-x (2003).

26 Stiban, J., Caputo, L. & Colombini, M. Ceramide synthesis in the endoplasmic reticulum can permeabilize mitochondria to proapoptotic proteins. *Journal of lipid research* **49**, 625-634, doi:10.1194/jlr.M700480-JLR200 (2008).

27 Morales, M. C. *et al.* 4-HPR-mediated leukemia cell cytotoxicity is triggered by ceramide-induced mitochondrial oxidative stress and is regulated downstream by Bcl-2. *Free radical research* **41**, 591-601, doi:10.1080/10715760701218558 (2007).

28 Luo, X., Budihardjo, I., Zou, H., Slaughter, C. & Wang, X. Bid, a Bcl2 interacting protein, mediates cytochrome c release from mitochondria in response to activation of cell surface death receptors. *Cell* **94**, 481-490 (1998).

29 Lin, C. F. *et al.* Bcl-2 rescues ceramide- and etoposide-induced mitochondrial apoptosis through blockage of caspase-2 activation. *The Journal of biological chemistry* **280**, 23758-23765, doi:10.1074/jbc.M412292200 (2005).

30 Morad, S. A. & Cabot, M. C. Ceramide-orchestrated signalling in cancer cells. *Nature reviews. Cancer* **13**, 51-65, doi:10.1038/nrc3398 (2013).

31 Cuvillier, O. *et al.* Sphingosine generation, cytochrome c release, and activation of caspase-7 in doxorubicin-induced apoptosis of MCF7 breast adenocarcinoma cells. *Cell Death Differ* **8**, 162-171, doi:10.1038/sj.cdd.4400793 (2001).

32 Dumitru, C. A., Carpinteiro, A., Trarbach, T., Hengge, U. R. & Gulbins, E. Doxorubicin enhances TRAIL-induced cell death via ceramide-enriched membrane platforms.

Apoptosis : an international journal on programmed cell death **12**, 1533-1541, doi:10.1007/s10495-007-0081-9 (2007).

33 Gouaze, V. *et al.* Glucosylceramide synthase blockade down-regulates P-glycoprotein and resensitizes multidrug-resistant breast cancer cells to anticancer drugs. *Cancer research* **65**, 3861-3867, doi:10.1158/0008-5472.can-04-2329 (2005).

34 Gouaze, V. *et al.* Overexpression of glucosylceramide synthase and P-glycoprotein in cancer cells selected for resistance to natural product chemotherapy. *Molecular cancer therapeutics* **3**, 633-639 (2004).

35 Gouaze-Andersson, V. *et al.* Ceramide and glucosylceramide upregulate expression of the multidrug resistance gene MDR1 in cancer cells. *Biochimica et biophysica acta* **1771**, 1407-1417, doi:10.1016/j.bbalip.2007.09.005 (2007).

36 Inokuchi, J. *et al.* Inhibition of experimental metastasis of murine Lewis lung carcinoma by an inhibitor of glucosylceramide synthase and its possible mechanism of action. *Cancer research* **50**, 6731-6737 (1990).

37 Lavie, Y., Cao, H.-t., Bursten, S. L., Giuliano, A. E. & Cabot, M. C. Accumulation of Glucosylceramides in Multidrug-resistant Cancer Cells. *Journal of Biological Chemistry* **271**, 19530-19536, doi:10.1074/jbc.271.32.19530 (1996).

38 Liu, Y. Y., Han, T. Y., Giuliano, A. E. & Cabot, M. C. Expression of glucosylceramide synthase, converting ceramide to glucosylceramide, confers adriamycin resistance in human breast cancer cells. *The Journal of biological chemistry* **274**, 1140-1146 (1999).

39 Lucci, A. *et al.* Glucosylceramide: a marker for multiple-drug resistant cancers. *Anticancer research* **18**, 475-480 (1998).

40 Morjani, H. *et al.* Elevation of glucosylceramide in multidrug-resistant cancer cells and accumulation in cytoplasmic droplets. *International journal of cancer* **94**, 157-165 (2001).

41 Radin, N. S. Chemotherapy by slowing glucosphingolipid synthesis. *Biochemical pharmacology* **57**, 589-595 (1999).

42 Cheng, J. C. *et al.* Radiation-induced acid ceramidase confers prostate cancer resistance and tumor relapse. *J Clin Invest* **123**, 4344-4358, doi:10.1172/jci64791 (2013).

43 Holman, D. H. *et al.* Lysosomotropic acid ceramidase inhibitor induces apoptosis in prostate cancer cells. *Cancer chemotherapy and pharmacology* **61**, 231-242, doi:10.1007/s00280-007-0465-0 (2008).

44 Roh, J.-L., Park, J. Y., Kim, E. H. & Jang, H. J. Targeting acid ceramidase sensitises head and neck cancer to cisplatin. *European Journal of Cancer* **52**, 163-172, doi:http://dx.doi.org/10.1016/j.ejca.2015.10.056 (2016).

45 Seelan, R. S. *et al.* Human acid ceramidase is overexpressed but not mutated in prostate cancer. *Genes, chromosomes & cancer* **29**, 137-146 (2000).

46 Strelow, A. *et al.* Overexpression of acid ceramidase protects from tumor necrosis factor-induced cell death. *The Journal of experimental medicine* **192**, 601-612 (2000).

47 Zhai, L., Sun, N., Han, Z., Jin, H. C. & Zhang, B. Liposomal short-chain C6 ceramide induces potent anti-osteosarcoma activity in vitro and in vivo. *Biochemical and biophysical research communications* **468**, 274-280, doi:10.1016/j.bbrc.2015.10.113 (2015).

48 Shabbits, J. A. & Mayer, L. D. Intracellular delivery of ceramide lipids via liposomes enhances apoptosis in vitro. *Biochimica et biophysica acta* **1612**, 98-106 (2003).

49 Kester, M. *et al.* Preclinical development of a C6-ceramide NanoLiposome, a novel sphingolipid therapeutic. *Biological chemistry* **396**, 737-747, doi:10.1515/hsz-2015-0129 (2015).

50 Zolnik, B. S. *et al.* Rapid distribution of liposomal short-chain ceramide in vitro and in vivo. *Drug metabolism and disposition: the biological fate of chemicals* **36**, 1709-1715, doi:10.1124/dmd.107.019679 (2008).

51 Kester, M. *et al.* Calcium phosphate nanocomposite particles for in vitro imaging and encapsulated chemotherapeutic drug delivery to cancer cells. *Nano Lett* **8**, 4116-4121, doi:10.1021/nl802098g (2008).

52 Stover, T. C., Kim, Y. S., Lowe, T. L. & Kester, M. Thermoresponsive and biodegradable linear-dendritic nanoparticles for targeted and sustained release of a pro-apoptotic drug. *Biomaterials* **29**, 359-369, doi:10.1016/j.biomaterials.2007.09.037 (2008).

53 Devalapally, H., Duan, Z., Seiden, M. V. & Amiji, M. M. Paclitaxel and ceramide co-administration in biodegradable polymeric nanoparticulate delivery system to overcome drug resistance in ovarian cancer. *International journal of cancer* **121**, 1830-1838, doi:10.1002/ijc.22886 (2007).

54 Devalapally, H., Duan, Z., Seiden, M. V. & Amiji, M. M. Modulation of drug resistance in ovarian adenocarcinoma by enhancing intracellular ceramide using tamoxifen-loaded biodegradable polymeric nanoparticles. *Clinical cancer research : an official journal of the American Association for Cancer Research* **14**, 3193-3203, doi:10.1158/1078-0432.ccr-07-4973 (2008).

55 Wu, C. H. *et al.* Trojan-horse nanotube on-command intracellular drug delivery. *Nano Lett* **12**, 5475-5480, doi:10.1021/nl301865c (2012).

56 Stancevic, B. & Kolesnick, R. Ceramide-rich platforms in transmembrane signaling. *FEBS letters* **584**, 1728-1740, doi:10.1016/j.febslet.2010.02.026 (2010).

57 Truman, J. P. *et al.* Endothelial membrane remodeling is obligate for anti-angiogenic radiosensitization during tumor radiosurgery. *PloS one* **5**, e12310, doi:10.1371/journal.pone.0012310 (2010).

58 Paris, F. *et al.* Natural ceramide reverses Fas resistance of acid sphingomyelinase(-/-) hepatocytes. *The Journal of biological chemistry* **276**, 8297-8305, doi:10.1074/jbc.M008732200 (2001).

59 Deng, X. *et al.* Ceramide biogenesis is required for radiation-induced apoptosis in the germ line of C. elegans. *Science* **322**, 110-115, doi:10.1126/science.1158111 (2008).

60 Kjellberg, M. A., Lönnfors, M., Slotte, J. P. & Mattjus, P. Metabolic Conversion of Ceramides in HeLa Cells - A Cholesteryl Phosphocholine Delivery Approach. *PloS one* **10**, e0143385, doi:10.1371/journal.pone.0143385 (2015).

61 Ji, L., Zhang, G., Uematsu, S., Akahori, Y. & Hirabayashi, Y. Induction of apoptotic DNA fragmentation and cell death by natural ceramide. *FEBS letters* **358**, 211-214, doi:http://dx.doi.org/10.1016/0014-5793(94)01428-4 (1995).

62 Su, X. *et al.* Co-delivery of doxorubicin and PEGylated C16-ceramide by nanoliposomes for enhanced therapy against multidrug resistance. *Nanomedicine (London, England)* **10**, 2033-2050, doi:10.2217/nnm.15.50 (2015).

63 Lu, C. H., Yang, H. H., Zhu, C. L., Chen, X. & Chen, G. N. A graphene platform for sensing biomolecules. *Angewandte Chemie (International ed. in English)* **48**, 4785-4787, doi:10.1002/anie.200901479 (2009).

64 Wang, Y. *et al.* Aptamer/graphene oxide nanocomplex for in situ molecular probing in living cells. *Journal of the American Chemical Society* **132**, 9274-9276, doi:10.1021/ja103169v (2010).

65 Song, Y., Chen, Y., Feng, L., Ren, J. & Qu, X. Selective and quantitative cancer cell detection using target-directed functionalized graphene and its synergetic peroxidase-like activity. *Chemical communications (Cambridge, England)* **47**, 4436-4438, doi:10.1039/c0cc05533f (2011).

66 Feng, L., Zhang, S. & Liu, Z. Graphene based gene transfection. *Nanoscale* **3**, 1252-1257, doi:10.1039/c0nr00680g (2011).

67 Chen, B. *et al.* Polyethylenimine-functionalized graphene oxide as an efficient gene delivery vector. *Journal of Materials Chemistry* **21**, 7736-7741, doi:10.1039/C1JM10341E (2011).

68 Bao, H. *et al.* Chitosan-functionalized graphene oxide as a nanocarrier for drug and gene delivery. *Small* **7**, 1569-1578, doi:10.1002/smll.201100191 (2011).

69 Hu, W. *et al.* Graphene-Based Antibacterial Paper. *ACS nano* **4**, 4317-4323, doi:10.1021/nn101097v (2010).

70 Park, S. Y. *et al.* Enhanced differentiation of human neural stem cells into neurons on graphene. *Advanced materials (Deerfield Beach, Fla.)* **23**, H263-267, doi:10.1002/adma.201101503 (2011).

71 Robinson, J. T. *et al.* Ultrasmall Reduced Graphene Oxide with High Near-Infrared Absorbance for Photothermal Therapy. *Journal of the American Chemical Society* **133**, 6825-6831, doi:10.1021/ja2010175 (2011).

72 Hummers, W. S. & Offeman, R. E. Preparation of Graphitic Oxide. *Journal of the American Chemical Society* **80**, 1339-1339, doi:10.1021/ja01539a017 (1958).

73 Kosynkin, D. V. *et al.* Longitudinal unzipping of carbon nanotubes to form graphene nanoribbons. *Nature* **458**, 872-876, doi:http://www.nature.com/nature/journal/v458/n7240/suppinfo/nature07872_S1.html (2009).

74 Yang, X. *et al.* High-Efficiency Loading and Controlled Release of Doxorubicin Hydrochloride on Graphene Oxide. *The Journal of Physical Chemistry C* **112**, 17554-17558, doi:10.1021/jp806751k (2008).

75 Xu, Z. *et al.* Delivery of paclitaxel using PEGylated graphene oxide as a nanocarrier. *ACS applied materials & interfaces* **7**, 1355-1363, doi:10.1021/am507798d (2015).

76 Misra, S. K., Kondaiah, P., Bhattacharya, S. & Rao, C. Graphene as a nanocarrier for tamoxifen induces apoptosis in transformed cancer cell lines of different origins. *Small* **8**, 131-143 (2012).

77 Sun, X. *et al.* Nano-Graphene Oxide for Cellular Imaging and Drug Delivery. *Nano Res* **1**, 203-212, doi:10.1007/s12274-008-8021-8 (2008).

78 Zhang, L., Xia, J., Zhao, Q., Liu, L. & Zhang, Z. Functional graphene oxide as a nanocarrier for controlled loading and targeted delivery of mixed anticancer drugs. *Small* **6**, 537-544, doi:10.1002/smll.200901680 (2010).

79 Chowdhury, S. M. *et al.* Graphene nanoribbons as a drug delivery agent for lucanthone mediated therapy of glioblastoma multiforme. *Nanomedicine : nanotechnology, biology, and medicine*, doi:10.1016/j.nano.2014.08.001 (2014).

80 Mullick Chowdhury, S., Manepalli, P. & Sitharaman, B. Graphene nanoribbons elicit cell specific uptake and delivery via activation of epidermal growth factor receptor enhanced by human papillomavirus E5 protein. *Acta biomaterialia* **10**, 4494-4504, doi:10.1016/j.actbio.2014.06.030 (2014).

81 Mullick Chowdhury, S. *et al.* Cell specific cytotoxicity and uptake of graphene nanoribbons. *Biomaterials* **34**, 283-293, doi:10.1016/j.biomaterials.2012.09.057 (2013).

82 Pakkanen, K. *et al.* Desipramine induces disorder in cholesterol-rich membranes: implications for viral trafficking. *Physical biology* **6**, 046004, doi:10.1088/1478-3975/6/4/046004 (2009).

83 Dobrowsky, R. T., Kamibayashi, C., Mumby, M. C. & Hannun, Y. A. Ceramide activates heterotrimeric protein phosphatase 2A. *The Journal of biological chemistry* **268**, 15523-15530 (1993).

84 Shabbits, J. A. & Mayer, L. D. High ceramide content liposomes with in vivo antitumor activity. *Anticancer research* **23**, 3663-3669 (2003).

85 Dhule, S. S. *et al.* The combined effect of encapsulating curcumin and C6 ceramide in liposomal nanoparticles against osteosarcoma. *Molecular pharmaceutics* **11**, 417-427, doi:10.1021/mp400366r (2014).

86 Nirala, N. K. *et al.* Survival response to increased ceramide involves metabolic adaptation through novel regulators of glycolysis and lipolysis. *PLoS genetics* **9**, e1003556, doi:10.1371/journal.pgen.1003556 (2013).

87 Mesicek, J. *et al.* Ceramide synthases 2, 5, and 6 confer distinct roles in radiation-induced apoptosis in HeLa cells. *Cellular signalling* **22**, 1300-1307, doi:10.1016/j.cellsig.2010.04.006 (2010).

88 Osawa, Y. *et al.* Roles for C16-ceramide and sphingosine 1-phosphate in regulating hepatocyte apoptosis in response to tumor necrosis factor-alpha. *The Journal of biological chemistry* **280**, 27879-27887, doi:10.1074/jbc.M503002200 (2005).

89 Thomas, R. L., Jr., Matsko, C. M., Lotze, M. T. & Amoscato, A. A. Mass spectrometric identification of increased C16 ceramide levels during apoptosis. *The Journal of biological chemistry* **274**, 30580-30588 (1999).

90 Eto, M. *et al.* C16 ceramide accumulates following androgen ablation in LNCaP prostate cancer cells. *The Prostate* **57**, 66-79, doi:10.1002/pros.10275 (2003).

91 Eto, M., Bennouna, J., Hunter, O. C., Lotze, M. T. & Amoscato, A. A. Importance of C16 ceramide accumulation during apoptosis in prostate cancer cells. *International journal of urology : official journal of the Japanese Urological Association* **13**, 148-156, doi:10.1111/j.1442-2042.2006.01249.x (2006).

92 Aflaki, E. *et al.* C16 ceramide is crucial for triacylglycerol-induced apoptosis in macrophages. *Cell death & disease* **3**, e280, doi:10.1038/cddis.2012.17 (2012).

93 Sassa, T., Suto, S., Okayasu, Y. & Kihara, A. A shift in sphingolipid composition from C24 to C16 increases susceptibility to apoptosis in HeLa cells. *Biochimica et biophysica acta* **1821**, 1031-1037, doi:10.1016/j.bbalip.2012.04.008 (2012).

94 Qiao, Y., Zhang, P., Wang, C., Ma, L. & Su, M. Reducing X-Ray Induced Oxidative Damages in Fibroblasts with Graphene Oxide. *Nanomaterials (Basel)* **4**, 522-534, doi:10.3390/nano4020522 (2014).

95 Valencia, A. & Kochevar, I. E. Ultraviolet A induces apoptosis via reactive oxygen species in a model for Smith-Lemli-Opitz syndrome. *Free radical biology & medicine* **40**, 641-650, doi:10.1016/j.freeradbiomed.2005.09.036 (2006).

96 Artyukhov, V. G., Trubitsyna, M. S., Nakvasina, M. A. & Solov'eva, E. V. DNA fragmentation of human lymphocytes in dynamics of development of apoptosis induced by action of UV radiation and reactive oxygen species. *Cell and Tissue Biology* **5**, 127-135, doi:10.1134/s1990519x11020039 (2011).

97 Degli Esposti, M. & McLennan, H. Mitochondria and cells produce reactive oxygen species in virtual anaerobiosis: relevance to ceramide-induced apoptosis. *FEBS letters* **430**, 338-342, doi:http://dx.doi.org/10.1016/S0014-5793(98)00688-7 (1998).

98 Gutierrez, G., Mendoza, C., Montano, L. F. & Lopez-Marure, R. Ceramide induces early and late apoptosis in human papilloma virus+ cervical cancer cells by inhibiting reactive oxygen species decay, diminishing the intracellular concentration of glutathione and increasing nuclear factor-kappaB translocation. *Anti-cancer drugs* **18**, 149-159, doi:10.1097/CAD.0b013e3280115111 (2007).

99 Hannun, Y. A. & Obeid, L. M. Principles of bioactive lipid signalling: lessons from sphingolipids. *Nat Rev Mol Cell Biol* **9**, 139-150 (2008).

100 Espaillat, M. P., Shamseddine, A. A., Adada, M. M., Hannun, Y. A. & Obeid, L. M. Ceramide and sphingosine-1-phosphate in cancer, two faces of the sphinx. *Translational Cancer Research* **4**, 484-499 (2015).

101 Best, C. *et al.* Paclitaxel disrupts polarized entry of membrane-permeable C6 ceramide into ovarian cancer cells resulting in synchronous induction of cell death. *Oncology Letters* **5**, 1854-1858, doi:10.3892/ol.2013.1305 (2013).

102 Kobayashi, T., Makino, A., Ishii, K. & Celis, J. Vital staining of cells with fluorescent lipids. *Cell Biology: a Laboratory Handbook, 3rd ed. Celis JE, Ed. Elsevier, Amsterdam*, 139-145 (2006).

Chapter 6

Conclusions and Future Work

Conclusions

Ceramide is a sphingolipid with many exciting potential applications in the treatment of cancer and other diseases, but the realization of this potential has thus far been held back by the lack of adequate methods for its therapeutic delivery. In Chapter 1, we reviewed the biology of ceramide, its role in apoptosis and cancer, and the currently available methods for its delivery. The metabolism of ceramide has been implicated in many levels of apoptotic signaling in cancer, and low levels of ceramide are associated with cancer resistance to drug and radiation treatment. Enzymes that metabolize cancer have also been shown to be overexpressed or upregulated in cancers that are resistant to treatment. Many attempts have been made to exploit this knowledge using the synthetic short-chain ceramide C_6. This ceramide is a potent inducer of apoptosis and has been shown to be effective in sensitizing cancers that are resistant to other treatment. The most common method of study is direct dissolution in organic solvents and subsequent addition to aqueous solution. However, for therapeutic treatment, liposomes have been studied the most extensively. Many different formulations of liposomes have been tried, with some more successful than others. However, a common problem is the rapid translocation of C_6 ceramide from the liposomes, making systemic delivery a difficult prospect. Other delivery methods have been tried, but thus far these methods have failed to translate into potential therapeutic applications. There have been either fewer attempts made at external delivery of long chain ceramides such as C_{16} or C_{24} ceramide. So far the only method available with potential *in vivo* applications has been liposomes, which, despite some successes, are riddled with issues such as complex, error-prone synthesis and poor uptake into cells. Thus there is a tangible need for new methods of ceramide delivery into cells. We suggested the use of oxidized graphene nanoribbons (O-GNRs) derived carbon nanotubes as potential delivery systems for ceramides, due to several

favorable properties such as the existence of hydrophobic regions along hydrophilic ones in their structure.

In Chapter 2, we described the process for developing a method to load ceramides onto O-GNRs. We first attempted to mix ceramides and O-GNRs together in ethanol and dimethylsulfoxide but found that there was no significant loading of ceramides onto the nanoparticles. We then tried fractional distillation, with ceramides and O-GNRs being placed in a mixture of high ethanol and low water with the goal of selectively boiling the ethanol out and forcing the ceramide to interact with the O-GNRs in more the more hydrophilic environment. However, we found that the mixing of solvents caused a high degree of irreversible O-GNR aggregation, which was the guiding factor for our subsequent attempts at developing a loading method. We found that by taking the opposite approach - by adding water to a completely hydrophilic environment using a burette - we were able to see some difference in the aggregation, but it was still quite high. So we revised our method in two ways: first, by switching to a syringe pump for more precision addition of water, and second, by adding in a small sonic cleaner to reduce aggregation. We found that a combination of a two-stage addition of water (2 mL/hr for one hour, then 7 mL/hr for 1 hour) and a sonication length of 1.5 hours produced ceramide loaded nanoparticles with a very low degree of aggregation. We found that we were able to load 70% of the ceramide in the initial solution of the nanoparticles. We concluded that O-GNRs could potentially be used as a delivery system for ceramides.

In Chapter 3, we tested our loading method with the short-chain C_6 ceramide. This is a ceramide that has been widely studied for external delivery due to its ease of use. That, combined with its direct, potent effects on cell viability, gave us a good way to test the efficacy of our delivery system. We tested O-GNRs as well as oxidized graphene nanoplatelets (GNPs) derived

from graphite. We found a high degree of loading for both particles, with 57% and 51.5% for O-GNRs and GNPs, respectively. We found that when delivered into cells, both kinds of particles were able to greatly reduce the viability of HeLa cells and that O-GNRs were more effective than GNPs at accomplishing this feat. We also found that there was a similar pattern in U87MG glioblastoma cells and MDA-MB-231 breast cancer cells tested with C_6 ceramide-loaded O-GNRs, while fibroblasts did not experience a significant reduction in viability at lower indications, indicating that C_6 ceramide-loaded O-GNRs could possibly induce toxicity to cancer cells while not harming normal cells nearby. We found that further solubilizing our C_6 ceramide-loaded O-GNRs and GNPs with DSPE-PEG did not reduce their efficacy. We also found a different uptake profile of ceramide loaded O-GNRs into HeLa cells versus free ceramide with the fluorescently tagged C_6 NBD ceramide. We found that there was not significant fluorescence from C_6 NBD ceramide-loaded O-GNRs until 24 minutes, while there was fluorescence from free ceramide almost immediately. We confirmed that the C_6 ceramide-loaded O-GNRs were actually entering into the cells using TEM. We concluded that O-GNRs were a promising delivery system for short-chain ceramide analogues.

In Chapter 4, we revealed a mechanism by which O-GNRs can protect cells from ultraviolet (UV) induced apoptosis. We found that O-GNRs had a significant effect on UV-irradiated HeLa cell viability down to the lowest concentration tested of 5 μg/mL. We found that GNPs were not capable of doing this at any concentration tested. We found that O-GNRs were able to significantly reduce UV-induced apoptosis by measuring caspase-3 activity. We found that this mechanism was dependent on the buffering of reactive oxygen species (ROS) using the ROS detector DCFDA. We concluded that our findings were in accordance with previous studies on this subject and that the differences observed between O-GNRs and GNPs were likely due to

a higher degree of oxidation with O-GNRs. We also concluded that O-GNRs may have the potential to interfere with therapeutic delivery systems that rely on ROS for signaling.

In Chapter 5, we explored the ability of O-GNRs to deliver the long chain ceramides C_{16} and C_{24}. We found that we were able to load 61.47% and 48.76% of the initial concentrations of C_{16} and C_{24} ceramide, respectively. We found that were able to deliver these ceramides to HeLa cells and induce significant biological effects in conjunction with C_6 ceramide or UV treatment measured by the Prestoblue viability assay and caspase-3 activity assay. However, we found that O-GNRs themselves exerted significant biological effects and interfered with C_6 ceramide and UV treatment. Using uptake inhibitors, we were able to reverse these effects and found that the pattern of reversal was in accordance with previous studies on the methods of O-GNR entry into cells, indicating that the loading of ceramide on O-GNRs did not have a significant effect on their uptake, which was further confirmed by TEM imaging. We also measured the levels of several different sphingolipid species in HeLa cells treated with O-GNRs and ceramide-loaded O-GNRs and found that while there were higher levels of C_{16} and C_{24} ceramide measured in their respective groups, there were also high levels of these ceramides in the background sham control. We also observed a large effect of O-GNRs on the levels of certain sphingolipids, indicating that their interference with UV and C_6 ceramide treatment may be due to altering sphingolipid metabolism. Using the fluorescent C_{12} NBD ceramide, we found that there was a difference in uptake between free ceramide and ceramide O-GNRs, with the O-GNR uptake inhibitors significantly reducing their fluorescence but having no effect on free ceramide fluorescence. We also found that the endosome disruptor had no effect on the localization of ceramide O-GNRs while completely release free ceramide from endosomes and spreading them

around the cells. We concluded that O-GNRs could potentially be a good delivery system for long chain ceramides, but that there is also much optimization that needs to be done.

This work represents an important achievement in the field of therapeutic ceramide delivery. Up until now, potential delivery methods have been few in number and with certain drawbacks. Even liposomes - the most promising of the methods - have thus far been unable to translate into therapeutic applications. In our work, we successfully delivered the short-chain C_6 ceramide into cells and induced apoptosis in several cell lines, yielding a system that has the potential to be a powerful treatment for cancer. This lack of a good delivery system has also limited the ability to understand the effects of externally delivered long chain ceramides on cells. Here we have successfully delivered the long chain ceramides C_{16} and C_{24}, revealing that C_{16} can potentially assist in sensitizing cells to apoptosis and that C_{24} can potentially protect cells from apoptosis. Although our O-GNRs exerted significant biological effects of their own, the ability to load significant quantities of these ceramides and introduce them into cells represents a critical step forward into fully understanding their effects. The exact effects of these ceramides on different types of cells remains an outstanding question in the study of ceramides, and one that will only be able to be answered with innovation and optimization in the field of ceramide delivery.

Future Work

The research at hand here has had mixed outcomes in the short term. However, in the long term, there is much potential and much room for improvement over the results currently observed. Below we discuss some ways to improve upon O-GNRs as a delivery system for ceramides and further elucidate the effects of O-GNRs on cells, as well alternate routes of progression.

1) First and foremost, there needs to be an extensive study of the effects of O-GNRs on ceramide metabolism in cancer cells. Although previous research points to an ROS-dependent mechanism for the protective effect of graphene oxide nanoparticles on oxidative stress, our results in Chapter 5 may point to a mechanism that may also be mediated by sphingolipid metabolism. This study should include (but not necessarily be limited to) quantification of the expression levels of important ceramide-metabolizing enzymes involved in cancer resistance such as glucosylceramide synthase and ceramidase. It should also not necessarily be limited to just O-GNRs, but also include graphene oxide nanoparticles synthesized by different methods as well.

2) Further testing of the potential of C_6 ceramide-loaded O-GNRs should be conducted. Although the 'holy grail' of this research is the delivery of long chain ceramides, the delivery of short chain ceramides is a worthy goal as well. Our results indicate that O-GNRs could be developed as a potent delivery system for C_6 ceramide. In this realm, co-delivery with other therapeutic reagents may be a promising avenue for development. In particular, inhibitors of ceramide-metabolizing enzymes such as glucosylceramide synthases and ceramidases could significantly enhance the toxicity of C_6 ceramide-loaded O-GNRs.

3) This research should also not just be limited to ceramide. There are many lipids out there with compelling and interesting properties. For example, in the realm of gene transfection, cationic lipids are extremely potent transfection reagents *in vitro*, but have difficulty *in vivo* for similar reason to other liposomes. However, if these cationic lipids were loading onto our O-GNRs using the loading method we developed for ceramide, it could make for a potent combination between the transfection power of these lipids and the stability of graphene nanoparticles.